UNIVERSIDADE FEDERAL DE MINAS GERAIS
Escola de Engenharia
Programa de Pós-Graduação em Engenharia Metalúrgica, Materiais e de Minas

Cássia Ribeiro Souza

CRYSTALLIZATION OF NIOBIUM COMPOUNDS FROM Fe-Nb ALLOY FINES ALKALINE LIQUOR

CRISTALIZAÇÃO DE COMPOSTOS DE NIÓBIO A PARTIR DO LICOR ALCALINO DE FINOS DE LIGA Fe-Nb

Belo Horizonte
2024

Cássia Ribeiro Souza

CRYSTALLIZATION OF NIOBIUM COMPOUNDS FROM Fe-Nb ALLOY FINES ALKALINE LIQUOR

CRISTALIZAÇÃO DE COMPOSTOS DE NIÓBIO A PARTIR DO LICOR ALCALINO DE FINOS DE LIGA Fe-Nb

Tese apresentada ao Programa de Pós-Graduação em Engenharia Metalúrgica, Materiais e de Minas da Escola de Engenharia da Universidade Federal de Minas Gerais, como requisito parcial para obtenção do título Doutora em Engenharia Metalúrgica, Materiais e de Minas.

Área de Concentração: Tecnologia Mineral

Orientadora: Profª Drª Sônia Denise Ferreira Rocha

Co-orientador: Prof. Dr. Frederico Marques Penha

Belo Horizonte
2024

Souza, Cássia Ribeiro.
S729c Crystallization of niobium compounds from Fe-Nb alloy fines alkaline liquor [recurso eletrônico] = Cristalização de compostos de nióbio a partir do licor alcalino de finos de liga Fe-Nb / Cássia Ribeiro Souza. –2024.
1 recurso online (168 f.: il., color.): pdf.

Orientadora: Sônia Denise Ferreira Rocha.
Coorientador: Frederico Marques Penha.

Tese (doutorado) - Universidade Federal de Minas Gerais, Escola de Engenharia.

Apêndices: f. 163-168.

Inclui bibliografia.

1. Engenharia de minas - Teses. 2. Tecnologia mineral - Teses. 3. Compostos de nióbio - Teses. 4. Solubilidade - Teses. 5. Cristalização - Teses. 6. Modelagem - Teses. 7. Termodinâmica - Teses. I. Rocha, Sônia Denise Ferreira. II. Penha, Frederico Marques. III. Universidade Federal de Minas Gerais. Escola de Engenharia. IV. Título.

CDU: 622(043)

Ficha catalográfica elaborada pelo bibliotecário Reginaldo César Vital dos Santos CRB/6 2165
Biblioteca Prof. Mário Werneck, Escola de Engenharia da UFMG

UNIVERSIDADE FEDERAL DE MINAS GERAIS
ENGENHARIA - COLEGIADO DE PÓS-GRADUAÇÃO EM ENGENHARIA METALÚRGICA MATERIAIS E DE MINAS - SECRETARIA

ATA DE DEFESA DE TESE

Às 09h do dia 20 (vinte) de dezembro de 2024, na sala 2240 do Bloco II do Prédio da Escola de Engenharia da UFMG, realizou-se a sessão pública de defesa de tese de Doutorado do(a) aluno(a) **CÁSSIA RIBEIRO SOUZA**, para a obtenção do grau de Doutor(a) em Engenharia Metalúrgica, Materiais e de Minas, na área de concentração de Tecnologia Mineral. O presidente da sessão, Drª Sônia Denise Ferreira Rocha (UFMG), orientador(a) do(a) aluno(a), apresentou a comissão examinadora, composta pelos seguintes membros: Dr. Frederico Marques Penha, Coorientador (KTH Royal Institute of Technology); Drª. Virginia Sampaio Teixeira Ciminelli (UFMG); Drª Viviane Santos Birchal (UFMG); Dr. Marcelo Martins Seckler (USP); Dr. Elbert Muller Nigri (SENAI). Na sequência, o(a) candidato(a) realizou a apresentação de sua Tese de Doutorado, intitulada **"CRYSTALLIZATION OF NIOBIUM COMPOUNDS FROM FE-NB ALLOY FINES ALKALINE LIQUOR"**. Após a apresentação, os examinadores procederam à arguição do(a) candidato(a). Concluída essa etapa, a comissão reuniu-se em caráter reservado, sem a presença do(a) candidato(a) e do público, e decidiu por **APROVAR** a Tese de Doutorado. O resultado final foi comunicado publicamente ao(à) candidato(a) pelo presidente da sessão. Não havendo mais nada a tratar, o presidente encerrou a sessão e lavrou a presente ata, que, após lida, foi assinada pelos membros da comissão examinadora e pelo coordenador do Programa.

Belo Horizonte, 20 de dezembro de 2024

Assinatura dos membros da banca examinadora:

Documento assinado eletronicamente por **Elbert Muller Nigri**, **Usuário Externo**, em 26/12/2024, às 17:49, conforme horário oficial de Brasília, com fundamento no art. 5º do Decreto nº 10.543, de 13 de novembro de 2020.

Documento assinado eletronicamente por **Sonia Denise Ferreira Rocha**, **Professora do Magistério Superior**, em 27/12/2024, às 12:36, conforme horário oficial de Brasília, com fundamento no art. 5º do Decreto nº 10.543, de 13 de novembro de 2020.

Documento assinado eletronicamente por **Frederico Marques Penha**, **Usuário Externo**, em 06/01/2025, às 11:30, conforme horário oficial de Brasília, com fundamento no art. 5º do Decreto nº 10.543, de 13 de novembro de 2020.

Documento assinado eletronicamente por **Virginia Sampaio Teixeira Ciminelli**, **Professora do Magistério Superior**, em 08/01/2025, às 14:12, conforme horário oficial de Brasília, com fundamento no art. 5º do Decreto nº 10.543, de 13 de novembro de 2020.

Documento assinado eletronicamente por **Viviane Santos Birchal**, **Diretor(a)**, em 08/01/2025, às 15:45, conforme horário oficial de Brasília, com fundamento no art. 5º do Decreto nº 10.543, de 13 de novembro de 2020.

Documento assinado eletronicamente por **Eduardo Henrique Martins Nunes**, **Coordenador(a) de curso de pós-graduação**, em 17/02/2025, às 09:42, conforme horário oficial de Brasília, com fundamento no art. 5º do Decreto nº 10.543, de 13 de novembro de 2020.

Documento assinado eletronicamente por **Marcelo Martins Seckler**, **Usuário Externo**, em 25/02/2025, às 12:03, conforme horário oficial de Brasília, com fundamento no art. 5º do Decreto nº 10.543, de 13 de novembro de 2020.

A autenticidade deste documento pode ser conferida no site https://sei.ufmg.br/sei/controlador_externo.php?acao=documento_conferir&id_orgao_acesso_externo=0, informando o código verificador **3817183** e o código CRC **07292FCB**.

Referência: Processo nº 23072.273123/2024-03 SEI nº 3817183

AGRADECIMENTOS

Agradeço a Deus por me guiar com sabedoria e proteger a cada dia.

Ao meu esposo, Stênio, que foi minha certeza de apoio incondicional e suporte. Que não mediu esforços para estar comigo durante meu intercâmbio e por ser meu grande incentivador. Me trouxe calmaria nos momentos difíceis e certeza de amor a cada dia. Juntos, à espera da Aurora, tenho ainda mais motivos para agradecer.

Aos meus pais, Cristóvão e Célia, que foram conforto e amparo incondicionais. Às minhas irmãs, e suas famílias, Consuelo e Clara, pela nossa linda amizade e parceria.

À minha orientadora, Profª Sônia, toda minha gratidão e admiração, pelas oportunidades proporcionadas ao longo destes anos que foram essenciais para meu crescimento profissional e pessoal, pela confiança, amizade, apoio e acolhimento e por me incentivar sempre a conquistar meus sonhos.

Ao meu coorientador, Profº Fred, pela amizade e dedicação. Que mesmo longe, sempre foi muito solícito e não mediu esforços para me ajudar quando precisei. A convivência durante o intercâmbio foi enriquecedora e tornou essa experiência muito mais especial.

Aos amigos do grupo de pesquisa Strategic Nb e colegas da UFMG pela amizade e ideias compartilhadas que enriqueceram meu percurso acadêmico. Em especial à Isabel, André, Daísa, Alice, Marina e Thaiara, pelo companheirismo e momentos de distração. À Andressa Mazur, por toda ajuda indispensável durante meu período em Estocolmo. Vocês foram essenciais.

À UFMG, ao PPGEM e ao DEMIN, professores, técnicos e colaboradores, pelos ensinamentos, disponibilidade e suporte. Em especial ao Laboratório de Processamento Aquoso (INCT-Acqua/UFMG) e ao Centro de Microscopia da UFMG pelas análises feitas. Ao KTH – Division of Resource Recovery, pelo apoio e suporte durante meu intercâmbio em Estocolmo.

À CAPES e CNPq (Project INOVA-NIÓBIO nº 408563/2022-2) pelo suporte financeiro durante meu doutorado.

Por fim, agradeço a todos que, de alguma forma, contribuíram para a realização deste trabalho, seja com palavras de incentivo, gestos de apoio ou compartilhando momentos ao longo desta jornada. A cada um de vocês, minha eterna gratidão. Este trabalho é fruto não só dos meus esforços, mas também da confiança, carinho e dedicação que recebi de tantas pessoas especiais.

ACKNOWLEDGMENTS

I thank God for guiding me with wisdom and protecting me every day.

To my husband, Stênio, who was my unwavering source of support and encouragement. He spared no effort to be by my side during my exchange program and has always been my greatest motivator. He brought me calm during challenging moments and certainty of love every single day. Together, as we await the arrival of our daughter Aurora, I have even more reasons to be grateful.

To my parents, Cristóvão and Célia, who provided unconditional comfort and support. To my sisters, and their families, Consuelo and Clara, for our beautiful friendship and partnership.

To my advisor, Prof. Sônia, my deepest gratitude and admiration for the opportunities provided over these years, which have been essential for my professional and personal growth. Thank you for your trust, friendship, support, and guidance, and for always encouraging me to pursue my dreams.

To my co-advisor, Prof. Fred, for your friendship and dedication. Despite the distance, you have always been extremely helpful and spared no effort to assist me whenever I needed. The time we spent together during the exchange was enriching and made this experience even more special.

To the friends of the Strategic Nb research group and colleagues at UFMG, thank you for the friendship and shared ideas that enriched my academic journey. A special thanks to Isabel, André, Daísa, Alice, Marina, and Thaiara for the friendship and for the moments of enjoyment.

To Andressa Mazur, for all the indispensable help during my time in Stockholm. You were all essential.

To UFMG, the PPGEM, and DEMIN, professors, staff, and collaborators, thank you for the teachings, availability, and support. Special thanks to the Laboratory of Aqueous Processing (INCT-Acqua/UFMG) and the Microscopy Center of UFMG for the analyses performed. To KTH – Division of Resource Recovery, for the support and assistance during my exchange in Stockholm.

To CAPES and CNPq (Project INOVA-NIÓBIO nº 408563/2022-2) for the financial support during my research time.

Finally, I extend my gratitude to everyone who, in some way, contributed to the completion of this work—be it with words of encouragement, gestures of support, or sharing moments along this journey. To each of you, my eternal gratitude. This work is not only the result of my efforts but also of the trust, care, and dedication I received from so many special people.

RESUMO

O consumo de compostos à base de nióbio aumentou nas últimas décadas devido à sua crescente gama de aplicações. Os avanços tecnológicos e industriais recentes elevaram a demanda por nióbio (Nb), especialmente nos setores de aviação, construção civil, componentes eletrônicos e de comunicação, energia, além das indústrias automotiva, metalúrgica e siderúrgica. Nesse contexto, embora essas aplicações ainda não tenham atingido o fim de vida, investigar a recuperação de Nb a partir de fontes secundárias torna-se necessária para a produção de novos compostos com alto valor econômico. Como fonte secundária modelo, foram escolhidas as partículas finas fora dos padrões comerciais que são descartadas no processamento de ligas Fe-Nb, tornando-se passivos para a indústria metalúrgica. A química do nióbio em meio aquoso é complexa e pouco explorada, havendo escassez de dados de solubilidade na literatura. Por isso, foi realizada uma avaliação termodinâmica das propriedades físico-químicas e da especiação do sistema Nb-K-H_2O utilizando os softwares PHREEQC e OLI Studio Stream Analyzer. O objetivo foi avaliar a influência de parâmetros de processos (composição química, pH, temperatura e supersaturação) na cristalização de niobato de potássio e ácido nióbico. Para o estudo experimental de solubilidade, o ácido nióbico (Nb_2O_5·nH2O HY-340) e o niobato de potássio (mistura cristalizada das fases $K_4Nb_6O_{17}$ e $KNbO_3$) foram avaliados em função da temperatura em diferentes concentrações de solução de KOH (0 a 2 mol/L). As medições experimentais de solubilidade foram realizadas utilizando o Crystal 16. O tempo de equilíbrio do ácido nióbico em meio alcalino também foi avaliado. Esses resultados são essenciais para o desenvolvimento do conhecimento científico e tecnológico sobre o nióbio em meio aquoso, que é escasso na literatura. Partículas finas de liga Fe-Nb foram lixiviadas em KOH a T= 96 ºC, produzindo um licor alcalino e permitindo a recuperação de compostos de nióbio a temperaturas relativamente baixas e pressão atmosférica. O niobato de potássio foi obtido por cristalização a partir do resfriamento da solução alcalina de potássio, sendo utilizado como precursor para a produção de ácido nióbico e, posteriormente, óxido de nióbio. Apesar da cinética de cristalização lenta, verificada à diferentes taxas de resfriamento, as análises de DRX e composição química confirmaram a formação de fases cristalinas – $KNbO_3$ e $K_4Nb_6O_{17}$ – e a microscopia óptica mostrou cristais em forma de placa isolados em sua maioria. Por outro lado, ácido nióbico amorfo foi obtido por precipitação de uma solução de niobato de potássio com H_2SO_4 a 0,50 e 0,25 mol/L. Um protocolo de lavagem foi implementado para eliminar as impurezas do ácido nióbico precipitado. Após calcinação a 900ºC por 5 horas, o DRX revelou a presença de uma fase de niobato de potássio ($K_2Nb_8O_{21}$) com morfologia em forma de bastões. Este trabalho fornece a base para a futura recuperação e valorização de produtos contendo nióbio a partir de resíduos em direção à circularidade e ressalta a viabilidade de recuperar compostos de nióbio a partir de fontes secundárias em condições amenas de temperatura e pressão.

Palavras-chave: compostos de nióbio; licor alcalina; solubilidade; cristalização; modelagem termodinâmica.

ABSTRACT

The consumption of niobium-based compounds has risen due to the broadening of the range of applications. Recent technological and industrial developments have increased the niobium (Nb) demand, particularly in aviation, construction, electronics, communication, energy as well as the automotive, metallurgical and steel industries. In this regard, although many of these applications have not yet reached their end-of-life, investigating the recovery of Nb from secondary sources is essential for the production of new compounds with high economic value. As a model secondary source, the alloy fines that are out of the commercial standard and are discarded in the Fe-Nb alloy processing were chosen, becoming a liability in the metallurgical industry. The chemistry of niobium in aqueous media it is complex and has been under-investigated, with limited solubility data available. Thus, a thermodynamic evaluation of physical-chemical properties and speciation of Nb-K-H_20 system was carried out using PHREEQC, OLI Studio Stream Analyzer. Aiming to evaluate the influence of process parameters (chemical composition, pH, temperature and supersaturation) on the crystallization of potassium niobate and niobic acid. To the experimental solubility study, niobic acid ($Nb_2O_5.nH_2O$ HY-340) and potassium niobate (crystallized mix of phases $K_4Nb_6O_{17}$ and $KNbO_3$) was evaluated as a function of temperature in different concentrations of KOH solution (0 to 2 mol/L). Crystal 16 was used in the experimental measurements of solubility. The equilibrium time of niobic acid in alkaline medium was also evaluated. These results are essential to develop scientific and technological knowledge about niobium behaviour in aqueous media, which is scarce in the literature. Fe-Nb alloy fines leached in KOH at 96 ºC, producing an alkaline liquor enabling the recovery of niobium compounds at relatively low temperatures and atmospheric pressure. Potassium niobate was obtained from the cooling crystallization of potassium alkaline liquor and was used as a precursor for producing niobic acid and further niobium oxide. Despite its low crystallization, observed at different cooling rates, the XRD and chemical analysis indicated that potassium niobate was formed in different crystalline phases – $KNbO_3$ and $K_4Nb_6O_{17}$ – with microscopy imagens showing isolated plate-like crystals. On the other hand, an amorphous niobic acid with residual potassium sulphate was obtained through precipitation from a potassium niobate solution with H_2SO_4 0.50 and 0.25 mol/L. A washing protocol was implemented in order to remove the impurities of precipitated niobic acid. After the calcination at 900ºC for 5h, the XRD shows the presence of a potassium niobate phase $K_2Nb_8O_{21}$ with rod-like morphology. This study provides the basis for future recovery and valorisation of niobium-containing products from waste materials towards circularity and highlights the feasibility of recovering niobium compounds from secondary sources under mild temperature and pressure conditions.

Keywords: niobium compounds; alkaline liquor; solubility; crystallization; thermodynamic modeling.

LIST OF FIGURES

LIST OF TABLES

SUMMARY

CHAPTHER 1 – INTRODUCTION / INTRODUÇÃO

1.1 Contextualization / Contextualização

English

Brazil is the largest niobium producer and holds the largest world reserves with around 98.5%, followed by Canada (1.0%) and Australia (0.5%). According to ANM (Brazilian National Mining Agency - *Agência Nacional de Mineração*), in 2020 niobium was the fifth highest-added value metal in exports, after iron, gold, aluminium and copper, which makes it a strategic metal (Decree nº 10.657, 2021). In addition, niobium is classified by the European Union as one of the thirty-four critical raw materials, as it presents a high risk of supply and high growth in demand (von Rennenberg, 2021; European Commission, 2023).

In Brazil, the main niobium reserves are concentrated in Araxá (Minas Gerais), Catalão and Ouvidor (Goiás), Presidente Figueiredo (Amazonas), and Itapuã do Oeste, Rio Crespo, Ariquemes (Rondônia). According to the ANM, Araxá holds approximately 90% of the reserves and has a measured reserve of 742 Mt of pyrochlore ore [$(Na,Ca)_2Nb_2O_6(OH,F)$] while Catalão and Ouvidor contain 82.3 Mt of pyrochlore ore. In Presidente Figueiredo, the Pitinga reserve contains a measured reserve of 108.2 Mt of columbite ore [$(Mg,Fe^{2+},Mn)(Nb,Ta)_2O_6$] while in Itapuã do Oeste, Rio Crespo and Ariquemes there are minor reserves of columbite-tantalite ore. The niobium contents in these ores range between 0.21 to 2.85% in Nb_2O_5. In the case of pyrochlore, the reserves are found in carbonatite bodies, while those of columbite–tantalite are in pegmatites associated with rapakivi granites (ANM, 2019).

Due to the industrialization and increased consumption of niobium, studies show its use in various applications such as electrolytic and ceramic capacitors, material for medical implants with excellent biocompatibility, optical films, battery alloys, semiconductor and microelectronic components, chemical products for specific applications in catalysis and optical lenses (Alves & Coutinho, 2015; Bruziquesi et al., 2019; Heisterkamp & Carneiro, 2001; Peiffert et al., 2010). Also, chemical solutions with niobium have received attention due to radioactive isotopes (Filella & May, 2020).

Niobium as Nb_2O_5 has gained prominence in electric batteries for its use as an anodic material for intercalation reactions, providing high volumetric capacity, and stability over a wide range of temperatures and pH (Lübke et al., 2016) and in hybrid supercapacitors starting from Nb_2O_5 microspheres synthesized from high porosity carbon matrices (Bruziquesi et al., 2019). Other niobium-containing products are alkaline niobates which have attracted attention because of their excellent optical, ferroelectric and photorefractive properties (Kanie et al., 2011; Bai et al., 2017; Andrade et al., 2000).

Due to its high melting point, niobium has been widely used as a component of various metallic alloys with a great impact on alloys refining, fostering an improvement of corrosion resistance and reducing weight (Labinger, 1982). These alloys are present in turbines, chemical and petrochemical equipment's, magnetic superconductors, metallic structures in civil construction and others (Alves & Coutinho, 2015; Deblonde et al., 2015, 2016).

The need for innovative and technological energies in a situation where non-renewable resources must be replaced and greenhouse gas emissions must be reduced, the use of electric batteries and solar panels stand out and niobium has been ultimately been studied for applications in this sector (Baktash et al., 2020; Dolganova et al., 2020; Lü et al., 2010; Nikolay et al., 2011; Park et al., 2013; Sasidharan et al., 2012; Lübke et al., 2016; Vasconcelos, 2019).

In the near future, it is expected that the implementation of technological innovations and advancements will require the increase in recyclability of niobium (today this rate is around 20-30% - mainly in European countries), with regulations that encourage niobium supply companies to work on the circular economy and obtain raw materials from secondary sources (Sociedade de Química, 2021; European Commission, 2014). In the case of critical raw materials, such as niobium, the application of circular economy principles aims to reduce dependence on suppliers and the processing of secondary resources (von Rennenberg, 2021). Urban mining is an alternative that involves the recycling or reusing of post-consumer goods as a means of economically reusing wastes that have a high added value and that can still be utilized to reduce environmental liabilities. It is a circular economy approach since the raw materials come from end-of-life objects and infrastructures that already exist. One of the benefits of urban mining is

the recovery of valuable metals from the ever-growing e-waste streams, especially those containing critical raw materials (Zeng et al., 2018, Tesfaye et al., 2017).

The Fe-Nb alloy is the main product of niobium, and its production begins with the ore fragmentation, which includes crushing, grinding, and desliming, followed by concentration. The impurities are removed from the ore by leaching and in the final stage the aluminothermic reduction with iron metallic produces the Fe-Nb alloy. Then, granulometric separation is carried to get the allow with adequate commercial size specification. However, alloy fines are generated in the crushing step and separated from the product. This material, out of commercial specification, needs subsequent processing.

In this context, the present study proposes to obtain niobium-containing compounds from Fe-Nb alloy fines. This will enable the development of technology to recover niobium from secondary sources and promote the circular economy. Thus, a thermodynamic study of physical-chemical properties and speciation of niobium-potassium-water system is essential to understand the variables of leaching and crystallization processes. For the crystallization step, solution composition, pH, supersaturation levels and temperature were investigated through thermodynamic modelling and with results from experiments addressed, to obtain high-quality niobium oxide, a precursor for many distinct niobium products.

Português

O Brasil é o maior produtor de nióbio e possui as maiores reservas mundiais, com cerca de 98,5%, seguido pelo Canadá (1,0%) e Austrália (0,5%). Segundo a ANM (Agência Nacional de Mineração), em 2020, o nióbio foi o quinto metal de maior valor agregado nas exportações, após ferro, ouro, alumínio e cobre, o que o torna um metal estratégico (Decreto nº 10.657, 2021). Além disso, o nióbio é classificado pela União Europeia como um dos trinta e quatro materiais críticos, devido ao alto risco de abastecimento e ao crescimento significativo na demanda (von Rennenberg, 2021; Comissão Europeia, 2023).

No Brasil, as principais reservas de nióbio estão concentradas em Araxá (Minas Gerais), Catalão e Ouvidor (Goiás), Presidente Figueiredo (Amazonas) e Itapuã do Oeste, Rio Crespo e Ariquemes (Rondônia). De acordo com a ANM, Araxá detém aproximadamente 90% das reservas, com uma reserva medida de 742 Mt de minério de pirocloro [$(Na,Ca)_2Nb_2O_6(OH,F)$], enquanto Catalão e Ouvidor possuem 82,3 Mt de minério de pirocloro. Em Presidente Figueiredo, a reserva de Pitinga possui uma reserva medida de 108,2 Mt de minério de columbita [$(Mg,Fe^{2+},Mn)(Nb,Ta)_2O_6$], enquanto em Itapuã do Oeste, Rio Crespo e Ariquemes há reservas menores de minério de columbita-tantalita. Os teores de nióbio nesses minérios variam entre 0,21% e 2,85% em Nb_2O_5. No caso do pirocloro, as reservas encontram-se em corpos de carbonatito, enquanto as de columbita-tantalita estão em pegmatitos associados a granitos rapakivi (ANM, 2019).

Devido à industrialização e ao aumento do consumo de nióbio, estudos apontam seu uso em diversas aplicações, como capacitores eletrolíticos e cerâmicos, materiais para implantes médicos com excelente biocompatibilidade, filmes ópticos, ligas para baterias, componentes semicondutores e microeletrônicos, produtos químicos para aplicações específicas em catálise e lentes ópticas (Alves & Coutinho, 2015; Bruziquesi et al., 2019; Heisterkamp & Carneiro, 2001; Peiffert et al., 2010). Além disso, soluções químicas com nióbio têm recebido atenção devido a isótopos radioativos (Filella & May, 2020).

O nióbio, na forma de Nb_2O_5, ganhou destaque em baterias elétricas por seu uso como material anódico para reações de intercalação, proporcionando alta capacidade volumétrica e estabilidade em ampla faixa de temperaturas e pH (Lübke et al., 2016), e em supercapacitores híbridos, a partir de microesferas de Nb_2O_5 sintetizadas a partir de matrizes de carbono de alta porosidade (Bruziquesi et al., 2019). Outros produtos contendo nióbio, como os niobatos alcalinos, têm atraído atenção devido às suas excelentes propriedades ópticas, ferroelétricas e fotorrefrativas (Kanie et al., 2011; Bai et al., 2017; Andrade et al., 2000).

Devido ao seu alto ponto de fusão, o nióbio tem sido amplamente utilizado como componente de várias ligas metálicas, com grande impacto no refinamento de ligas, promovendo melhoria na resistência à corrosão e redução de peso (Labinger, 1982). Essas ligas estão presentes em turbinas, equipamentos químicos e petroquímicos, supercondutores magnéticos, estruturas metálicas na construção civil, entre outros (Alves & Coutinho, 2015; Deblonde et al., 2015, 2016).

Com a necessidade de energias inovadoras e tecnológicas, em um contexto onde recursos não renováveis precisam ser substituídos e as emissões de gases de efeito estufa devem ser reduzidas, destacam-se o uso de baterias elétricas e painéis solares. O nióbio tem sido estudado para aplicações nesse setor (Baktash et al., 2020; Dolganova et al., 2020; Lü et al., 2010; Nikolay et al., 2011; Park et al., 2013; Sasidharan et al., 2012; Lübke et al., 2016; Vasconcelos, 2019).

No futuro próximo, espera-se que a implementação de inovações tecnológicas exija um aumento na reciclabilidade do nióbio (atualmente, essa taxa é de cerca de 20-30%, principalmente em países europeus), com regulamentações que incentivem as empresas fornecedoras de nióbio a trabalharem na economia circular e a obterem matérias-primas de fontes secundárias (Sociedade de Química, 2021; Comissão Europeia, 2014). No caso de materiais críticos, como o nióbio, a aplicação de princípios de economia circular visa reduzir a dependência de fornecedores e o processamento de recursos secundários (von Rennenberg, 2021). A mineração urbana é uma alternativa que envolve a reciclagem ou reutilização de bens de consumo pós-uso como forma de reaproveitar economicamente resíduos de alto valor agregado, ainda utilizáveis, para reduzir passivos ambientais. Trata-se de uma abordagem de economia circular, pois as matérias-primas provêm de objetos e infraestruturas de fim de vida que já existem. Um dos benefícios da mineração urbana é a recuperação de metais valiosos provenientes de fluxos crescentes de lixo eletrônico, especialmente os que contêm materiais críticos (Zeng et al., 2018; Tesfaye et al., 2017).

A liga Fe-Nb é o principal produto do nióbio, e sua produção começa com a fragmentação do minério, que inclui britagem, moagem e deslamagem, seguida da concentração. As impurezas são removidas do minério por lixiviação, e, na etapa final, a redução aluminotérmica com ferro metálico produz a liga Fe-Nb. Em seguida, é realizada a separação granulométrica para obter a liga com especificações comerciais adequadas. No entanto, finos da liga são gerados na etapa de britagem e separados do produto. Este material, fora das especificações comerciais, necessita de processamento subsequente.

Nesse contexto, o presente estudo propõe obter compostos contendo nióbio a partir de finos da liga Fe-Nb. Isso permitirá o desenvolvimento de tecnologias para a recuperação de nióbio de fontes secundárias e promoverá a economia circular. Assim, um estudo termodinâmico das propriedades físico-químicas e da especiação do sistema nióbio-potássio-água é essencial para compreender as variáveis dos processos de lixiviação e

cristalização. Para a etapa de cristalização, foram investigadas, por meio de modelagem termodinâmica e experimentos, a composição da solução, pH, níveis de supersaturação e temperatura, com o objetivo de obter óxido de nióbio de alta qualidade, precursor de diversos produtos distintos de nióbio.

1.2 Justificative and Relevance / Justificativa e Relevância

English

In 2019, Brazil was responsible for 88% of niobium production worldwide, followed by Canada with 10% (Padilha, 2020). About 90% of niobium is commercialized in the form of Fe-Nb alloy and the other part as Nb_2O_5 (Sumário Mineral Brasileiro, 2017; Barky and Zeng, 2022).

The high added-value of niobium ores, as well as the fact that Brazil is the world leader in reserves, contribute to the attractiveness of national and international production and commercialization. Hence, there is a need for scientific knowledge of the physico-chemical changes that occur during the industrial processes, as well as their social, economic, and environmental aspects.

The aim of this research is the production of high added-value niobium compounds by the hydrometallurgical processing of Fe-Nb alloy fines, composed of niobium, iron, potassium, silicon, and aluminium. The crystallization process variables such as pH, temperature, solution concentration, and chemical species distribution were evaluated to understand the behaviour of the system. Equilibrium calculation which requires the thermodynamic data on niobium systems were also essential to guide the experiments.

The relevance and impact of this project for scientific, technological and innovation development are in the generation of specific knowledge, essential for the development of new niobium applications and products. This knowledge, which is scarce in the literature, will allow advancements in the chemistry of niobium compounds and provide the potential to obtain niobium products from secondary materials for new applications. The processing of these materials will ease the urban mining and the circular economy in the niobium chain.

As a result, this thesis intends to contribute for a better use of mineral resources with a more effective use of niobium-bearing minerals, as well as the use of wastes from the iron-niobium extraction process to obtain new products, improving sustainability to niobium chain. Considering i) the growth in the use of niobium in the world; ii) the interest in obtaining high-purity niobium compounds, and iii) the need of understanding the effect of process variables in the processing of Nb-bearing liquors, this project also proposes to carry out fundamental studies of solubility to design properly the crystallization and precipitation processes.

Português

Em 2019, o Brasil foi responsável por 88% da produção mundial de nióbio, seguido pelo Canadá, com 10% (Padilha, 2020). Cerca de 90% do nióbio é comercializado na forma de liga Fe-Nb, e o restante como Nb_2O_5 (Sumário Mineral Brasileiro, 2017; Barky e Zeng,2022).

O alto valor agregado dos minérios de nióbio, bem como o fato de o Brasil ser líder mundial em reservas, contribui para a atratividade da produção e comercialização nacional e internacional. Assim, torna-se necessário o conhecimento científico das mudanças físico-químicas que ocorrem durante os processos industriais, bem como de seus aspectos sociais, econômicos e ambientais.

O objetivo desta pesquisa é a produção de compostos de nióbio de alto valor agregado por meio do processamento hidrometalúrgico de finos da liga Fe-Nb, compostos de nióbio, ferro, potássio, silício e alumínio. Foram avaliadas as variáveis do processo de cristalização, como pH, temperatura, concentração da solução e distribuição de espécies químicas, para compreender o comportamento do sistema. Os cálculos de equilíbrio, que exigem dados termodinâmicos sobre sistemas contendo nióbio, também foram essenciais para orientar os experimentos.

A relevância e o impacto deste projeto para o desenvolvimento científico, tecnológico e de inovação residem na geração de conhecimentos específicos, essenciais para o desenvolvimento de novas aplicações e produtos de nióbio. Esse conhecimento, escasso

na literatura, permitirá avanços na química de compostos de nióbio e proporcionará o potencial para obter produtos de nióbio a partir de materiais secundários para novas aplicações. O processamento desses materiais facilitará a mineração urbana e a economia circular na cadeia do nióbio.

Como resultado, esta tese pretende contribuir para um melhor aproveitamento dos recursos minerais, com o uso mais eficaz de minerais que contêm nióbio, bem como para o reaproveitamento de resíduos do processo de extração de ferro-nióbio para obtenção de novos produtos, promovendo maior sustentabilidade na cadeia do nióbio. Considerando: i) o crescimento no uso do nióbio no mundo; ii) o interesse em obter compostos de nióbio de alta pureza; e iii) a necessidade de compreender o efeito das variáveis de processo no tratamento de soluções contendo Nb, este projeto também propõe a realização de estudos fundamentais de solubilidade para projetar adequadamente os processos de cristalização e precipitação.

1.3 References

Alves, A. R., & Coutinho, A. Dos R. (2015). The Evolution of the Niobium Production in Brazil. Materials Research, 18(1), 106–112.

ANM. Anuário Mineral Brasileiro. Disponível em: <www.anm.gov.br>.

Andrade, J. S., Pinheiro, A. G., Vasconcelos, I. F., De Araújo, M. A. B., Valente, M. A., & Sombra, A. S. B. (2000). Structural studies of KNbO3 in niobate glass-ceramics. Journal of Physics and Chemistry of Solids, 61(6), 899–906. https://doi.org/10.1016/S0022-3697(99)00387-X.

Bai, S., Zhang, J., Chen, Z., Wang, Y., Hong, M., & Karaki, T. (2017). Near-room-temperature synthesis of niobate hydrate particles with hexagonal-platelike morphologies. Materials Chemistry and Physics, 199, 230–238. https://doi.org/10.1016/j.matchemphys.2017.06.048.

Baktash, A., Amiri, O., & Saadat, M. (2020). High efficient perovskite solar cells base on niobium doped TiO2 as a buffer layer. Journal of Nanostructures, 10(1), 119–127. https://doi.org/10.22052/JNS.2020.01.013.

Bruziquesi, C. G. O., Balena, J. G., Pereira, M. C., Silva, A. C., & Oliveira, L. C. A. (2019). Niobium: A strategic chemical element for brazil. Quimica Nova, 42(10), 1184–1188. https://doi.org/10.21577/0100-4042.20170442.

Deblonde, G. J. P., Chagnes, A., Bélair, S., & Cote, G. (2015). Solubility of niobium(V) and tantalum(V) under mild alkaline conditions. Hydrometallurgy, 156(June), 99–106. https://doi.org/10.1016/j.hydromet.2015.05.015.

Deblonde, G. J. P., Chagnes, A., Roux, M. A., Weigel, V., & Cote, G. (2016). Extraction of Nb(v) by quaternary ammonium-based solvents: toward organic hexaniobate systems. Dalton Transactions, 45(48), 19351–19360. https://doi.org/10.1039/C6DT03873E.

Dolganova, I., Rödl, A., Bach, V., Kaltschmitt, M., & Finkbeiner, M. (2020). A review of life cycle assessment studies of electric vehicles with a focus on resource use. Resources, 9(3), 4–8. https://doi.org/10.3390/resources9030032.

European Comission (2023). Study on the Critical Raw Materials for the EU 2023 – Final Report.

Filella, M., & May, P. M. (2020). The aqueous solution thermodynamics of niobium under conditions of environmental and biological interest. Applied Geochemistry, 122, 104729. https://doi.org/10.1016/j.apgeochem.2020.104729.

Kanie, K., Numamoto, Y., Tsukamoto, S., Takahashi, H., Mizutani, H., Terabe, A., Nakaya, M., Tani, J., & Muramatsu, A. (2011). Hydrothermal synthesis of sodium and potassium niobates fine particles and their application to lead-free piezoelectric material. Materials Transactions, 52(11), 2119–2125. https://doi.org/10.2320/matertrans.M2011148.

Labinger, J. A. (1982). Niobium and Tantalum. In Niobium and tantalum (pp. 705–782).

Lü, X., Mou, X., Wu, J., Zhang, D., Zhang, L., Huang, F., Xu, F., & Huang, S. (2010). Improved-Performance Dye-Sensitized solar cells using Nb-Doped TiO2 electrodes: Efficient electron Injection and transfer. Advanced Functional Materials, 20(3), 509–515. https://doi.org/10.1002/adfm.200901292.

Lübke, M., Sumboja, A., Johnson, I. D., Brett, D. J. L., Shearing, P. R., Liu, Z., & Darr, J. A. (2016). High power nano-Nb2O5 negative electrodes for lithium-ion batteries. Electrochimica Acta, 192, 363–369. https://doi.org/10.1016/j.electacta.2016.01.226.

Nikolay, T., Larina, L., Shevaleevskiy, O., & Ahn, B. T. (2011). Electronic structure study of lightly Nb-doped TiO2 electrode for dye-sensitized solar cells. Energy and Environmental Science, 4(4), 1480–1486. https://doi.org/10.1039/c0ee00678e.

Heisterkamp, F., & Carneiro, T. (2001). Niobium: Future possibilities - Technology and the market place. Niobium, Science and Technology, 1, 1109–1159.

Park, G., Gunawardhana, N., Lee, C., Lee, S. M., Lee, Y. S., & Yoshio, M. (2013). Development of a novel and safer energy storage system using a graphite cathode and Nb2O5 anode. Journal of Power Sources, 236, 145–150. https://doi.org/10.1016/j.jpowsour.2012.10.102.

Peiffert, C., Nguyen-Trung, C., Palmer, D. A., Laval, J. P., & Giffaut, E. (2010). Solubility of B-Nb2O5 and the hydrolysis of niobium(V) in aqueous solution as a function of temperature and ionic strength. Journal of Solution Chemistry, 39(2), 197–218. https://doi.org/10.1007/s10953-010-9495-z.

Sasidharan, M., Gunawardhana, N., Yoshio, M., & Nakashima, K. (2012). Nb2O5 hollow nanospheres as anode material for enhanced performance in lithium ion batteries. Materials Research Bulletin, 47(9), 2161–2164. https://doi.org/10.1016/j.materresbull.2012.06.004.

Tesfaye, F., Lindberg, D., Hamuyuni, J., Taskinen, P., & Hupa, L. (2017). Improving urban mining practices for optimal recovery of resources from e-waste. Minerals Engineering, 111(April), 209–221. https://doi.org/10.1016/j.mineng.2017.06.018.

Von Rennenberg, T. 2021. Towards a circular economy of critical raw materials: The case of niobium.

Vasconcelos, Y. O Polêmico Nióbio. Revista Fapesp, p. 64–69, mar. 2019.

Zeng, X., Mathews, J. A., & Li, J. (2018). Urban Mining of E-Waste is Becoming More Cost-Effective Than Virgin Mining. Environmental Science and Technology, 52(8), 4835–4841. https://doi.org/10.1021/acs.est.7b04909.

CHAPTER 2 – OBJECTIVES

2.1 General Objectives

The overall aim of this thesis is to design a crystallization- and precipitation-based process for the recovery of niobium-based compounds from potassium alkaline liquor containing Nb and Fe. This includes the determination of solubilities of potassium niobate and niobic acid in aqueous systems, in the presence and absence of electrolytes, and in diverse temperatures, to develop a process that allows circular economy for both primary and secondary materials and the obtaining solids with adequate properties for new applications.

2.2 Specific Objectives

- Thermodynamic and experimental study of the dissolution kinetics and solubility of niobium compounds in pure aqueous systems and in the presence of electrolytes under specific conditions of pH and temperature;
- Development of the crystallization of potassium niobate from liquor of Fe-Nb alloy fines produced via leaching with KOH solution;
- Investigating the process parameters for the crystallization of potassium niobate;
- Investigate the use of potassium niobate as a precursor for the precipitation of niobic acid;
- Evaluate process conditions for obtaining niobium oxide by calcination from the niobic acid;
- Extensive characterization of all solids produced in this study.

CHAPTER 3 – CRYSTALLIZATION-BASED RECOVERY OF NIOBIUM COMPOUNDS FROM ALKALINE LEACHING OF FE-NB ALLOY FINES

3.1 Introduction

The growth of the niobium industry has sparked interest in exploring its potential applications. Niobium is a refractory metallic solid of low density (8.57 g/cm^3), high thermal and electrical conductivity (Dolganova et al., 2020). It is soft, ductile and presents very high melting and boiling points of 2468 ºC and 4744 °C, respectively (Hagelüken, 2014; Nico et al., 2016). Vast literature can be found related to metallic alloys, ceramic capacitors, material for medical implants with excellent biocompatibility, optical films and lenses, semiconductor and microelectronic components, and chemical products catalysis (Alves and Dos Reis Coutinho, 2015; Bruziquesi et al., 2019; Heisterkamp and Carneiro, 2001; Peiffert et al., 2010). Moreover, niobium has received special attention for recent applications in electric batteries and solar panels (Baktash et al., 2020; Dolganova et al., 2020; Lü et al., 2010; Lübke et al., 2016; Nikolay et al., 2011; Park et al., 2013; Patat et al., 2022; Sasidharan et al., 2012; Yi et al., 2021).

The increase in niobium production is directly linked to the expanded use of Fe-Nb alloy in the construction of high-pressure pipelines, offshore oil drilling platforms, and as major components in the automotive industry. Niobium has been widely applied as a component of various metallic alloys with a great impact on alloys refining, as it improves corrosion resistance and reduces the weight of vehicles, decreasing the fuel consumption and increasing their efficiency (Alves and Dos Reis Coutinho, 2015; Bakry et al., 2023; Labinger, 1982; Mackay and Simandl, 2014). Meanwhile, superalloys account for approximately 8% of niobium use (Von Rennenberg, 2021), with widespread use in the aircraft and automotive industries.

Brazil is the highest niobium world producer, followed by Canada, Australia and Angola (Gasik et al., 2020; USGS, 2017). In 2019, Brazil was responsible for 88% of niobium world production and about 90% of niobium is commercialized as Fe-Nb alloy (ANM, 2020; Bakry et al., 2023). In general, beneficiation for both columbite-tantalite or pyrochlore ores starts with the enrichment of the Nb_2O_5 grade by physical and chemical

methods, including magnetic separation, flotation and impurities leaching. The concentration process is followed by an aluminothermic reduction to produce the main product, the Fe-Nb alloy and/or to a hydrometallurgical process to produce the high a purity niobic oxide, Nb_2O_5.

The Fe-Nb alloy production involves the griding of the Fe-Nb alloy followed by particle size separation to get the product with the required commercial size specification. The grinded alloy out of granulometric specification (fines) is either recycled to the pyrometallurgical step, which makes the process more expensive due to the high energy consumption or stored as a lower added-value material for optional subsequent processing.

Niobium and its compounds are very stable and almost insoluble in inorganic acid. Unlike many metals, niobium is resistant to most organic and mineral acids, except hydrofluoric acid, at all concentrations below 100 ºC, (Gupta & Suri, 1994; Wang et al., 2009). Due to environmental and health concerns related to the high toxicity of fluorine-based techniques, and the comparatively high solubility of niobium in alkaline media, hydrometallurgical processes using KOH or NaOH are gaining space in the processing of niobium ores (De Cock et al., 2017; Deblonde et al., 2015, 2016, 2019; Wang et al., 2009, 2018; Zhou et al., 2005a, 2005b). In alkaline solutions, niobium undergoes hydrolysis and, according to Schweitzer (2003), the affinity with Na or K-based solutions can be related to its embrittlement in presence of potassium and sodium salts.

Zhou and co-workers (2005a) studied the dissolution of Nb_2O_5 in highly concentrated KOH solution and showed that the formation of a soluble phase of potassium niobate is favoured at high KOH concentrations (84 wt.%). Same authors (2005b) evaluated the decomposition of a low-grade niobium-tantalum-ore by concentrated KOH solution in an alkali-to-ore mass ratios of 10:1, 7:1 and 3:1. The conversion rate of Nb increases slowly rising the alkali-to-ore ratio in the beginning of reaction and conversion of less than 10% was obtained at the lowest ratio.

Wang and co-workers (2009) studied the niobium alkaline leaching of a low-grade refractory ore. They adjusted the Nb/Ta ratio with Nb_2O_5 to get good extraction. The KOH: ore mass ratio was reduced from 7:1 to 2:1 to cut the need for concentrating the initial solution and hence reducing the energy consumption. In another study (2018), they

investigated the leaching kinetics of niobium-bearing mineralization (Nb_2O_5 ~14 wt.%) in a hydrothermal system using KOH (alkali-to-solid mass ratio 4:1) and reported the obtaining of a potassium niobate phase.

In this chapter, we propose a new destination for Fe-Nb alloy fines to achieve an efficient resource utilization, considering that the process can be used for the recovery of niobium from other secondary sources, such as spent batteries and alloys thus promoting the circular economy. Moreover, the crystallization of potassium niobate from an aqueous solution under mild conditions of temperature and atmospheric pressure, distinct from the majority studies in literature which report complex hydrothermal methods (Bai et al., 2011; Cao et al., 2012; Hayashi, H., Hakuta, Y., & Kurata, 2004; Yang et al., 2023).

Figure 1 shows the process diagram for obtaining new niobium compounds from Fe-Nb alloy fines at relatively low temperatures and atmospheric pressure (except for the calcination step). After Nb leaching from the fines with KOH, potassium niobate was crystallized from the leachate. Subsequently, potassium niobate was dissolved in distilled water and used in the precipitation of niobic acid (hydrated niobium oxide). Finally, the calcination of niobic acid produced the niobium oxide.

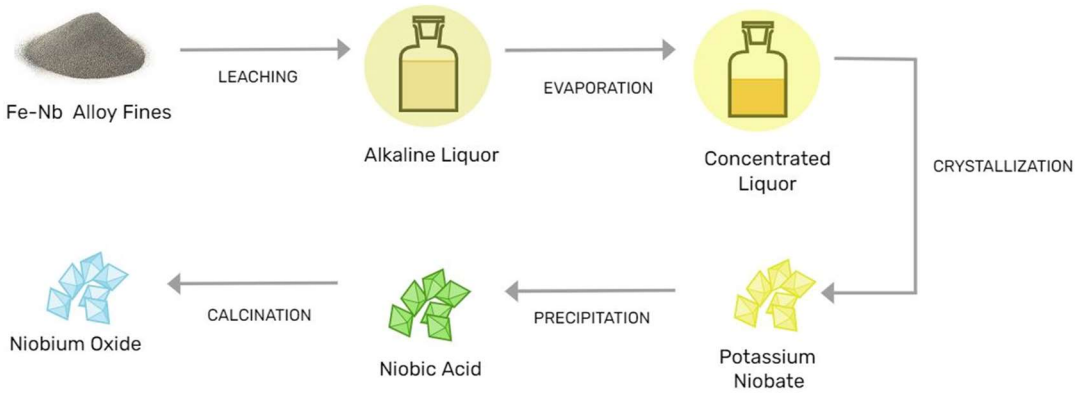

Figure 3.1. Schematic overview of process for niobium recovery from Fe-Nb alloy fines.

3.2 Materials and methods

3.2.1 Materials

The Fe-Nb alloy fines were prepared by quartering and submitted to dry granulometric analysis using vibrating sieves with openings of 600, 300, 212, 106, 75 and 53 µm for 20 minutes at 7 rpm (ENGETOTUS LTDA 701640). Particles with size < 106 µm were selected to be used in the subsequent leaching.

All solutions were prepared with distilled water. Analytical grade $KOH_{(s)}$ (85%, CAS: 1310-58-3 - Êxodo Científica) and H_2SO_4 (98%, CAS: 7664-93-9 - Êxodo Científica) were used without further purification.

3.2.2 Leaching of Fe-Nb alloy fines

Alkaline leaching was conducted in two steps. First, the activation of solids was done where a mixture of (i) 75 g of Fe-Nb alloy fines, 125 g of KOH and 50 mL of distilled water were added to a jacketed reactor, and kept for 1 hour without stirring; then (ii) 500 mL of distilled water was added to the 1 L reactor and the suspension was stirred at 300 rpm for 2 hours under atmospheric pressure and maintained at 96 ºC. A condenser attached to the reactor allowed to recycle the water to the reactor minimizing the losses. The liquor was filtered using a membrane filter (0.45 µm).

The extent of leaching (X) was calculated using Equation 3.1.

$$(\mathrm{X})\% = \left(1 - \frac{M_R}{M_o}\right) x\ 100 \tag{3.1}$$

M_R and M_0 are the calculated mass of the element in the residue from the leaching step and in the Fe-Nb alloy fines, respectively.

3.2.3 Crystallization

The liquor was concentrated by evaporation at around 100 ºC, until 40% reduction of the initial volume was obtained. Potassium niobate was then crystallized by cooling the liquor in a 1.5 L reactor. The temperature inside the crystallizer was controlled by circulating

water from a thermostatic bath (BROOKFIELD TC-502) into the jacket of the vessel. The liquor was stirred at 300 rpm during cooling at 2 ºC/min from 100 to 30 °C and remained under stirring for an additional 1 hour at 30 °C. The solids obtained were vacuum filtered on a quantitative strip filter paper (0.45 μm) and dried at 80 ºC for 12 hours prior to analysis.

3.2.4 Precipitation

Niobic acid was precipitated by adding H_2SO_4 to a potassium niobate solution. The initial solution was prepared dissolving 30 g of the previously crystallized potassium niobate into 300 mL of distilled water for 30 minutes at 90 ± 0.5 ºC. At the end of dissolution, the pH of solution was about 11.6. A solution of 0.5 mol/L H_2SO_4 was used as precipitant agent, that was added at a rate of 2.0 ± 0.5 mL/min to the potassium niobate solution until pH 3 was attained and then maintained constant. During the precipitation of niobic acid, the temperature of the system was kept at 90 ± 1.2 ºC and under stirring at 300 rpm. The solids obtained were vacuum filtered on a strip filter paper and dried at 80 ºC for 12 hours prior to analysis.

3.2.5 Calcination

The dehydration of niobic acid ($Nb_2O_5.nH_2O$ - hydrated niobium oxide) into niobium oxide (Nb_2O_5) was carried out in a furnace (NOVUS-N1040) at 900 ºC for 5 hours using a platinum crucible.

3.2.6 Chemical analysis and characterization

The chemical composition of the aqueous solutions was determined by ICP-OES (Perkin Elmer, model Optima 7300DV). The detection limits were < 0.005 mol/L and Lutecium (1 mg/kg) was used as an internal standard to evaluate the instrument performance and precision of analysis. The crystalline phases in solids were identified using a PHILIPS X-ray Diffractometer (PANalytical - controller PW3710/31, generator PW1830/10 and detector PW3020/00), with a Cu (Kα) radiation and a scanning rate of 0.06 °/s in the 2 θ. The chemical composition of the solids was obtained by X-Ray Fluorescence (XRF) in

spectrometer with wavelength dispersion (WDXRF-ARL PERFORM'X, Thermo Scientific GEN-X 4200W) and Rd tube.

Structural characteristics were analysed with Fourier Transform Infrared with an attenuated total reflectance (FTIR-ATR) spectroscopy (Bruker Alpha spectrometer) at a resolution of 4 cm^{-1} and 128 scans from 4000 to 350 cm^{-1}. The collected spectra were normalized using the band at 1625 cm^{-1} as reference. Additionally, RAMAN spectroscopy (Horiba Jobin Yvon - LabRamHR800) was used to identify the structure and phases of the solids with a helium-neon laser (λ = 632.8 nm) and a microscope (Olympus BX-41, 100x). The crystallized and precipitated solids were also imaged using optical microscopy (NOVEL- BM2100POL) and Scanning Electron Microscopy (SEM) (FEI Quanta 3D FEG).

3.3 Results and discussions

3.3.1 Samples preparation and leaching

Figure 3.2 shows the temperature profile during the leaching of Fe-Nb alloy particles (< 106 μm) with KOH solution. The leaching involves the oxidation of Nb and the H reduction, thus causing the H_2 evolution (Equation 3.2). After 60 minutes of reaction the temperature was stabilized and maintained at 96 ºC.

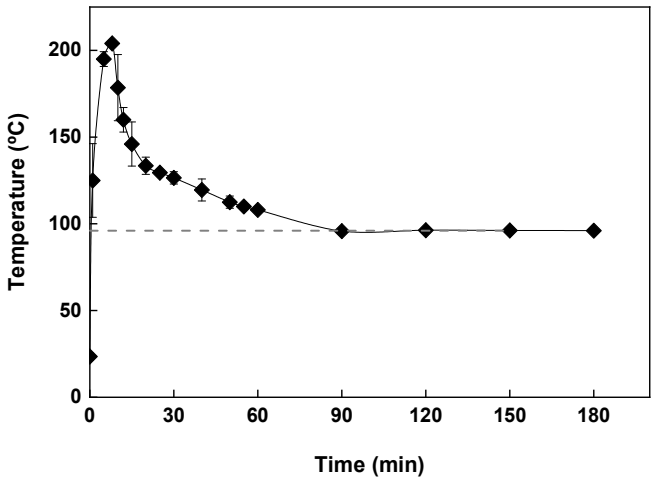

$$2Nb + 2KOH + 2H2O \rightarrow 2\,KNbO_{3\,(aq)} + 3H_{2\,(g)} \quad (3.2)$$

Figure 3.2. Temperature profile during alkaline leaching of the alloy fines (dashed line: fixed temperature at 96 ºC).

Table 3.1 shows the chemical composition of feed and the residue after leaching. The extraction of niobium was approximately 77% w/w. According to Wang et al. (2009), lower KOH concentrations in the leaching could positively influence niobium extraction and improve leaching efficiency as it would reduce the viscosity of the liquor as well as the resistance to mass transfer at the solid-liquid interface. The liquor obtained contained 0.65 mol Nb/kg_{liquor} and 2.7 mol K/kg_{liquor} However, leaching optimization was not the primary objective of this study, but to obtain a niobium-rich alkaline liquor for further crystallization of potassium niobate.

Table 3.1. Chemical composition of Fe-Nb alloy fines and residue from the alkaline leaching.

Grade (%)*	Nb	Fe	K	Al	Mn	Si	Ti	Ta	P
Fe-Nb alloy fines	47.67	22.52	<0.01	0.66	0.11	2.01	0.23	0.1	0.11
Residue	11.10	21.00	11.58	0.20	0.10	1.50	0.19	0.02	0.06

* The content of each element was calculated considering the initial mass of Fe-Nb alloy fines and the residual mass after the alkaline leaching.

Figure 3.3 shows the XRD of the Fe-Nb alloy fines and the residue. As expected, for Fe-Nb alloy peaks related to both iron and niobium metallic are present. In addition to Fe and SiO_2, the leached mass shows peaks that may be related to potassium niobium oxide silicate and potassium iron niobium oxide phases. The identification of these phases indicates the reaction between KOH and the alloy fines.

The high alkaline concentration may result in the oxidation of silicon and favour the formation of silicate molecules ($Si(OH)_x$) (Čekerevac et al., 2012) which reacts with potassium and niobium and forms the oxidized phase. As showed by Zhou et al. (2015), iron can be slightly dissolved during the alkaline leaching but as result of oxidation it can also react in the medium and form stable phases.

According to Masoud (2005), the potassium niobium silicate phase $K_6Nb_6Si_4O_{26}$ is labelled as the stable high-temperature phase that results from the chemical reaction of $KNbO_3$ with the silica rich grain boundary. Feizpour et al. (2014) also found this phase in the solids after a low-temperature calcined powder reaction. This may indicate that the

insoluble potassium niobate phase may be formed during leaching when temperature rises to 200ºC through reaction with silicate and iron.

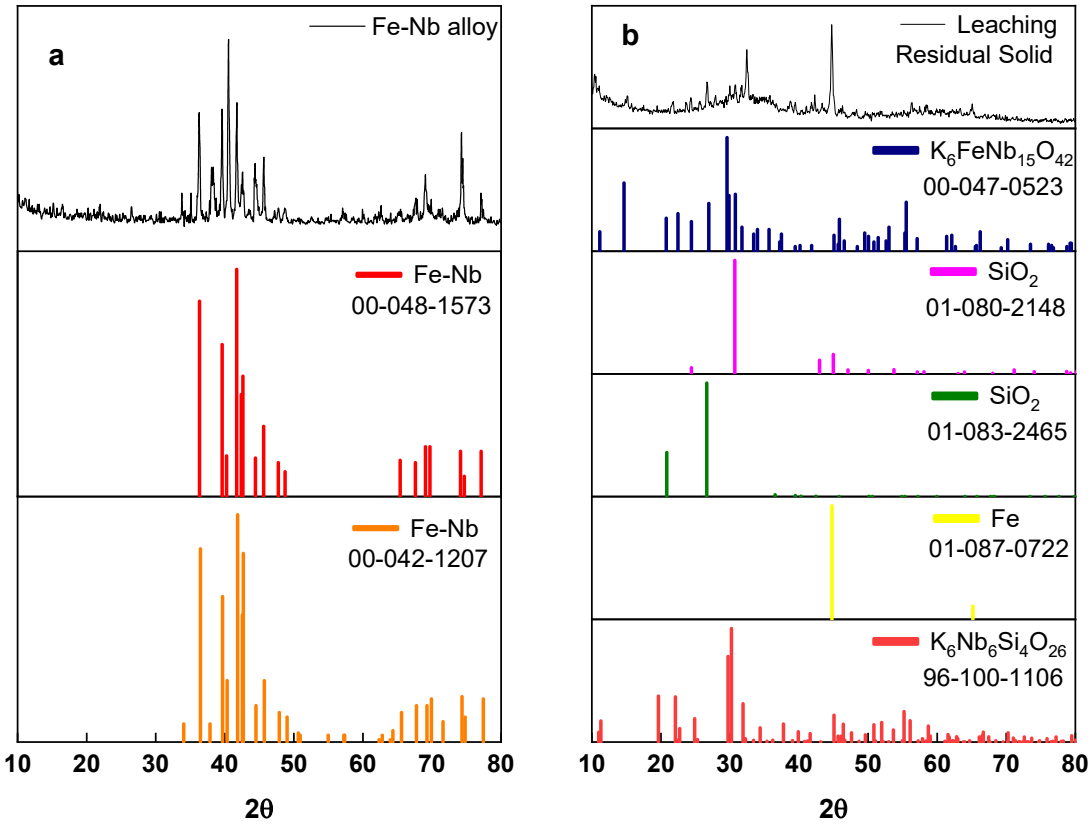

Figure 3.3. Diffractogram of (a) Fe-Nb alloy fines and (b) leaching residual solid.

3.3.2 Crystallization of Potassium Niobate

A niobium-rich alkaline liquor was successfully produced (88% of extraction) for further crystallization at a relatively middle condition. It was not the objective of this work a detailed study of the leaching step, and just obtain a solution rich in niobium with certain amount of contamination by iron. Higher levels of extraction can be obtained by increasing temperature or pressure. The initial composition of the alkaline liquor obtained from fines alloy Fe-Nb leaching (32.78 g/L) and the variation of Nb, Fe and K concentrations are shown in Table 3.2. According to the theoretical calculations based on Nb concentration, the crystallization yield was 89 %. The extent of crystallization based on the variation of experimental niobium concentration in the evaporation and post-

crystallization step is approximately 80 %. It is noteworthy that the theoretical concentration in cooling crystallization of Nb and K was considered here as the solubility of $KNbO_3$ at 30 ºC as obtained from thermodynamic simulations (OLI Studio Stream Analyzer). However, solubility studies are necessary, since multiple potassium niobates phases that can be formed.

Table 3.2. Variation of chemical composition of the liquors after the steps of leaching, concentration and colling.

Liquor	**Nb (mol/kg$_{liquor}$)**		**K (mol/kg$_{liquor}$)**		**Fe (mol/kg$_{liquor}$)**		**Density (g/cm^3)**
Steps	Theoretical*	Real[a]*	Theoretical	Real[a]	Theoretical	Real[a]	
Leaching	0.74[b]	0.65	3.6	2.7	0.58[b]	0.001	1.23
Evaporation	1.04	1.05	5.0	4.1	0	0.003	1.38
Cooling crystallization	0.095[c]	0.22	0.095[c]	3.9	0	0.002	1.16

[a] Real concentration of the liquors: Detection limit by ICP-OES <0.005mol/L.
[b] Considering that all Nb and Fe were recovered from Fe-Nb alloy fines.
[c] Based on the solubility of $KNbO_3$ in 5 mol/L KOH at 30 ºC obtained from OLI Studio.
* Theoretical: mass balance data; Real: experimental data.

Two potassium niobate phases were identified in the crystallized solids (Figure 3.4): the dominant and metastable phase $K_4Nb_6O_{17}$ and the stable phase $KNbO_3$. The unknown peaks may be related to the soluble intermediate hexaniobate phase $K_8Nb_6O_{19}.nH_2O$ (Bai et al., 2017a, 2011; Kanie et al., 2011). This may indicate that the $KNbO_3$ formation may involve the intermediate $K_4Nb_6O_{17}$ or hydrated phases in the first stage.

Mixtures of potassium niobate phases ($K_4Nb_6O_{17}$ and $KNbO_3$) were reportedly formed by hydrothermal crystallization under different temperatures and initial concentrations of niobium and potassium hydroxide. Hayashi et al. (2004) observed that the $K_4Nb_6O_{17}$ was preferably formed under medium KOH concentration (0.5 mol/L) and Kudo et al., (2004) noticed that $K_4Nb_6O_{17}$ was firstly formed thus enabling the formation of the stable phase $KNbO_3$. Temperature of the system is crucial to determine which phase will be formed. The distinct phase, $K_8Nb_6O_{19}$, was obtained by Wang et al. (2009) from an alkaline liquor containing higher KOH concentration, 6.8 mol/L. According to studies, highest concentration of KOH is favourable to formation of $K_8Nb_6O_{19}$ phase (Bai et al., 2017b; Kaseda et al., 2011; Kong et al., 2013). According to Zhou et al. (2005) (H. Zhou et al., 2005), the increase in the KOH concentration increases the activity of OH^- and likely

hinders the formation of the most stable phase of potassium niobate ($KNbO_3$). As the initial concentration of KOH used in this work (4.1 mol/L) was quite lower than that used by Wang et al. (2009) (Wang et al., 2009), lower concentration of KOH may favour the formation of $K_4Nb_6O_{17}$ or its mixture with the $KNbO_3$ phase, coherent with the results observed.

Amini et al. (2009) (Amini and Mirzaee, 2009) produced a potassium niobate with similar profile and attributed to a metastable phase of $KNbO_3$. The formation of a hexaniobate phase could be expected, since complex soluble hexaniobate phases can be formed during the reaction of Nb and KOH (Bai et al., 2017; Kong et al., 2013).

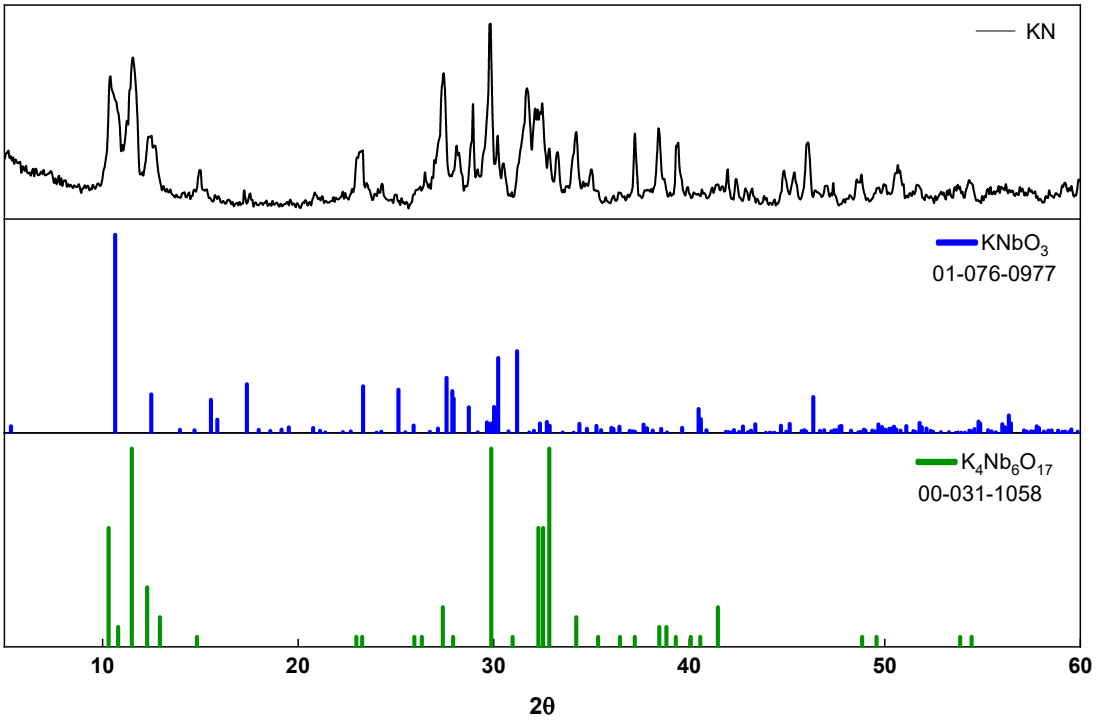

Figure 3.4. Diffractogram of the crystallized potassium niobate at 30.0±0.8 ºC and 300 rpm.

Figure 3.5 (a) shows the FT-IR spectra obtained for potassium niobate sample. The bands observed around 3500 to 2500 cm^{-1} are attributed to OH group and to water in the structure of the solid. The bands in the range of 1000 and 2000 cm^{-1} are related to adsorbed water molecules or regions with H-bonds of water (Feizpour et al., 2014), and they indicate hydrated Lindqvist ions. Its structure is related to hexaniobate salts $H_xNb_6O_{19}^{(x-}$

[8)] which are dominant species for Nb(V) in aqueous medium with pH ≥ 8 (Deblonde et al., 2016b, 2015b, 2015c; Nyman, 2011; Nyman et al., 2006) and are also precursors for several polyoxoniobates, including $Nb_7O_{22}^{9-}$, $Nb_{10}O_{28}^{6-}$, $Nb_{20}O_{54}^{8-,}$ and $Nb_{24}O_{72}H_9^{15-}$ (Petrus et al., 2022; Ye et al., 2013).

The bands at wavenumbers smaller than 1000 cm^{-1} are characteristic of niobates and are related to Nb-O octahedral vibrations which indicate the formation of perovskite structure (K-Nb-O) (De Andrade et al., 2000; Feizpour et al., 2014; Wang et al., 2009). The shoulders in this region may be attributed to the presence of the more crystalline perovskite structure (Leal Marchena et al., 2016). Similar spectra to potassium niobate are reported in literature (De Andrade et al., 2000; Piskin et al., 2021; Santos et al., 2002; Wang et al., 2007).

In the Raman spectra (Figure 3.5 (b)) bands associated to $K_4Nb_6O_{17}$ and $KNbO_3$ phases were identified. The band at 200-300 cm^{-1} may be related to hydrated $K_4Nb_6O_{17}$ (De Andrade et al., 2000; Mączka et al., 2011). The band at 530 cm^{-1} is characteristic of potassium niobate phases and belong to the NbO_6 oxygen octahedral vibration (Hajdara et al., 2012; Mączka et al., 2011). Stretching vibrations and short Nb-O bonds can be observed at 800-1100 cm^{-1} (Mączka et al., 2011). Galutskiy et al., (2020) (Galutskiy et al., 2020), related the band around 800 cm^{-1} with a high proportion of ideal structure of a single crystal growth in orthorhombic phase of potassium niobate.

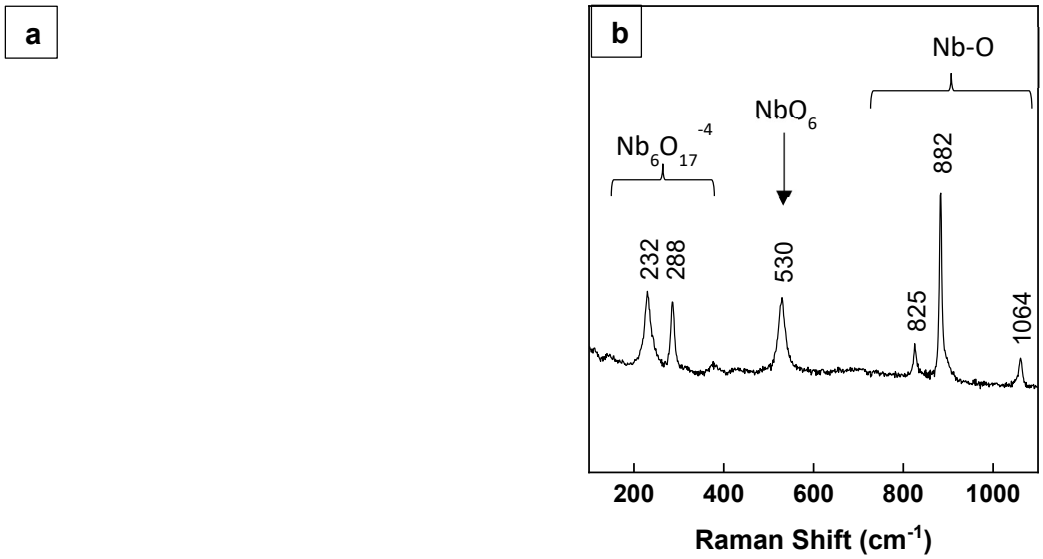

Figure 3.5. (a) FTIR and (b) Raman spectra of potassium niobate solid crystallized at 30.0 ± 0.8 ºC for 1 hour and 300 rpm.

Mostly isolated single crystals of potassium niobate exhibiting a rectangular shape with long-side lengths are shown in Figure 3.6 (a). The low temperature of crystallization when compared to hydrothermal synthesis allowed fewer defective particles to be formed, with more homogeneous structures. This observation is in agreement with the study of Bai et al. (2017) (Bai et al., 2017b) that investigated the crystallization of potassium niobate from Nb_2O_5- KOH solution, at relatively low temperatures, and in the presence of sodium dodecyl benzene sulfonate surfactant. According to these authors, a relatively lower temperature can provide the needed driving force for crystal growth. Reducing the temperature from 200 to 60ºC slowed the dissolution of Nb_2O_5 and this could have stabilized the precursor and prompted more heterogeneous nucleation. When the synthesis was performed at 200ºC, mainly fractured particles were obtained, probably due to fast dissolution of Nb_2O_5 in the alkaline solution. In addition, at the lower temperature of reaction, the particles exhibited improved hexagonal morphology. It is noteworthy from the SEM image (Figure 3.6 (b)) that the crystals surface is rough, which points out to high supersaturations. In cooling crystallization, the supersaturation was driven by a cooling rate of 2 °C/min. Hence, lower cooling rates would likely favour the formation of single crystals with smoother surfaces and possibly the most stable forms. The

chemical mapping (Figure 3.6 (c-f)) confirms the uniform composition of niobium, potassium and oxygen in the solids.

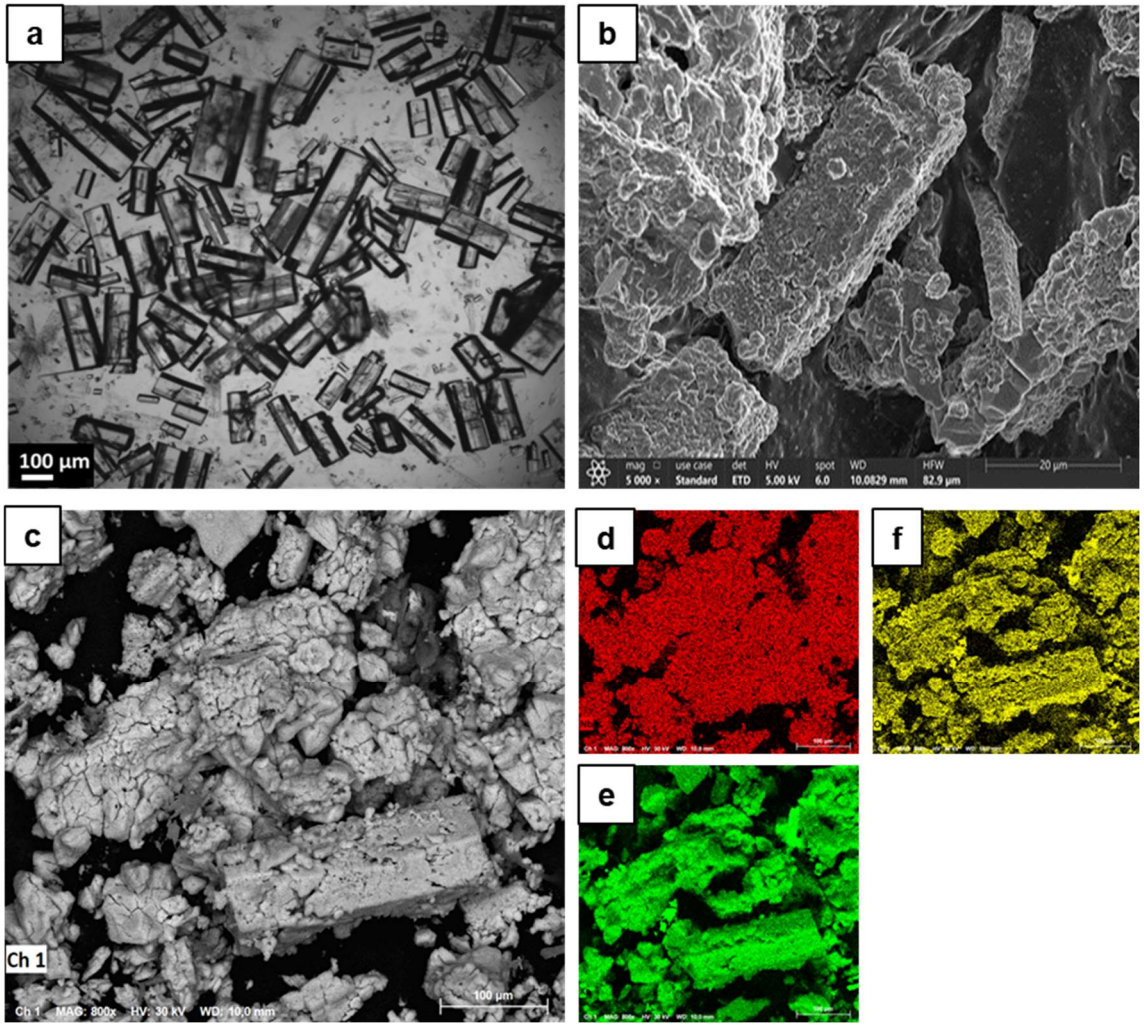

Figure 3.6. (a) Optical Microscopy, (b) and SEM image of potassium niobate crystallized at 30.0±0.8 ºC for 1 hour and 300 rpm. Chemical mapping: c) background, d) Nb, e) K, and f) O.

The control of potassium niobate crystals shape and morphology is dependent of the supersaturation in alkaline medium. This is related to the phases solubility, and according to literature, the particles size may decrease with increasing KOH concentration (Kanie et al., 2011; Kong et al., 2013). In general, the particle size decreases with higher initial concentration of KOH. This phenomenon is derived from homogeneous nucleation and

enhancement of the number of potassium niobate nuclei by the increasing KOH concentration.

3.3.3 Precipitation of Niobic Acid

Dissolution of crystallized potassium niobate supplied the solution to precipitate niobic acid. This was done at 90 °C to maximize the dissolution of the potassium niobate, which solubility increases with temperature, as proven by its prior crystallization via cooling. The yield of the process was 90 % from the expected, based on Nb concentration and the efficiency of precipitation was higher than 99%, revealing that all dissolved niobium was precipitated as niobic acid.

Figure 3.7 shows the diffractogram of precipitated niobic acid, with characteristics of amorphous structure, without virtually distinctive peaks due to low intensities and broad bumps, in accordance with the literature (Brandão et al., 2009; Chan et al., 2017; Chen et al., 2022; Guo and Qian, 1993; Lebarbier et al., 2012; Tanabe, 1987). Only two small diffraction peaks were observed, that could be derived from arcanite – potassium sulphate phase. This was supported by the chemical composition obtained by XRF (Table 3.3) that confirms the presence of potassium and residual sulphur in the solid. In order to provide a high-quality niobic acid and further niobium oxide, washing protocols with distilled water could be implemented for the solid yield, based on the higher solubility of K- and S-based solids (Eysseltová and Bouaziz, 2012) when compared to Nb-based compounds (highly insoluble) (Filella and May, 2020). This was not the objective of the present study.

According to Lebarbier et al. (2012), the crystallinity of niobic acid can be enhanced with heat treatment at temperatures higher than 300ºC. The complexity in the structure of amorphous niobic acid makes it difficult to further control the acidity by structure manipulation which may influence its catalytic properties (Fan et al., 2013).

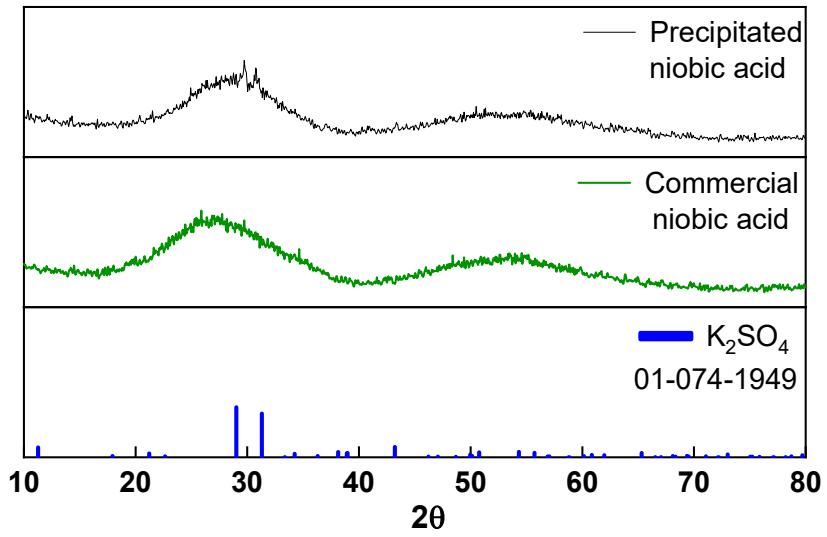

Figure 3.7. XRD pattern of precipitated niobic acid precipitated with 0.5 mol/L H_2SO_4 at 90±1.2 ºC and 300 rpm.

The SEM images (Figure 3.8) show that niobic acid was composed of aggregates of small particles. It was possible to identify regions with the presence of larger potassium sulphate particles (Figure 3.8 (a-b)), confirmed by the chemical mapping (Figure 3.8 (c-g)), with higher crystallinity, corroborating the XRD results. Deposits of niobic acid can be seen on top of the potassium sulphate particles. Figure 6c, shows amorphous deposits on top of a much larger crystal. The chemical mapping highlights that the amorphous phase is comprised of Nb and that the presence of K and S can be related to the large crystal where the small irregular material is deposited.

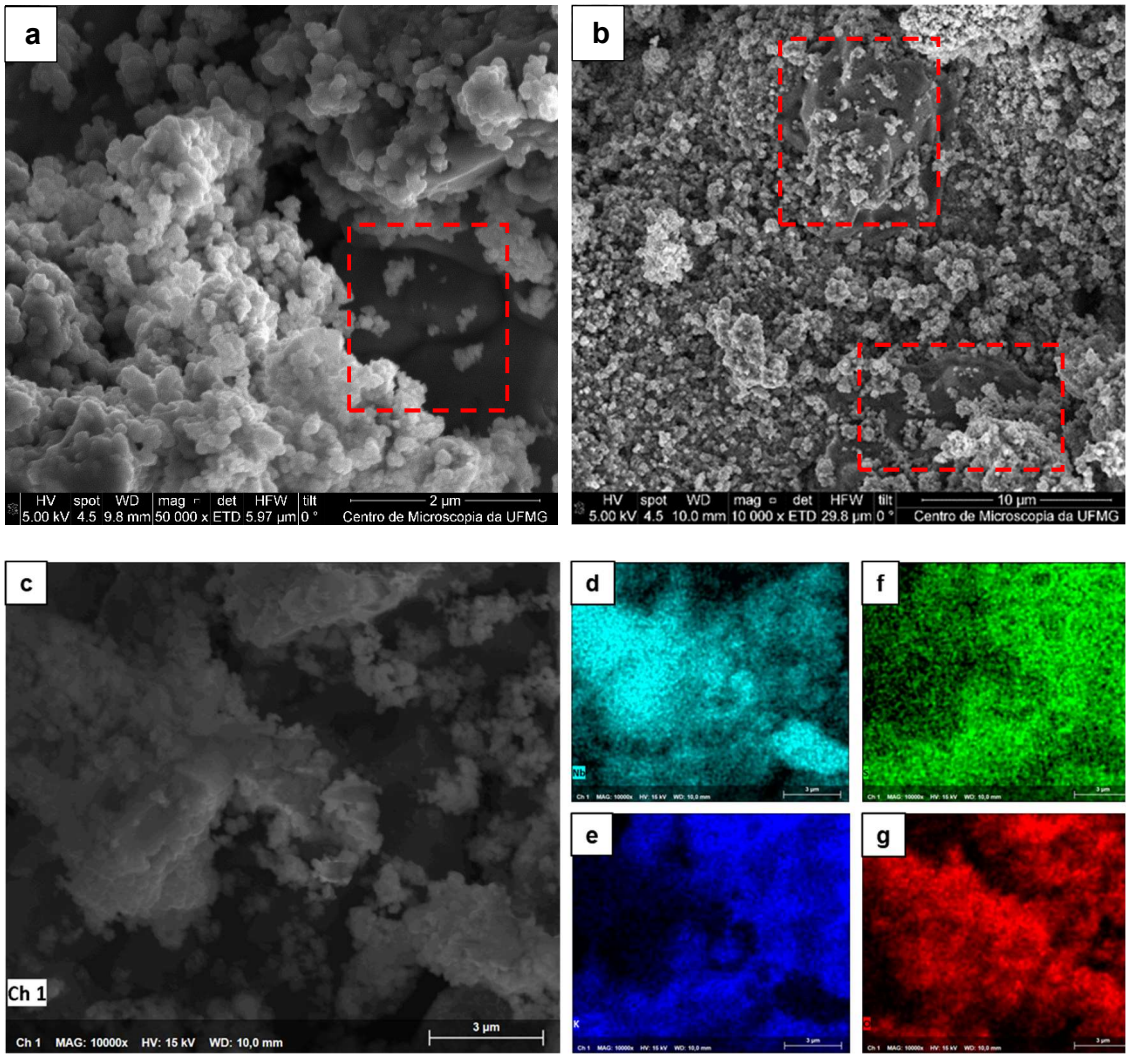

Figure 3.8. SEM images of precipitated niobic acid 0.5 mol/L H_2SO_4 at 90 ± 1.2 ºC and 300 rpm. Dashed line: region with sulphur and potassium. Chemical mapping: c) background, d) Nb, e) K, f) S and g) O.

The FTIR spectra of the niobic acid sample is presented in Figure 3.9 (a). The band observed around 3500 and 2500 cm^{-1} is related to the Nb-OH of adsorbed H_2O, implying the presence of water in the samples. The absorption peak around 800 and 1000 cm^{-1} can be assigned to the stretching vibrations of the oxygen bonds (O–O) (Uekawa et al., 2003) and to Nb=O, also associated to NbO_4 tetrahedra (Lewis acid sites), and Nb-O-Nb bonds typical of niobium solids (Hughes, 1964; Nakajima et al., 2011). These features, as well as the shoulder observed at ca. 500 cm^{-1} are characteristic of the hydrated niobium oxide. Weak bands around 750, 500, and 400 cm^{-1} can be associated to Nb-O bonds and HSO_4^-, respectively, in hydrated niobium oxide (Brandão et al., 2009; Prasetyoko et al., 2008).

Figure 3.9 (b) shows the Raman analysis, that was conducted across two different regions of the precipitated niobic acid. These regions are characterized by the presence and absence of potassium and sulphate in the niobic acid, as evidenced by SEM images (Figure 3.8). The spectrum obtained from the analysis of region 1 shows characteristic peaks of niobic acid without the presence of impurities (Brandão et al., 2009; Chan et al., 2017; Lebarbier et al., 2012). However, region 2 exhibits bands that are related to the presence of sulphate in the solids. According to Qiu et al. (2019) (Qiu et al., 2019), the bands at 400 to 1150 cm^{-1} are characteristic of potassium sulphate phase K_2SO_4.

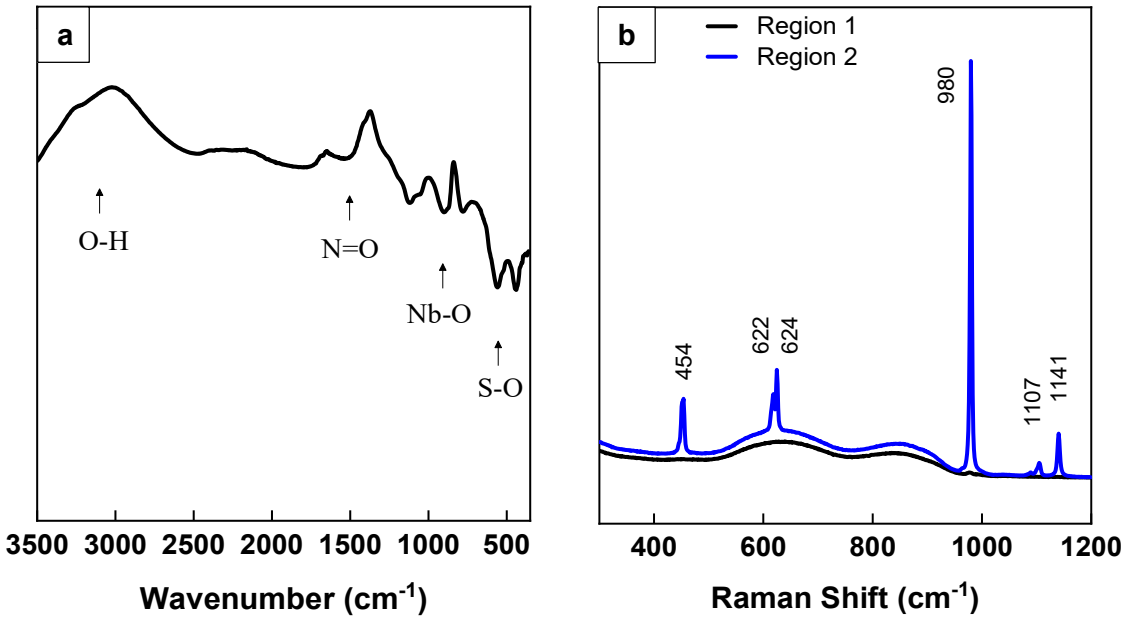

Figure 3.9. (a) FTIR and (b) RAMAN spectra precipitated niobic acid precipitated with 0.5 mol/L H_2SO_4 at 90±1.2 ºC and 300 rpm.

3.3.4 Calcination

The calcined niobic acid (900 ºC, 5 h) yielded a product containing a proportion of 87.5% of Nb_2O_5 and impurities such as potassium and sulphur (Table 3.3). Due to the presence of the impurities in the solids, the XRD analysis (Figure 10) after calcination shows a potassium niobate phase as the majority phase in addition to the niobium oxide phase. The unidentified peaks are likely related to another minor intermediate phase.

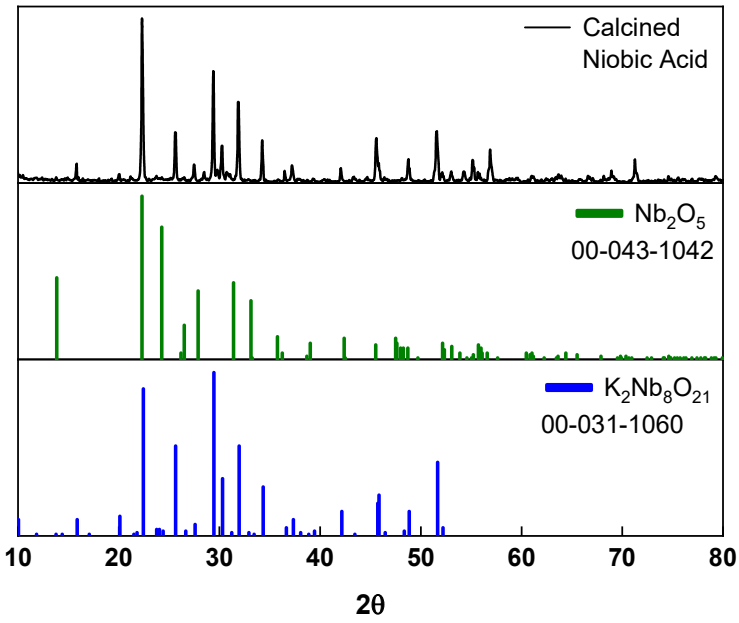

Figure 3.10. XRD of calcined precipitated niobic acid at 900ºC for 5 hours.

Figure 3.11 shows the SEM image of calcined niobic acid. The thermal treatment changed the morphology and crystalline structure of the solid from the aggregates of small amorphous particles to crystalline rod-like crystals. According to Guo et al (2020) (Guo et al., 2020), the $K_2Nb_8O_{21}$ particles with columnar structure can stuck to each other and form a cluster. This behaviour also was observed in the obtained solid, along with some dispersed particles. As the crystalline structure of Nb_2O_5 changes due to heat treatment, its columnar structure is also reported in other studies (Jun Park et al., 2021, Xiao et al., 2008).

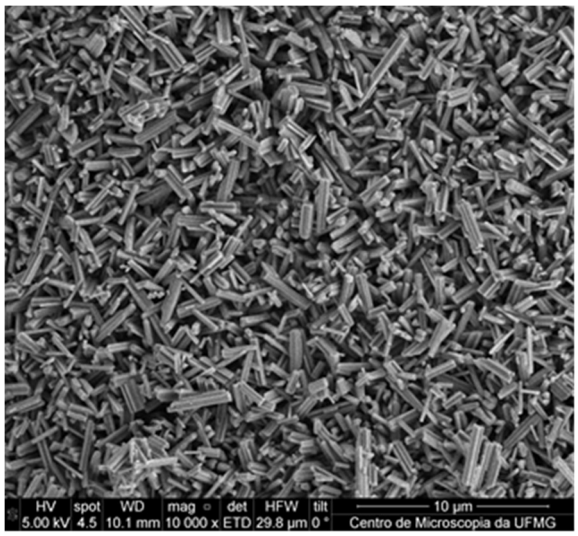

Figure 3.11. SEM image of calcined precipitated niobic acid at 900ºC for 5 hours.

The chemical composition of calcinated niobic acid (Table 3.3) also confirmed the presence of potassium as an impurity. Since no washing protocol of niobic acid was implemented after its precipitation, the solid contained 11.7% of K. During calcination, the sulphur was removed, and potassium remained in the solids leading to the formation of a potassium niobate phase, $K_2Nb_8O_{21}$ that was identified by the XRD. According to Cheng et al (2018) (Cheng et al., 2018), this phase exhibit a high structural stability and electrochemical reversibility with a potential material do be used for lithium storage. Additionally, it has dielectric properties and high level of photocatalytic activity (Chandel and Jindal, 2023). However, since the intention of this work was to obtain niobium oxide, this result reinforces the need to implement a washing procedure after the precipitation process of niobic acid to reduce the presence of contaminants in the solids and produce high-quality niobium oxide.

Table 3.3. Chemical composition of potassium niobate, niobic acid and niobium oxide by XRF analysis.

Content (%)	**Nb**	**K**	**S**	**O**	**Fe**	**Si**	**Al**	**Ta**	**P**	**Ca**
Potassium Niobate	42.3	24.7	0.04	23.3	<0.01	<0.01	<0.01	0.02	<0.01	<0.01
Niobic Acid	54.7	11.7	2.4	30.3	0.24	0.37	0.04	<0.01	<0.01	<0.01
Niobium Oxide	61.2	12.1	1.9	32.6	0.24	0.32	0.04	<0.01	<0.01	<0.01

Considering the metallic secondary source of niobium, the presence of impurities is critical factor in the recovery process. It is important to notice that the produced niobium compounds were not influenced by the presence of the main impurities from the starting material such as Fe, Si and Al. Yet, as the application of niobium compounds in industry is greatly dependent on purity level, the amount of impurity increases the level of difficult in recovery Nb, implementing a pretreatment step in the leachate, prior to the crystallization step, could help minimize further the presence of impurities in the final product. Moreover, applying a washing protocol on the solids could also act to enhancing purity.

Specific conditions for the crystallization of potassium niobate by cooling and the acid precipitation of niobic acid were investigated and are presented in the following chapters.

3.4 Conclusions

A new route was developed and validated for the recovery of niobium compounds from Fe-Nb alloy fines containing Al and Si as main impurities, at relatively low temperatures and atmospheric pressure.

A niobium-rich liquor was obtained through alkaline leaching of Fe-Nb alloy fines with KOH, which recovered approximately 88 % of the Nb. The crystallization of potassium niobate and the subsequent synthesis of niobic acid highlighted the efficiency of the method. Both $KNbO_3$ and $K_4Nb_6O_{17}$ phases (stable and metastable, respectively) were formed from the cooling crystallization. With a recovery of 66% of Nb from the initial liquor.

An amorphous niobic acid was obtained by precipitation with H_2SO_4, subsequently used as a precursor to produce niobium pentoxide via calcination. In addition to Nb_2O_5, a potassium niobate phase ($K_2Nb_8O_{21}$) was also seen in the calcined solid due to residual potassium present in the solid. The improvement of the purity of niobium oxide products can be achieved by implementing an impurity removal procedure – such as a washing protocol.

In addition, this study successfully demonstrated the feasibility of producing niobium compounds from Nb-alloys containing iron, silicon, and aluminium without significant contamination. This approach establishes a viable route for efficient niobium recovery from secondary sources and offers a promising opportunity for sustainable niobium production.

3.5 References

Alves, A.R., Dos Reis Coutinho, A., 2015. The evolution of the niobium production in Brazil. Mater. Res. 18, 106–112. https://doi.org/10.1590/1516-1439.276414

Amini, M.M., Mirzaee, M., 2009. Effect of solvent and temperature on the preparation

of potassium niobate by hydrothermal-assisted sol-gel processing. Ceram. Int. 35, 2367–2372. https://doi.org/10.1016/j.ceramint.2009.01.009

Antonio, M.R., Nyman, M., Anderson, T.M., 2009. Direct observation of contact ion-pair formation in aqueous solution. Angew. Chemie - Int. Ed. 48, 6136–6140. https://doi.org/10.1002/anie.200805323

Bai, S., Zhang, F., Karaki, T., Adachi, M., 2011. Effect of surfactants on morphology of niobate hydrate particles in hydrothermal synthesis. Jpn. J. Appl. Phys. 50, 1–5. https://doi.org/10.1143/JJAP.50.09ND12

Bai, S., Zhang, J., Chen, Z., Wang, Y., Hong, M., Karaki, T., 2017a. Near-room-temperature synthesis of niobate hydrate particles with hexagonal-platelike morphologies. Mater. Chem. Phys. 199, 230–238. https://doi.org/10.1016/j.matchemphys.2017.06.048

Bai, S., Zhang, J., Chen, Z., Wang, Y., Hong, M., Karaki, T., 2017b. Near-room-temperature synthesis of niobate hydrate particles with hexagonal-platelike morphologies. Mater. Chem. Phys. 199, 230–238. https://doi.org/10.1016/j.matchemphys.2017.06.048

Bakry, M., Li, J., Zeng, X., 2023. Evaluation of global niobium flow modeling and its market forecasting. Front. Energy 17, 286–293. https://doi.org/10.1007/s11708-022-0823-y

Baktash, A., Amiri, O., Saadat, M., 2020. High efficient perovskite solar cells base on niobium doped TiO2 as a buffer layer. J. Nanostructures 10, 119–127. https://doi.org/10.22052/JNS.2020.01.013

Brandão, R.F., Quirino, R.L., Mello, V.M., Tavares, A.P., Peres, A.C., Guinhos, F., Rubim, J.C., Suarez, P.A.Z., 2009. Synthesis, characterization and use of Nb2O5 based catalysts in producing biofuels by transesterification, esterification and pyrolysis. J. Braz. Chem. Soc. 20, 954–966. https://doi.org/10.1590/S0103-50532009000500022

Bruziquesi, C.G.O., Balena, J.G., Pereira, M.C., Silva, A.C., Oliveira, L.C.A., 2019. Niobium: A strategic chemical element for brazil. Quim. Nova 42, 1184–1188. https://doi.org/10.21577/0100-4042.20170442

C. K. Gupta & A. K. Suri, 1994. Extractive Metallurgy of Niobium. Taylor & Francis Group.

Cao, Y., Zhu, K., Qiu, J., Pang, X., Ji, H., 2012. Sol-gel processing and characterization of potassium niobate nano-powders by an EDTA/citrate complexing method. Solid State Sci. 14, 655–660. https://doi.org/10.1016/j.solidstatesciences.2012.03.011

Čekerevac, M., Simičić, M., Bujanović, L.N., Popović, N., 2012. The influence of silicate and sulphate anions on the anodic corrosion and the transpassivity of iron and silicon-rich steel in concentrated KOH solution. Corros. Sci. 64, 204–212. https://doi.org/10.1016/j.corsci.2012.07.019

Chan, X., Pu, T., Chen, X., James, A., Lee, J., Parise, J.B., Kim, D.H., Kim, T., 2017. Effect of niobium oxide phase on the furfuryl alcohol dehydration. Catal. Commun. 97, 65–69. https://doi.org/10.1016/j.catcom.2017.04.019

Chandel, R., Jindal, S., 2023. Fabrication technique of smart ferroelectric materials and its applications. AIP Conf. Proc. 2735. https://doi.org/10.1063/5.0140223

Chen, Y., Wang, Z., Liu, S., Zhang, G., 2022. Modified niobic acid via acidification by various liquid acids for dehydration of succinic acid to succinic anhydride. Colloids Surfaces A Physicochem. Eng. Asp. 650, 129644. https://doi.org/10.1016/j.colsurfa.2022.129644

Cheng, X., Zhu, H., Yu, H., Ye, W., Zheng, R., Liu, T., Peng, N., Shui, M., Shu, J., 2018. K2Nb8O21 nanotubes with superior electrochemical performance for ultrastable lithium storage. J. Mater. Chem. A 6, 8620–8632. https://doi.org/10.1039/c8ta01411f

De Andrade, J.S., Pinheiro, A.G., Vasconcelos, I.F., De Araújo, M.A.B., Valente, M.A., Sombra, A.S.B., 2000. Structural studies of KNbO3 in niobate glass-ceramics. J. Phys. Chem. Solids 61, 899–906. https://doi.org/10.1016/S0022-3697(99)00387-X

De Cock, B., Delaunay, N., Deblonde, G., Bosi, V., Pasti, L., Mangelings, D., Vander Heyden, Y., 2017. Kinetic study of niobium and tantalum hexameric forms and their substituted ions by capillary electrophoresis in alkaline medium. Talanta 175, 127–134. https://doi.org/10.1016/j.talanta.2017.07.025

Deblonde, G.J.P., Bengio, D., Beltrami, D., Bélair, S., Cote, G., Chagnes, A., 2019. A

fluoride-free liquid-liquid extraction process for the recovery and separation of niobium and tantalum from alkaline leach solutions. Sep. Purif. Technol. 215, 634–643. https://doi.org/10.1016/j.seppur.2019.01.052

Deblonde, G.J.P., Chagnes, A., Bélair, S., Cote, G., 2015a. Solubility of niobium(V) and tantalum(V) under mild alkaline conditions. Hydrometallurgy 156, 99–106. https://doi.org/10.1016/j.hydromet.2015.05.015

Deblonde, G.J.P., Chagnes, A., Roux, M.A., Weigel, V., Cote, G., 2016a. Extraction of Nb(v) by quaternary ammonium-based solvents: toward organic hexaniobate systems. Dalt. Trans. 45, 19351–19360. https://doi.org/10.1039/C6DT03873E

Deblonde, G.J.P., Chagnes, A., Weigel, V., Cote, G., 2016b. Direct precipitation of niobium and tantalum from alkaline solutions using calcium-bearing reagents. Hydrometallurgy 165, 345–350. https://doi.org/10.1016/j.hydromet.2015.12.009

Deblonde, G.J.P., Coelho-Diogo, C., Chagnes, A., Cote, G., Smith, M.E., Hanna, J. V., Iuga, D., Bonhomme, C., 2016c. Multinuclear Solid-State NMR Investigation of Hexaniobate and Hexatantalate Compounds. Inorg. Chem. 55, 5946–5956. https://doi.org/10.1021/acs.inorgchem.6b00345

Deblonde, G.J.P., Delaunay, N., Lee, D., Chagnes, A., Cote, G., Gareil, P., 2015b. First investigation of polyoxoniobate and polyoxotantalate aqueous speciation by capillary zone electrophoresis. RSC Adv. 5, 64119–64124. https://doi.org/10.1039/c5ra11521c

Deblonde, G.J.P., Moncomble, A., Cote, G., Bélair, S., Chagnes, A., 2015c. Experimental and computational exploration of the UV-visible properties of hexaniobate and hexatantalate ions. RSC Adv. 5, 7619–7627. https://doi.org/10.1039/c4ra14866e

Deblonde, G.J.P., Weigel, V., Bellier, Q., Houdard, R., Delvallée, F., Bélair, S., Beltrami, D., 2016d. Selective recovery of niobium and tantalum from low-grade concentrates using a simple and fluoride-free process. Sep. Purif. Technol. 162, 180–187. https://doi.org/10.1016/j.seppur.2016.02.025

Dolganova, I., Bosch, F., Bach, V., Baitz, M., Finkbeiner, M., 2020. Life cycle assessment of ferro niobium. Int. J. Life Cycle Assess. 25, 611–619.

https://doi.org/10.1007/s11367-019-01714-7

Etxebarria, N., Fernandez, L.A., Madariaga, J.M., 1994. On the hydrolysis of niobium(V) and tantalum(V) in 3mol/dm3 KCl at 25ºC. PART 1: Construction of a thermodynamic model for Nb(V). J. Chem. Soc. Dalt. Trans. 3055–3059.

Eysseltová, J., Bouaziz, R., 2012. IUPAC-NIST Solubility Data Series. 93. Potassium Sulfate in Water. J. Phys. Chem. Ref. Data 41. https://doi.org/10.1063/1.3679678

Fan, W., Zhang, Q., Deng, W., Wang, Y., 2013. Niobic acid nanosheets synthesized by a simple hydrothermal method as efficient Brønsted acid catalysts. Chem. Mater. 25, 3277–3287. https://doi.org/10.1021/cm400192q

Feizpour, M., Barzegar Bafrooei, H., Hayati, R., Ebadzadeh, T., 2014. Microwave-assisted synthesis and sintering of potassium sodium niobate lead-free piezoelectric ceramics. Ceram. Int. 40, 871–877. https://doi.org/10.1016/j.ceramint.2013.06.081

Filella, M., May, P.M., 2020. The aqueous solution thermodynamics of niobium under conditions of environmental and biological interest. Appl. Geochemistry 122, 104729. https://doi.org/10.1016/j.apgeochem.2020.104729

Galutskiy, V. V., Ivashko, S.S., Stroganova, E. V., 2020. Growth of lithium niobate and potassium niobate single crystals using the Czochralski method with liquid and ceramic charging. Solid State Sci. 108, 106355. https://doi.org/10.1016/j.solidstatesciences.2020.106355

Gasik, M., Bizhanov, V., Dashevskii, A., 2020. Ferroalloys - Theory and Practice.

Guo, C., Qian, Z., 1993. Acidic and catalytic properties of niobic acid crystallized at low temperature. Catal. Today 16, 379–385. https://doi.org/10.1016/0920-5861(93)80077-E

Guo, Z., Liu, L., Hou, Z., Wang, Y., Yu, J., Jiang, H., 2020. Fabrication of K2Nb8O21 microcrystalline with good dispersion by molten salt synthesis. Ferroelectrics 554, 197–203. https://doi.org/10.1080/00150193.2020.1705111

Hagelüken, C., 2014. Recycling of (critical) metals, 1st ed, Critical Metals Handbook. John Wiley & Sons, Ltd. https://doi.org/10.1002/9781118755341.ch3

Hajdara, I., Lengyel, K., Kovács, L., Péter, Á., Szaller, Z.S., 2012. Effect of alkali

doping on the Raman spectra of potassium lithium niobate crystals. Ferroelectrics 428, 57–63. https://doi.org/10.1080/00150193.2012.675271

Hayashi, H., Hakuta, Y., & Kurata, Y., 2004. Hydrothermal synthesis of potassium niobate photocatalysts under subcritical and supercritical water conditions. Mater. Chem. 14, 2046–2051. https://doi.org/10.1039/b400130n

Heisterkamp, F., Carneiro, T., 2001. Niobium: Future possibilities - Technology and the market place. Niobium, Sci. Technol. 1109–1159.

Hughes, M.A., 1964. Thermal studies on niobium compounds. I. Niobic acid and some niobic acid/amine derivatives. J. Less-Common Met. 6, 232–238. https://doi.org/10.1016/0022-5088(64)90104-3

Jehng, J. -M, Wachs, I.E., 1991. Niobium oxide solution chemistry. J. Raman Spectrosc. 22, 83–89. https://doi.org/10.1002/jrs.1250220207

Jo, Y., Garbev, K., Çevirim-Papaioannou, N., Blanco, O.D., de Blochouse, B., Altmaier, M., Gaona, X., 2022. Solubility of niobium(V) in cementitious systems relevant for nuclear waste disposal: Characterization of the solubility-controlling solid phases. J. Hazard. Mater. 440, 129810. https://doi.org/10.1016/j.jhazmat.2022.129810

Kanie, K., Numamoto, Y., Tsukamoto, S., Takahashi, H., Mizutani, H., Terabe, A., Nakaya, M., Tani, J., Muramatsu, A., 2011. Hydrothermal synthesis of sodium and potassium niobates fine particles and their application to lead-free piezoelectric material. Mater. Trans. 52, 2119–2125. https://doi.org/10.2320/matertrans.M2011148

Kaseda, K., Takesue, M., Aida, T.M., Watanabe, M., Hayashi, H., Smith, R.L., 2011. Restructuring mechanism of NbO6 octahedrons in the crystallization of KNbO3 in supercritical water. J. Supercrit. Fluids 58, 279–285. https://doi.org/10.1016/j.supflu.2011.06.009

Klemperer, W.G., Marek, K.A., 2013. An 17O NMR study of hydrolyzed NbV in weakly acidic and basic aqueous solutions. Eur. J. Inorg. Chem. 28, 1762–1771. https://doi.org/10.1002/ejic.201201231

Kong, X., Hu, D., Wen, P., Ishii, T., Tanaka, Y., Feng, Q., 2013. Transformation of

potassium Lindquist hexaniobate to various potassium niobates: Solvothermal synthesis and structural evolution mechanism. Dalt. Trans. 42, 7699–7709. https://doi.org/10.1039/c3dt00062a

Korzhinskaya, V.S., Kotova, N.P., Shapovalov, Y.B., 2017. Experimental study of natural pyrochlore and niobium oxide solubility in Alkaline hydrothermal solutions. Dokl. Earth Sci. 475, 793–796. https://doi.org/10.1134/S1028334X17070157

Kotova, N.P., 2012. Experimental study of concentration dependence of niobium oxide solubility in fluoride solutions at T=550oC, P=500 bar and low oxygen fugacity (Co–CoO buffer). Vestn. Otd. Nauk Zemle 4, 1–3. https://doi.org/10.2205/2012NZ

Kotova, N.P., 2011. Experimental study of concentration dependence of Ta2O5 and Nb2O5 solubility in the alkaline and carbonate solutions at T=550oC, P=500 bar and low oxygen fugacity (Co-CoO buffer). Vestn. Otd. Nauk o Zemle RAN 3, 1–7. https://doi.org/10.2205/2011nz000185

Kudo, K., Kakiuchi, K., Mizutani, K., Fukami, T., Hoshikawa, K., 2004. Non-stoichiometry in potassium niobate crystals grown by directional solidification. J. Cryst. Growth 267, 150–155. https://doi.org/10.1016/j.jcrysgro.2004.03.032

Labinger, J.A., 1982. Niobium and Tantalum, in: Niobium and Tantalum. pp. 705–782.

Leal Marchena, C., Saux, C., Dinamarca, R., Pecchi, G., Pierella, L., 2016. Alkaline niobates ANbO3 (A = Li, Na, K) as heterogeneous catalysts for dipropyl sulfide oxidation. RSC Adv. https://doi.org/10.1039/c6ra21749d

Lebarbier, V., Houalla, M., Onfroy, T., 2012. New insights into the development of Bronsted acidity of niobic acid. Catal. Today 192, 123–129. https://doi.org/10.1016/j.cattod.2012.02.061

Lothenbach, B., Ochs, M., Wanner, H., Mikazu, Y., 1999. Thermodynamic Date for the Speciation and Solubility of Pd,Pb,Sn,Sb,Nb,and Bi in Aqueous Solution.

Lü, X., Mou, X., Wu, J., Zhang, D., Zhang, L., Huang, F., Xu, F., Huang, S., 2010. Improved-Performance Dye-Sensitized solar cells using Nb-Doped TiO 2 electrodes: Efficient electron Injection and transfer. Adv. Funct. Mater. 20, 509–515. https://doi.org/10.1002/adfm.200901292

Lübke, M., Sumboja, A., Johnson, I.D., Brett, D.J.L., Shearing, P.R., Liu, Z., Darr, J.A., 2016. High power nano-Nb2O5 negative electrodes for lithium-ion batteries. Electrochim. Acta 192, 363–369. https://doi.org/10.1016/j.electacta.2016.01.226

Mackay, D.A.R., Simandl, G.J., 2014. Geology, market and supply chain of niobium and tantalum—a review. Miner. Depos. 49, 1025–1047. https://doi.org/10.1007/s00126-014-0551-2

Mączka, M., Ptak, M., Majchrowski, A., Hanuza, J., 2011. Raman and IR spectra of K4Nb6O17and K 4Nb6O17·3H2O single crystals. J. Raman Spectrosc. https://doi.org/10.1002/jrs.2668

Maiorov, V.G., Nikolaev, A.I., Kopkov, V.K., 2013. Preparation of alkaline Nb(V) solutions using K(I) compounds. Russ. J. Appl. Chem. 86, 108–111. https://doi.org/10.1134/S1070427213010199

Masoud, M., 2005. Diffusivity and Ionic Conductivity in Lithium Niobate and Related Glasses and Glass Composites. Arbeit.

Nakajima, K., Baba, Y., Noma, R., Kitano, M., N. Kondo, J., Hayashi, S., Hara, M., 2011. Nb2O5•nH2O as a heterogeneous catalyst with water-tolerant lewis acid sites. J. Am. Chem. Soc. 133, 4224–4227. https://doi.org/10.1021/ja110482r

Nico, C., Monteiro, T., Graça, M.P.F., 2016. Niobium oxides and niobates physical properties: Review and prospects. Prog. Mater. Sci. 80, 1–37. https://doi.org/10.1016/j.pmatsci.2016.02.001

Nikolaev, A.I., Kirichenko, N. V., Maiorov, V.G., 2009. Niobium, tantalum, and titanium fluoride solutions. Russ. J. Inorg. Chem. 54, 505–511. https://doi.org/10.1134/S0036023609040032

Nikolay, T., Larina, L., Shevaleevskiy, O., Ahn, B.T., 2011. Electronic structure study of lightly Nb-doped TiO2 electrode for dye-sensitized solar cells. Energy Environ. Sci. 4, 1480–1486. https://doi.org/10.1039/c0ee00678e

Niu, J., Pengtao, M., Niu, H., Li, J., Zhao, J., Song, Y., Wang, J., 2007. Giant polyniobate clusters based on [Nb7O22] 9- Units derived from a Nb6O19 precursor. Chem. - A Eur. J. 13, 8739–8748. https://doi.org/10.1002/chem.200700612

Noseck, U., Becker, D., Flügge, J., Fah-, C., Herbert, H., Kull, H., Meleshyn, A., Wolf, J., 2021. Scientific basis for a safety case of deep geological repositories.

Nyman, M., 2011. Polyoxoniobate chemistry in the 21st century. Dalt. Trans. 40, 8037–8248.

Nyman, M., Alam, T.M., Bonhomme, F., Rodriguez, M.A., Frazer, C.S., Welk, M.E., 2006. Solid-state structures and solution behavior of alkali salts of the [Nb6O19]8- Lindqvist ion. J. Clust. Sci. 17, 197–219. https://doi.org/10.1007/s10876-006-0049-x

Ozmen, O., Ozsoy-Keskinbora, C., Suvaci, E., 2018. Chemical stability of KNbO3, NaNbO3, and K0.5Na0.5NbO3 in aqueous medium. J. Am. Ceram. Soc. 101, 1074–1086. https://doi.org/10.1111/jace.15291

Park, G., Gunawardhana, N., Lee, C., Lee, S.M., Lee, Y.S., Yoshio, M., 2013. Development of a novel and safer energy storage system using a graphite cathode and Nb2O5 anode. J. Power Sources 236, 145–150. https://doi.org/10.1016/j.jpowsour.2012.10.102

Patat, S., Rahman, S., Dokan, F.K., 2022. The effect of sodium and niobium co-doping on electrochemical performance of Li4Ti5O12 as anode material for lithium-ion batteries. Ionics (Kiel). 28, 3177–3185. https://doi.org/10.1007/s11581-022-04579-3

Peiffert, C., Nguyen-Trung, C., Palmer, D.A., Laval, J.P., Giffaut, E., 2010. Solubility of B-Nb2O5 and the hydrolysis of niobium(V) in aqueous solution as a function of temperature and ionic strength. J. Solution Chem. 39, 197–218. https://doi.org/10.1007/s10953-010-9495-z

Petrus, E., Segado-Centellas, M., Bo, C., 2022. Computational Prediction of Speciation Diagrams and Nucleation Mechanisms: Molecular Vanadium, Niobium, and Tantalum Oxide Nanoclusters in Solution. Inorg. Chem. 1–13. https://doi.org/10.1021/acs.inorgchem.2c00925

Philip A. Schweitzer, P.E., 2003. METALLIC MATERIALS: Physical, mechanical and corrosion properties, Marcel Dekker, Inc. https://doi.org/10.1201/9781315177281-4

Piskin, C., Karacasulu, L., Bortolotti, M., Vakifahmetoglu, C., 2021. Synthesis of potassium–sodium niobate (KNN) from NbO2. Open Ceram. 7, 100159. https://doi.org/10.1016/j.oceram.2021.100159

Prasetyoko, D., Ramli, Z., Endud, S., Nur, H., 2008. Characterization and catalytic performance of niobic acid dispersed over titanium silicalite. Res. Lett. Mater. Sci. 2008. https://doi.org/10.1155/2008/345895

Qiu, J., Li, X., Qi, X., 2019. Raman Spectroscopic Investigation of Sulfates Using Mosaic Grating Spatial Heterodyne Raman Spectrometer. IEEE Photonics J. 11, 1. https://doi.org/10.1109/JPHOT.2019.2939222

Santandrea, R., Brasil, S.L.D.C., Reznik, L.Y., Carvalho, L.J., 2018. Estudo dos diagramas E-pH aplicados a revestimentos à base de pentóxido de nióbio. Intercorr 2018 10.

Santos, I.C.M.S., Loureiro, L.H., Silva, M.F.P., Cavaleiro, A.M.V., 2002. Studies on the hydrothermal synthesis of niobium oxides. Polyhedron 21, 2009–2015. https://doi.org/10.1016/S0277-5387(02)01136-1

Sasidharan, M., Gunawardhana, N., Yoshio, M., Nakashima, K., 2012. Nb2O5 hollow nanospheres as anode material for enhanced performance in lithium ion batteries. Mater. Res. Bull. 47, 2161–2164. https://doi.org/10.1016/j.materresbull.2012.06.004

Souza, R.M.F. de, Fernandes, L.E., Guerra, W., 2013. Nióbio. Química Nov. na Esc. 35, 68–69.

Tanabe, K., 1987. Niobic acid as an unusual acidic solid material. Mater. Chem. Phys. 17, 217–225. https://doi.org/10.1016/0254-0584(87)90057-5

Theresa Von Rennenberg, 2359. Towards a circular economy of critical raw materials: The case of niobium.

Timofeev, A., 2018. Department of Earth and Planetary Sciences, McGill University, The Solubility, Speciation, and Transport of the High Field Strength Elements (HFSE) Niobium, Tantalum, and Uranium. Montreal, Canada.

Uekawa, N., Kudo, T., Mori, F., Wu, Y.J., Kakegawa, K., 2003. Low-temperature

synthesis of niobium oxide nanoparticles from peroxo niobic acid sol. J. Colloid Interface Sci. 264, 378–384. https://doi.org/10.1016/S0021-9797(03)00460-0

USGS, 2017. Zirconium and Hafnium Chapter V of Critical Mineral Resources of the United States — Economic and Environmental Geology and Prospects for Future Supply Professional Paper 1802 – V U . S . Department of the Interior. U.S. Geol. Surv. Prof. Pap. 1802, Prep. by Jones, J.V., Piatak, N.M., Bedinger, G.M. V1–V26, Reston, Virginia.

Wang, X., Jia, Y., Ma, S., Zheng, S., Sun, Q., 2018. Effect of mechanical activation on the leaching kinetics of niobium-bearing mineralisation in KOH hydrothermal system. Hydrometallurgy 181, 123–129. https://doi.org/10.1016/j.hydromet.2018.08.012

Wang, X., Zheng, S., Xu, H., Zhang, Y., 2009. Leaching of niobium and tantalum from a low-grade ore using a KOH roast-water leach system. Hydrometallurgy 98, 219–223. https://doi.org/10.1016/j.hydromet.2009.05.002

Wang, Y., Yi, Z., Li, Y., Yang, Q., Wang, D., 2007. Hydrothermal synthesis of potassium niobate powders. Ceram. Int. 33, 1611–1615. https://doi.org/10.1016/j.ceramint.2006.07.013

Yang, D., Wang, Y., Chen, C., Su, Y., Li, L., Miao, L., Gu, H., Zhao, W., Ding, L., Hu, D., 2023. Oriented Plate-like KNbO3 Polycrystals: Topochemical Mesocrystal Conversion and Piezoelectric and Photocatalytic Responses. Inorg. Chem. 62, 10408–10419. https://doi.org/10.1021/acs.inorgchem.3c01286

Ye, Y., Chen, C., Feng, H., Zhou, J., Ma, J., Chen, J., Yuan, J., Kong, L., Qian, Z., 2013. Visible photoluminescence of polyoxoniobates in aqueous solution and their high electrocatalytic activities for water oxidation. Open J. Inorg. Chem. 03, 59–69. https://doi.org/10.4236/ojic.2013.33009

Yi, T.F., Sari, H.M.K., Li, Xuezhong, Wang, F., Zhu, Y.R., Hu, J., Zhang, J., Li, Xifei, 2021. A review of niobium oxides based nanocomposites for lithium-ion batteries, sodium-ion batteries and supercapacitors. Nano Energy 85, 105955. https://doi.org/10.1016/j.nanoen.2021.105955

Zhou, H., Zheng, S., Zhang, Y., 2005. Leaching of a low-grade niobium-tantalum ore

by highly concentrated caustic potash solution. Hydrometallurgy 80, 83–89. https://doi.org/10.1016/j.hydromet.2005.07.006

Zhou, H.M., Yi, D.Q., Zhang, Y., Zheng, S.L., 2005a. The dissolution behavior of Nb2O5, Ta2O5 and their mixture in highly concentrated KOH solution. Hydrometallurgy 80, 126–131. https://doi.org/10.1016/j.hydromet.2005.07.010

Zhou, H.M., Zheng, S.L., Zhang, Y., Yi, D.Q., 2005b. A kinetic study of the leaching of a low-grade niobium-tantalum ore by concentrated KOH solution. Hydrometallurgy 80, 170–178. https://doi.org/10.1016/j.hydromet.2005.06.011

CHAPTER 4 – INVESTIGATION OF SOLUBILITY OF NIOBIUM COMPOUNDS UNDER ALKALINE CONDITIONS

4.1 Introduction

Niobium (Nb) is a transition metal in group V of the periodic table. Oxidation states from +I to +VII are possible, but only Nb(V) exists under usual redox conditions in biological and environmental systems (Filella and May, 2020). In addition, it is a refractory metallic solid of lower density (8.57 g/cm^3), has high thermal and electrical conductivity (Dolganova et al., 2020; CBMM, 2021), is soft, ductile and presents a very high melting point of 2468 ºC (Hagelüken, 2013), being very resistant to corrosion as a result of the creation of a surface oxide film (Souza et al., 2013) .

Due to its complexity, the chemistry of niobium has been under investigated (Filella and May, 2020). The speciation diagram is the most employed tool to study the aqueous system and evaluate the effect of pH and total niobium concentration on the species formation. The solubility data of niobium compounds in aqueous media are scarce in the literature and an effort is needed to collect them.

In pure aqueous media, Nb(V) is stable in the water stability field (Deblonde et al., 2016a, 2015c; Jo et al., 2022), while Nb(III) is very unstable and rapidly oxidates into Nb(V) (Santandrea et al., 2018). Nb(V) complexes can exist in alkaline and acidic media with a tendency to hydrolyze due to their low stability in aqueous solutions and strong oxygen bonds (Deblonde et al., 2015c; Jehng and Wachs, 1991). Additionally, these complexes produce insoluble oxides with amphoteric behavior in both acidic and basic conditions. These oxides produce anionic species above pH 4 and cationic species below pH 4 (Peiffert et al., 2010).

Mononuclear species of Nb(V) can exist in aqueous media as $Nb(OH)_3^{2+}$, $Nb(OH)_4^{+}$, $Nb(OH)_7^{2-}$, $Nb(OH)_5^{0}$ and $Nb(OH)_6^{-}$. Jo and co-workers (2022) described that the increase in Nb concentration, due to the increase in the solubility observed in pH values higher than 12.5, enables the formation of hydrolyzed species of Nb(V) in addition to

$Nb(OH)_7^{2-}$ and in pH values higher than 14.5 the formation of $NbO_2(OH)_4^{3-}$ species is predicted.

In alkaline medium, niobium is known for Lindqvist type ions $H_xM_6O_{19}^{(x-8)}$ (M= metal) and the formation of the cluster M_6O_{19} has been reported (Deblonde et al., 2015b; Petrus et al., 2022). This structure ($H_xNb_6O_{19}^{(x-8)}$) is the dominant specie for Nb(V) in aqueous medium in pH ≥ 8, related to hexaniobate salts formation (Deblonde et al., 2016c, 2016d, 2015a, 2015c; Nyman et al., 2006). The hexaniobate ions are also precursors for several polyoxoniobates, including $Nb_{10}O_{28}^{6-}$, $Nb_{20}O_{54}^{8-,}$ and $Nb_{24}O_{72}H_9^{15-}$ (Ye et al., 2013). Petrus et al. (2022) predicted in the speciation diagram the formation of new species $Nb_{10}O_{28}^{6-}$, $Nb_7O_{22}^{9-}$ and $H_9Nb_{24}O_{72}^{9-}$, being the $Nb_{10}O_{28}^{6-}$ specie predominant from acid to neutral pH values. The $H_9Nb_{24}O_{72}^{9-}$ is also formed in similar pH but in higher niobium concentrations. Therefore, the $Nb_7O_{22}^{9-}$ is probably a transient intermediate and rapidly reacts to form the aforementioned species. Additionally, Jehng and Wachs (1991) speculate that hexaniobate species begin to degrade into tetrameric ($Nb_4O_{16}^{12-}$) and monomeric ($NbO_2(OH)_4^{3-}$) species in alkaline and dilute solutions.

The hexaniobate ion is an excellent precursor for the synthesis of heteropolyoxoniobates. When associated with elements such as K, Na, Rb, Cs and Li (reaction rate: Cs>Rb>K>Na>Li), these can be introduced to this structure and produce new compounds, e.g., the potassium ion, for example, can form species such as $K_4(Nb_6O_{19})^{4-}$, $K_8(Nb_6O_{19})$ and $K_{10}(Nb_6O_{19})^{2+}$ (Antonio et al., 2009; Nyman et al., 2006).

In acid medium, niobium may form niobic acid, a hydrous niobium oxide ($Nb_2O_5.nH_2O$) that has low solubility in water. Niobic acid can be calcinated to produce anhydrous niobium pentoxide. Niobic acid is a more reactive compound than its equivalents and is produced by hydrometallurgical route (Deblonde et al., 2015), either by $NbCl_{5(aq)}$ neutralization or by precipitation through the acidification of alkaline Nb solutions.

Little is known about the solubility of many niobium compounds. Most of the found in literature refers to niobium pentoxide and niobic acid, as compiled in Table 4.1.

Table 4.1. Solubility studies for niobium compounds.

COMPOUND	METHOD	SOLUBILITY Nb (mol/Kg)	CONDITION	REFERENCE
Nb_2O_5	Precipitation with KNO_3	1.4×10^{-5}	I= 1 to 6 mol/L $KNbO_3$, 19 °C; pH = 0 to 7	Babko et al., 1963
Nb_2O_5	Precipitation (reagents not reported)	1×10^{-8}	I= 0.1 mol/L NaCl; 25 ºC pH= 2 to 8	Yajima et al., 1992 and Yajima 1994 – cited by Lothenbach et al. 1999
Nb_2O_5	Recrystallization	6×10^{-10}	I= 0.1 - 6 mol/kg $NaClO_4$; 10 - 70°C, pH= 1 to 9 monoclinic phase	Peiffert et al., 2010
Nb_2O_5	Not reported	$\sim 10^{-4}$ to 10^{-7}	0.1 – 1 mol/Kg NaOH and Na_2CO_3, 550 ºC	Kotova, 2011
Nb_2O_5	Not reported	10^{-4} to $10^{-3.5}$ $10^{-1.5}$ to $10^{-0.5}$	10^{-2} mol/Kg HF and > 1 mol/kg HF at 550 ºC, 1000 bar, Co-CoO oxidizing medium	Kotova, 2012
Nb_2O_5	Not reported	10^{-5} to 10^{-4}	0.1 and 1 mol/kg HCl and KCl, 300 and 500 ºC, 100 MPa Co-CoO oxidizing medium	Kotova, 2015
Nb_2O_5	Not reported	$\sim 10^{-7}$ to 10^{-8}	I= 10^{-5} a 10^{-4} mol/L HF, 150, 200 and 250 °C; pH < 3	Timofeev et al., 2018
$Nb_2O_5.nH_2O$	Hydrolysis with $NbCl_5$	5.4×10^{-6}	I=0.12 mol/L NaCl/ NaOH/ Na_2CO_3; 25 °C; pH= 6 to 12	Deblonde et al., 2015a
$Na_7HNb_6O_{19}.15H_2O$	Hydrothermal Nb_2O_5 and KOH	$\sim 10^{-3}$	I= 0.09-0.18 NaCl/KCl; 25 °C; pH= 11 to 12	

As can be seen in the table 4.1, niobium oxide has low solubility in the aqueous medium. In hydrofluoric acid solution, niobium has higher solubility when compared to other aqueous acids, due to less prone to form polymeric species (Nikolaev et al., 2009).

Babko et al. (1963) investigated the solubility of freshly precipitated niobium hydroxide (probably an amorphous phase) in the presence of HNO_3. This study was used by Etxebarria et al. (1994) to estimate the solubility product of niobium pentoxide. On the other hand, Lothenbach et al. (1999) used the data of Yajima et al. (1992) and Yajima (1994) of the Nb_2O_5 solubility in NaCl to calculate solubility products from this study (publications Yajima et al. (1992) and Yajima (1994) not available).

Peiffert et al. (2010) studied the effect of temperature, ionic strength and pH on the solubility of the monoclinic phase of Nb_2O_5, obtained at moderate temperatures (~ 600 – 900 ºC). The results show the increase of solubility with the increase in temperature and ionic strength, and the presence of polyoxoniobates was reported at higher pH values.

Kotova (2011, 2012, 2015), studied the solubility of niobium oxide in the presence of different electrolytes such as NaOH, Na_2CO_3, KCl, HCl and HF. Co-CoO buffer with low oxygen fugitiveness was used due to the negative influence of an increase in oxygen fugitiveness on the solubility (Korzhinskaya et al., 2017). Niobium pentoxide showed low solubility in presence of NaOH, Na_2CO_3 and the effect of niobium chloride complexes in the niobium solubility was insignificant. However, the solubility of Nb_2O_5 increases strongly with rise in the concentrations of fluoride solutions. Timofeev et al. (2018) also investigated the solubility of Nb_2O_5 in HF solutions at lower pH values by adding $HClO_4$. They also notice that a decrease in the pH increases the solubility of niobium oxide at low HF concentration.

However, for niobates, there is a lack of solubility data in the literature. To the best of our knowledge, only Deblond et al. (2015a) studied the solubility of a sodium niobate phase in NaCl/KCl medium at 25 ºC. This study shows the effect of the common-ion in the solubility, where an increase in Na^+ caused a decrease in the solubility of sodium niobate. Moreover, the authors report an increase in the solubility influenced by the potassium ions, related to the interaction of potassium with hexaniobate ions. Same authors also studied the solubility of niobic acid increases with the rise in pH and showed that the hexaniobate ions play a major role in the solubility of niobic acid in aqueous medium.

Due to scenario of the scarcity of solubility data for niobium compounds, an effort was made here to measure the solubility of potassium niobate (mix of phases $K_4Nb_6O_{17}$ and $KNbO_3$) and niobic acid ($Nb_2O_5.nH_2O$) in different temperature and concentrations of KOH solution. An equilibrium study was conducted to investigate the solubility of niobic acid in KOH solutions of 0.10, 0.25, and 0.50 mol/L at 30 ºC. Additionally, solubility experiments for both potassium niobate and niobic acid in alkaline media (0 to 2 mol/L KOH) were performed using Crystal 16 equipment. Thermodynamic modeling was made for the system Nb-K-H_2O by OLI Studio stream analyser and PHREEQC.

4.2 Materials and methods

4.2.1 Reagents

Potassium niobate (KN) was synthesized by cooling crystallization from Fe-Nb alloy fines alkaline liquor, as shown in Chapter 3. Niobic acid HY-340 (NA) was obtained from CBMM (Brazilian Company of Metallurgy and Mining, from Portuguese: *Companhia Brasileira de Metalurgia e Mineração*). Analytical grade $NaOH_{(s)}$ (Êxodo Científica, CAS: 1310-73-2) and $KOH_{(s)}$ (Sigma Aldrich, CAS: 1310-58-3) were used without further purification. Solutions were prepared with deionized and distilled water.

4.2.2 Thermodynamic modeling

To obtain the solution description parameters, such as composition data, saturation index, distribution of the species in the solution and possible solid phases formed in the multicomponent systems, thermodynamic modelling was performed using OLI Studio Stream Analyser (version 11) and PHREEQC (version 3.4.12927; Parkhurst and Appelo, 2013). The thermodynamic framework AQ (aqueous model) and MSE (Mixed Solvent Electrolyte) were used in OLI. The AQ thermodynamic framework includes both stable phases – $KNbO_3$ and Nb_2O_5 – and is applied to electrolytes dissolved in water, using the Bromley-Zemaitis activity model. In contrast, the MSE framework contains only the Nb_2O_5 and utilizes the MSE activity model, which uses (i) the extended Debye-Huckel term that accounts for long-range interactions, (ii) an UNIQUAC term that accounts for short-range interactions, and a middle-range term that includes the ionic interactions. In

PHREEQC, the SIT (Specific ion Interaction Theory) database (sit.dat) was used as the aqueous model.

In addition, the speciation diagram of hexaniobates species were made based on the calculations shown by Etxebarria et al., (1994) using the equilibrium constants of the hydrolysis products of Nb(V) at 25 ºC, as a function of pH (Table A1). According to the Equations 4.1 to 4.9:

$$[C]_T = [\mathrm{Nb_6O_{19}^{8-}}] + [\mathrm{HNb_6O_{19}^{7-}}] + [H_2\mathrm{Nb_6O_{19}^{6-}}] + [H_3\mathrm{Nb_6O_{19}^{5-}}] \quad (4.1)$$

$$[\mathrm{Nb_6O_{19}^{8-}}] = \frac{[\mathrm{C}]_T}{1 + (K_1.[H^+]) + (K_2.[2.H^+]) + (K_3.[3.H^+])} \quad (4.2)$$

$$[\mathrm{HNb_6O_{19}^{7-}}] = [\mathrm{Nb_6O_{19}^{8-}}].K_1.[H^+] \quad (4.3)$$

$$[H_2\mathrm{Nb_6O_{19}^{6-}}] = [\mathrm{Nb_6O_{19}^{8-}}].K_2.[H^+]^2 \quad (4.4)$$

$$[H_3\mathrm{Nb_6O_{19}^{5-}}] = [\mathrm{Nb_6O_{19}^{8-}}].K_3.[H^+]^3 \quad (4.5)$$

$$\alpha_1 = \frac{[\mathrm{Nb_6O_{19}^{8-}}]}{[C]_T} \quad (4.6)$$

$$\alpha_2 = \frac{[\mathrm{HNb_6O_{19}^{7-}}]}{[C]_T} \quad (4.7)$$

$$\alpha_3 = \frac{[H_2\mathrm{Nb_6O_{19}^{6-}}]}{[C]_T} \quad (4.8)$$

$$\alpha_4 = \frac{[H_3\mathrm{Nb_6O_{19}^{5-}}]}{[C]_T} \quad (4.9)$$

4.2.3 Experimental

The equilibrium study was performed for the commercial niobic acid HY-340 at different concentrations of KOH solution. A mass of niobic acid was mixed into 10 mL of KOH solutions with concentrations from 0.10 to 0.50 mol/L in polyethylene vessels (Table 4.2). The experiments were carried out in a shaker (SOLAB SL-222) at 30 ± 0.5 ºC and 200 rpm. The achievement of the steady-state conditions was assessed by monitoring Nb concentration in solution as a function of time (0 - 300 hours). The samples were filtrated using a 0.45 μm syringe filter (MILLIPORE MILLEX-HV PVDF 0.45 μm). The pH measurements and quantification of Nb quantification were performed after the filtration process.

Table 4.2. Conditions of equilibrium study of niobic acid in alkaline medium at 30 ± 0.5 ºC and 200 rpm for 312 hours.

Mass of Niobic Acid (g)	KOH (mol/L)
0.20	0.10
0.20	0.25
0.50	0.50

The Nb in the aqueous solution was determined by ICP-OES (Perkin Elmer, model Optima 7300DV; detection limits < 0.005 mol/L) and UV-vis (BEL-M51 spectrophotometer) methods.

The Nb quantification with UV-Vis was performed using a methodology adapted from Deblonde and co-workers (2015b). Each sample was diluted in 4 M NaOH solution 10 minutes before the measurement and recorded against the corresponding blank sample using a quartz cuvette. The absorbance (A) was measured at 246.5 nm, using an optical path length (l) of 1 cm and the extinction coefficient (ε) was 15900±600 L/mol.cm to $Nb_6O_{19}^{-8}$ and 14300±400 L/mol.cm to $HNb_6O_{19}^{-7}$ species. The Beer-Lambert law was used for the determination of niobium concentration (c), according to Equation 4.10.

$$A = \varepsilon . c . l \quad (4.10)$$

Crystal 16 (Technobis Crystallization Systems® – software v. 2.3.2.5300) was used to estimate the solubility of potassium niobate and niobic acid. The equipment is a multi-reactor crystalliser that consists of 16 reactors (4 rows with 4 vials of 1 mL each) and to determine the solubility, clear and cloud points (dissolution and recrystallization, respectively) should be collected based on the transmissivity of each vial.

Different masses of solute were analysed in deionized water and KOH solution (0 to 2 mol/L). Each cycle of measurements was made of a temperature ramp from 20 to 70 ºC, with a heating rate of 0.1 ºC/min and stirring speed of 700 rpm. In this study, only the clear points were collected, when 100% of transmissivity were achieved.

Table 4.3 shows the initial experimental conditions used for estimating the solubility of potassium niobate and niobic acid under different concentrations of KOH. Were carried out 4 cycles for each condition described in the following Table 4.3.

Table 4.3. Experimental data for estimating the solubility of potassium niobate (KN) and niobic acid (NA) in different concentrations of KOH solution in a temperature ramp from 20 to 70 ºC using Crystal 16.

KN			**NA**		
KOH (mol/L)	**MASS (mg)**		**KOH (mol/L)**	**MASS (mg)**	
	MIN	**MAX**		**MIN**	**MAX**
0	80	300	0.75	5	80
0.10	30	80	1.00	5	60
0.25	10	80	1.50	10	80
0.50	10	80	2.00	10	60
1.00	10	50			

4.3 Results and discussion

4.3.1 Niobium Speciation

The speciation diagram of niobium in aqueous media was the first step to understanding the system and was also essential to elucidate the formation of niobium complexes. Figure 4.1 (a) shows the Nb-H_2O speciation diagram, simulating of the hydrolysis of Nb(V) in a broad pH range at 25, 50 and 100 ºC. According to the PHREEQC modeling, the specie $Nb(OH)_5$ is dominant at lower pH values. As the pH increases the species $Nb(OH)_6^-$ and $Nb(OH)_7^{-2}$ become predominant. At 100 ºC the predominance area of these species changes, becaming available at lower pH values. However, the hexaniobates species were not available in the PHREEQC database, reason why they do not appear in this diagram. Hence, the hexaniobates speciation (Lindqvist ions structure) was previewed considering the equilibrium equations shown in Table A1 at 25 ºC (Etxebarria et al., 1994; Petrus et al., 2022 - Figure 4.1 (b)).

According to literature (Deblonde et al., 2015b; Petrus et al., 2022), the hexaniobate species are present in an alkaline medium. Figure 4.1 (b) shows the distribution of species and the major formation of hexaniobates occurs at pH > 8 and only the third protonation occurs at lower pH values.

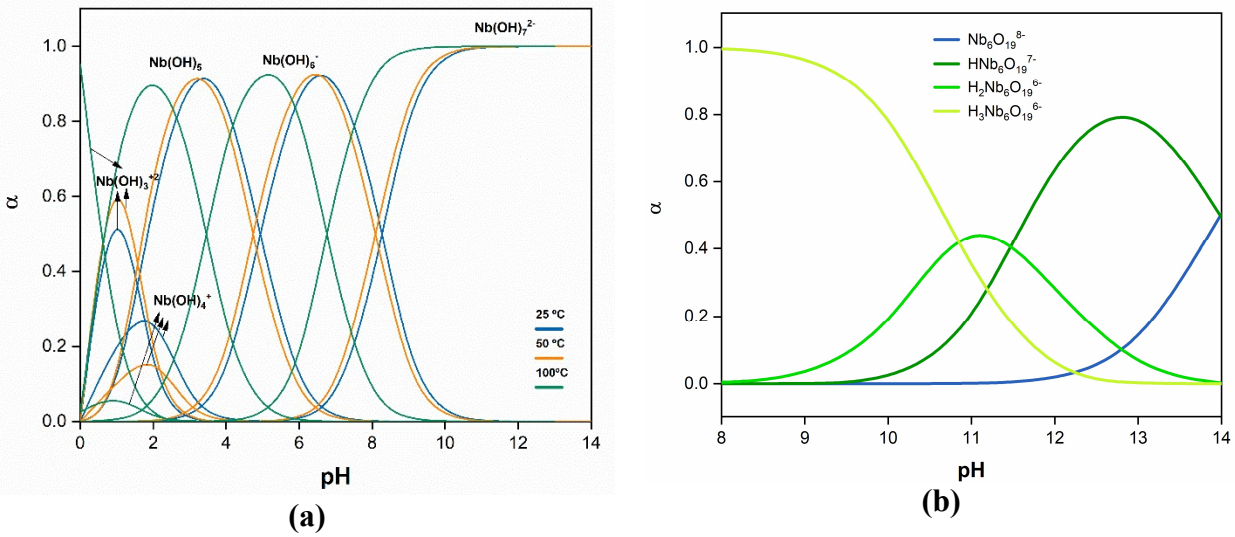

Figure 4.1. Speciation diagram of Nb-H_2O system by (a) PHREEQC - SIT databank at 25, 50 and 100 ºCand (b) data from the literature for hexaniobate species in an alkaline medium at 25 ºC. Initial conditions: [Nb] = 1 mol/L and 1 atm.

The system K-Nb-H_2O was modelled on OLI Studio and considered the formation of solid phases that may occur in aqueous medium, as shown in Figure 4.2. It is noticeable that Nb_2O_5 is the dominant solid at lower pH values and the $KNbO_3$ is formed with the increase in pH (pH > 4). However, on the OLI database only the stable phase $KNbO_3$ information is presented and the formation of metastable phases, such as $K_4Nb_6O_{17}$, are not considered.

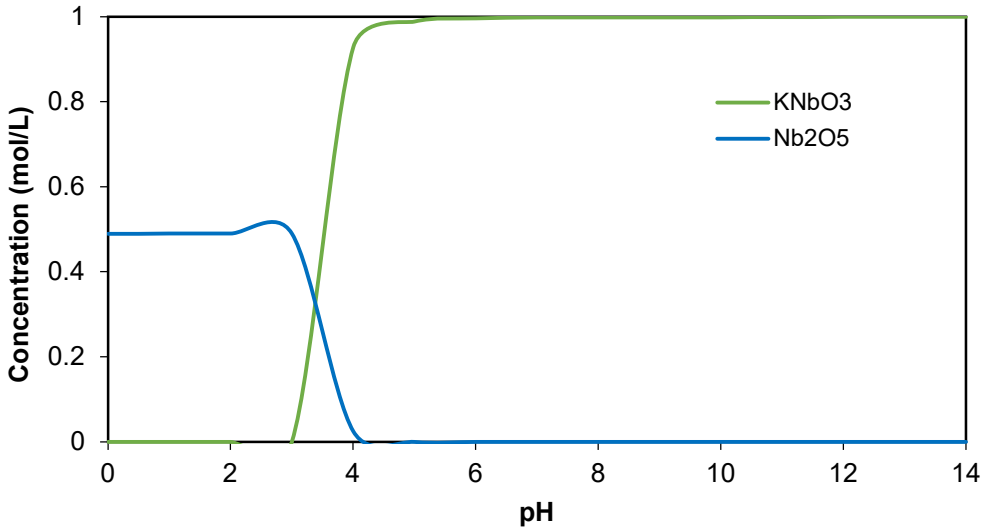

Figure 4.2. Speciation diagram of K-Nb-H_2O system at 25ºC and 1atm. (Initial [$KNbO_3$] = 1 mol/L – OLI Studio databank – AQ thermodynamic framework).

4.3.2 Kinetic of niobic acid dissolution in alkaline medium

The dissolution of niobic acid was monitored as a function of the concentration of KOH solution throughout 312 hours of an experiment at 30 ± 0.5 °C and 200 rpm, as shown in Figures 4.3 - 4.5. If all niobium was dissolved in KOH solution, the niobium concentration would be 0.15 (at 0.10 and 0.25 mol/L KOH solution) and 0.37 mol/L (at 0.50 mol/L KOH solution) (dashed grey line in the figures).

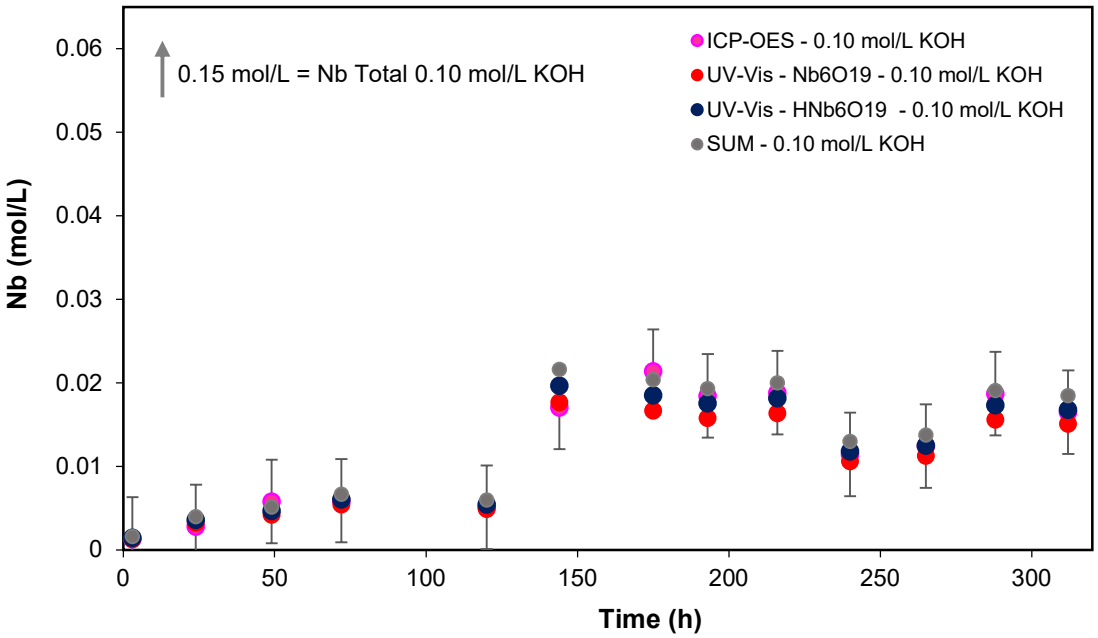

Figure 4.3. Aqueous niobium concentration measured by ICP-OES and UV-spectroscopy (γ=246.5 nm) from equilibrium study of niobic acid in 0.10 mol/L KOH solution at 30 ± 0.5 ºC, 200rpm and pH=12.8 ± 0.4. (Blue circle: $HNb_6O_{19}^{-7}$ and red circle: $Nb_6O_{19}^{-8}$ by UV-Vis method and pink circle: Nb total by ICP-OES, grey circle: sum of species $HNb_6O_{19}^{-7}$ and $Nb_6O_{19}^{-8}$, dashed line: maximum of niobium concentration).

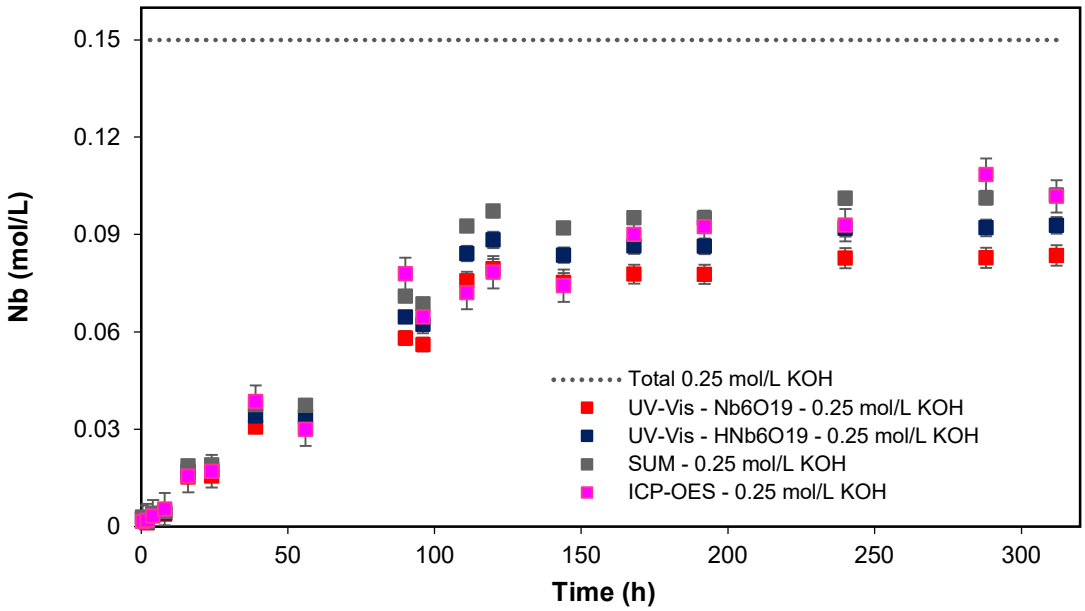

Figure 4.4. Aqueous niobium concentration measured by ICP-OES and UV-spectroscopy (γ=246.5 nm) from of niobic acid in 0.25 mol/L KOH solution at 30 ± 0.5 ºC, 200 rpm

and pH=13.5 ± 0.1. (Blue square: $HNb_6O_{19}^{-7}$ and red square: $Nb_6O_{19}^{-8}$ by UV-Vis method and pink square: Nb total by ICP-OES, grey square: sum of species $HNb_6O_{19}^{-7}$ and $Nb_6O_{19}^{-8}$, dashed line: maximum of niobium concentration).

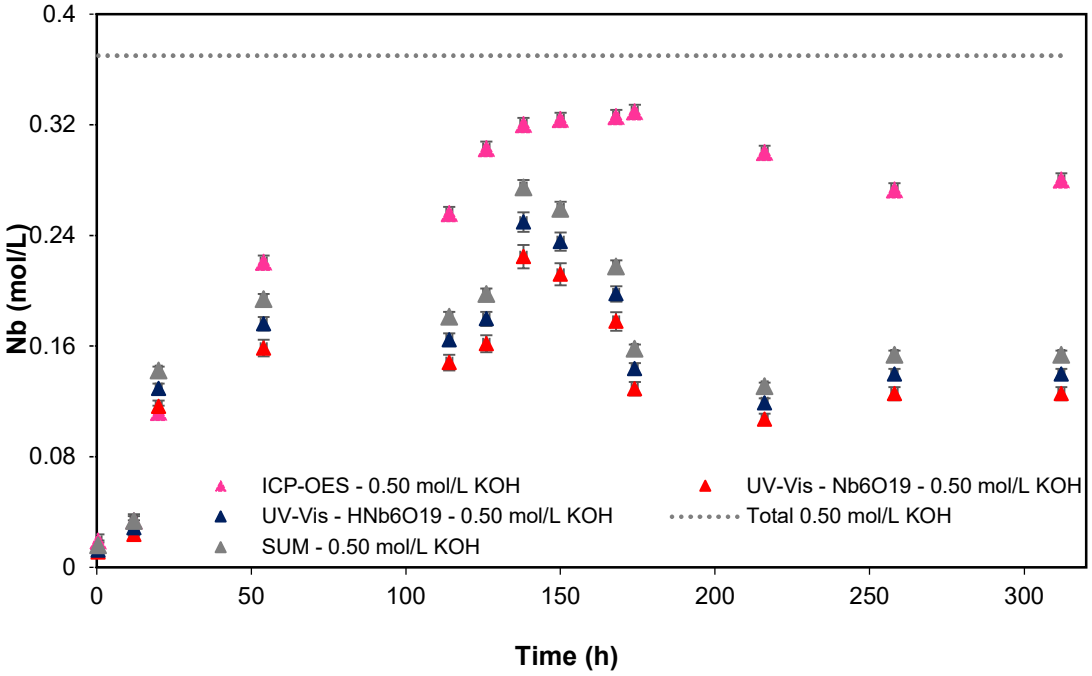

Figure 4.5. Aqueous niobium concentration measured by ICP-OES and UV-spectroscopy (γ=246.5 nm) from equilibrium study of niobic acid in 0.50 mol/L KOH solution at 30 ± 0.5 ºC, 200 rpm and pH=13.8 ± 0.6. (Blue triangle: $HNb_6O_{19}^{-7}$ and red triangle: $Nb_6O_{19}^{-8}$ by UV-Vis method and pink triangle: Nb total by ICP-OES, grey triangle: sum of species $HNb_6O_{19}^{-7}$ and $Nb_6O_{19}^{-8}$, dashed line: maximum of niobium concentration).

The niobium content in the solution was measured by UV-spectroscopy through the hexaniobates species $Nb_6O_{19}^{8-}$ and $HNb_6O_{19}^{7-}$ quantification. During the study of equilibrium, the pH value was above 12 and because of this, the UV-spectroscopy method could be effectively used (Deblonde et al., 2015a). As mentioned before, in alkaline media the niobium is complexed into hexaniobate and the species $Nb_6O_{19}^{8-}$ and $HNb_6O_{19}^{7-}$ are dominant at higher pH values (see Figure 1(b)). The pH behavior of niobic acid in KOH solutions with time is given in Table A2 (Appendix).

A difference in the niobium quantification between the ICP-OES and UV-vis methods is noted and its variation increases with the increase in KOH concentration and, consequently, an increase in Nb dissolved in the solution. According to the method used in this work, based on the study of Deblonde et al. (2015b), the nature of the alkali ion alters the wavelength in which maximum absorbance is observed (246.5 and 247.5 in NaOH and KOH solution, respectively). This occurs due to the ion-pairing effect that increases as the size of the cation increases (Cs > K > Na) and is reflected on the stabilization of the electron. However, an equilibrium between the deprotonated and the monoprotonated cluster is observed at 240 nm – close to the wavelength of Nb quantification. The hydroxide concentration also has an influence on the system, showing that an increase in the ionic strength makes the equilibrium constant decrease.

Additionally, some studies reported the presence of species as $H_xNb_7O_{22}^{x-9}$ as an intermediate from decaniobate $Nb_{10}O_{28}^{6-}$ and monoprotonated $H_xNb_6O_{19}^{x-8}$, at high pH values, in the same region of hexaniobates (Klemperer and Marek, 2013; Niu et al., 2007; Nyman, 2011; Petrus et al., 2022). This may result in an underestimation of the total of aqueous niobium. There is a lack of accurate data on speciation for the niobium system in a range of concentrations. It is necessary to account that the limitations of the method and the stability of polyoxoniobates may influence the measurements. In another study made by our research group (in preparation), the data of kinetics of dissolution of niobic acid was modeled in 0.10 and 0.25 mol/L KOH solution using machine learning techniques. The random forest model was used to fit and to compare to the linear regression of the data. As a result, the ICP-OES data fit better to the proposed model, due to the difference between the square error calculation for both methods: ICP-OES and UV-vis.

According to OLI Studio simulation, the solubility of niobium oxide increases with the growth of KOH concentration in the aqueous medium, when the formation of additional phases from the reaction of Nb(V) and KOH is not considered. Experimentally, following OLI prediction, the increase in KOH concentration favors the dissolution of niobic acid, a hydrated niobium oxide phase. The concentration of aqueous Nb increases with time until the concentration of niobium in solution is considered constant (less than 10% variation). The time of equilibrium was achieved after 100 hours of experiment in all the tested concentrations of KOH. Although, it is possible to observe a variation on Nb

concentration in the experiment with higher KOH concentration – 0.50 mol/L, between 140 to 170 minutes. This variation could be related to the kinetics of formation of polyoxoniobates in solution that directly influence the solubility of niobic acid.

From this study was possible to predict the solubility of niobic acid in KOH solution in the mentioned conditions, at 30 ± 0.5 ºC and 200 rpm. At the end of each experiment, the niobium concentrations for each studied condition (0.10, 0.25 and 0.50 mol/L KOH) given by ICP-OES were 0.016, 0.101 and 0.286 mol/L and by UV-vis method were 0.018, 0.102 and 0.154 mol/L, respectively. Even though Lindqvist ions have been known for a long time (Nyman, 2011), the properties of polyoxometalates ions in different electrolytes are scarce, especially for niobium. The remained solid was characterized by FTIR and XRD and is presented in Figure A1.

Figure 4.6 shows that the dependence of solubility of niobic acid with the KOH concentration. Niobic acid is known to be insoluble in water, especially at low pH. This result is in agreement with the literature, which reports an increase in the presence of Nb(V) in an alkaline medium with the pH (De Cock et al., 2017; Deblonde et al., 2015a; Petrus et al., 2022; Wang et al., 2009). The fitted equation of the solubility from equilibrium study is shown in Table A3.

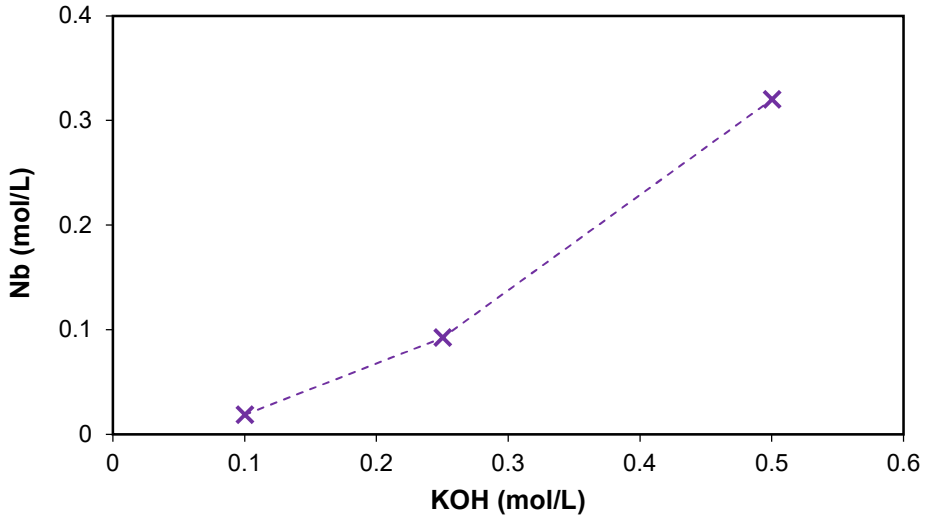

Figure 4.6. Solubility of niobic acid versus KOH concentration in solution from the equilibrium study at 30 ± 0.5 ºC. Aqueous niobium concentration measured by ICP-OES.

4.3.3 Dissolution of niobium compounds in alkaline medium: experimental and modeling

Thermodynamic modeling by the OLI Studio was also used to predict the solubility of niobic acid ($Nb_2O_5.nH_2O$) and potassium niobate crystallized from an alkaline liquor (Souza et al., 2024) (mix of phases: $K_4Nb_6O_{17}$ and $KNbO_3$). The detailed composition of the solids was analyzed via XRF (Table A4). For the potassium niobate, the clear points collected from the Crystal 16 were plateaus of transmissivity close but not at 100 %, the real solubility was not determined. Nonetheless, a pseudo-solubility could be estimated based on the maximum dissolution of the niobium compounds in an alkaline medium.

For the solubility simulations the temperature and concentration of niobium in aqueous media – with and without the presence of electrolytes – were considered. Figure 4.7 shows the results of niobic acid in different concentrations of KOH solution obtained from Crystal 16 and OLI Studio simulation.

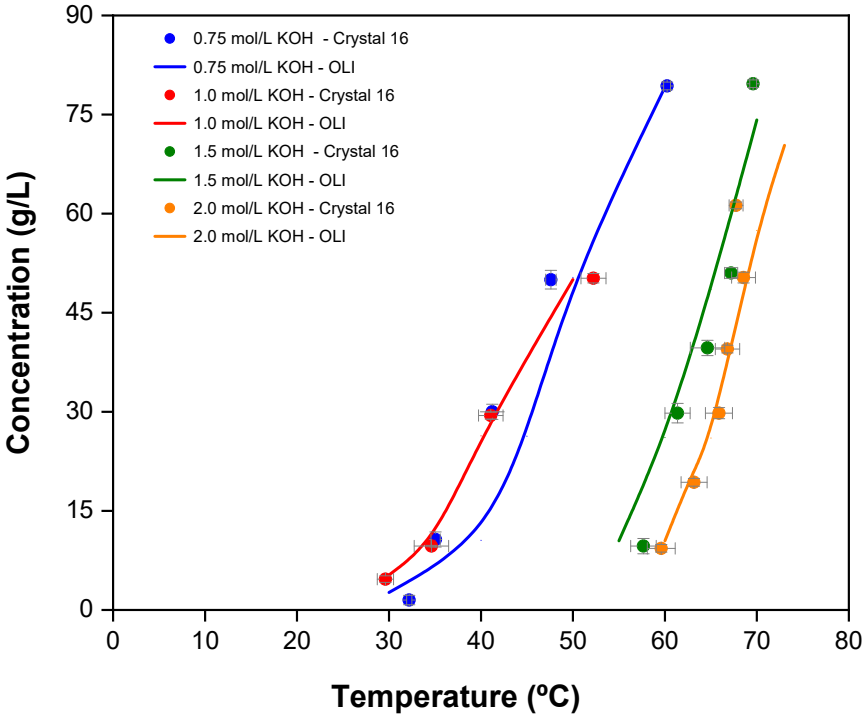

Figure 4.7. Pseudo-solubility of niobic acid ($Nb_2O_5.nH_2O$) in KOH versus temperature, obtained from Crystal 16 and predicted by OLI Studio.

It can be seen that OLI and experimental results show good fit, with an expressive increase in the solubility of niobic acid with the temperature in the range of 20 to 70 ºC and slight decrease with the increase in the KOH concentration. The OLI Studio simulation shows the formation of potassium niobate as the stable phase ($KNbO_3$) for concentrations higher than 1.5 mol/L (Figure A2). The Crystal 16 methodology adopted in this study was based on the dissolution of a known amount of solids in a known amount of solvent with the increase of temperature. The solubility data is collected when this solid is fully dissolved. Hence, no solid phase remained to be analysed at the end of the experiment, since the maximum dissolution of the solid in the aqueous medium was taken into account. No evidence of formation of any solids from the reaction of dissolved Nb(V) in a highly concentrated KOH solution was found, even when the solution temperature was subsequently lowered to 20 °C and kept under stirring for over 48 h, likely due to the slow kinetics of potassium niobate formation.

The solubility of niobic acid in distinct media has been reported in the literature in the past years (Table 4.1). It is noteworthy that similar studies for niobic acid were not found in the same conditions used in this work, so that the difference between the values in Table 4.1 and those determined in this work are not comparable. The presence of -niobate species should be considered in the system. It is known that polyoxoniobates ($Nb_6O_{19}^{x-8}$, $Nb_7O_{22}^{x-9}$, $Nb_{10}O_{28}^{6-}$) form in alkaline solutions and that their formation depends on the media (Klemper and Marek, 2013).

The pseudo-solubility of potassium niobate was evaluated in a range of 0 to 1.0 mol/L of KOH solution, as shown in Figure 4.8. To our knowledge, no quantitative data has been reported on the solubility of any potassium niobate phase in an alkaline medium. As an overall trend, the pseudo-solubility of crystallized potassium niobate (KN) increases with temperature. On the other hand, it decreases with the increase of KOH concentration, such that even the lowest concentration of KOH investigated (0.10 mol/L) lowers the solubility by roughly 70 %.

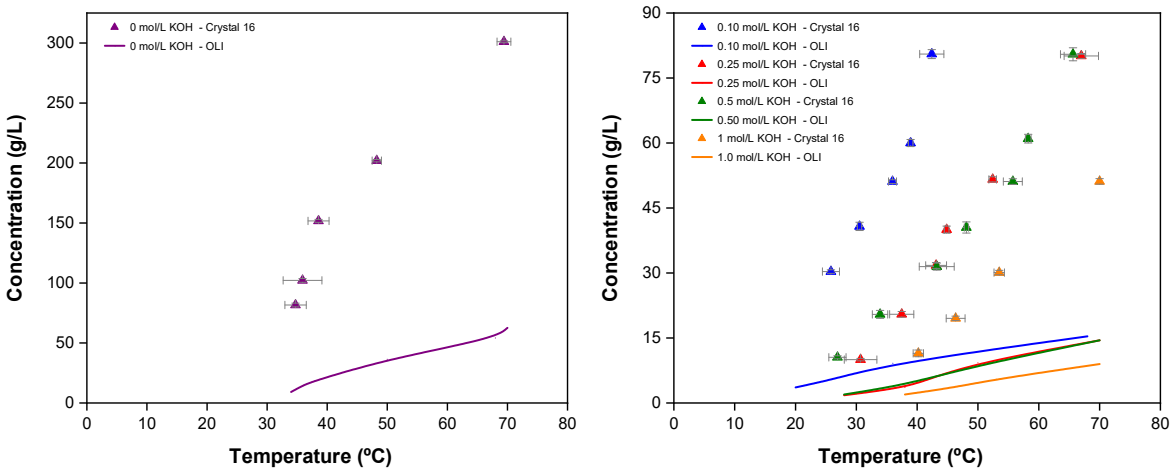

(a) **(b)**

Figure 4.8. Pseudo-solubility of crystallized potassium niobate (mix of phases) in KOH dependence on temperature, obtained from Crystal 16 and predicted by OLI Studio stream analyser.

According to the physicochemical analysis of the material, showed on the Chapter 3, two main potassium niobate crystals are present in the solids: the dominant and metastable phase $K_4Nb_6O_{17}$ and the stable phase $KNbO_3$. This indicates that the crystallization of the stable phase may occur via a metastable phase in the first stage. Consequently, these phases could exhibit different solubilities in aqueous medium. Moreover, as the potassium niobate used in this study was produced by cooling crystallization from an alkaline liquor from the leaching of Fe-Nb alloy fines, the presence of impurities is expected, as was presented in the chemical composition of the potassium niobate in Table 4.5. The impurities may have a considerable effect on the solubility of a system by combining and reacting chemically in the solution and forming complexes.

Crystallized potassium niobate was shown to be more soluble than the stable phase when compared to the solubility results from OLI Studio. This is expected since the potassium niobate used in the experiment is majority formed of a metastable phase, usually more soluble than the stable phase of the K-Nb-H_2O system.

An effort was made to measure of solubility of hydrothermal $KNbO_3$, as stable phase of the system, also using Crystal 16. However, due to the very slow kinetics of dissolution

associated to the perovskite-type of structure (Ozmen et al., 2018), it was not possible to determine the solubility by Crystal 16. No changes were visible in the transmissivity, even after leaving the vials at 80 °C for 48h.

The formation of hexaniobates species depends on the degree of alkalinity of the solution according to the suggested reactions shown in Equations 4.11 – 4.14. In dissolution, $K_4Nb_6O_{17}$ first dissolves into $Nb_6O_{17}^{4-}$ complex and afterward transforms into the $Nb_6O_{19}^{8-}$ hexaniobate ion. The same is observed in the $KNbO_3$ phase, which first dissolves into NbO_6^{7-} and then into the Lindqvist ion form.

$$K_4Nb_6O_{17} = Nb_6O_{17}^{4-} + 4K^+ \quad (4.11)$$

$$Nb_6O_{17}^{4-} + 4OH^- = Nb_6O_{19}^{8-} + 2H_2O \quad (4.12)$$

$$KNbO_3 + 6OH^- = NbO_6^{7-} + K^+ + 3H_2O \quad (4.13)$$

$$NbO_6^{7-} + 17H_2O = Nb_6O_{19}^{8-} + 34OH^- \quad (4.14)$$

According to Deblonde et al. (2015a), the interaction between potassium and hexaniobate ions prevents the determination of solubility products of niobium in a potassium medium. These interactions may alter the free ions concentration and change the equilibrium of the solution. The formation of ion pairs has an important influence on the determination of solubility. There is a lack of literature concerning the mechanisms of the formation of niobate complexes in aqueous solutions.

4.4 Conclusions

In this study we have investigated the solubility of niobic acid and potassium niobate under alkaline conditions experimentally and supported by the thermodynamic modeling from OLI Studio Stream Analyser.

The use of UV-Vis as method of quantification of niobium in equilibrium study of niobic acid shows that the hexaniobates may not be the only complexes formed during the reaction with KOH and that depends on the stability of polyoxoniobates in the solution.

A change in the structure of niobic acid occurs after 100 hours of reaction and the presence of hexaniobate was confirmed by the characterization of the remained solid.

The solubility of niobic acid measured by Crystal 16 shows a slight decrease in the dissolution of the solid with increase in KOH concentration – from 0 to 2 mol/L KOH at 20 to 70 ºC. The strong interaction of K^+ ions with hexaniobate ions may increases the solubility of niobic acid up to a certain minimum concentration of KOH.

The pseudo-solubility of a mixed-phases potassium niobate increases with temperature but decreases with the increase of KOH concentration, e.g., at 40 ºC, for example, the solubility of potassium niobate is 11.5 g/L in 1 mol/L KOH and 80.5 g/L in 0.10 mol/L KOH. The presence of the metastable phase $K_4Nb_6O_{17}$ suggests that the mixed phases exhibit higher solubility compared to the predictions of thermodynamic modeling for the stable phase $KNbO_3$.

The results from this study help address the gap in the literature of aqueous solubility of niobium compounds under alkaline conditions and highlight the importance of solubility data of niobium for the development of hydrometallurgical process.

4.5 References

Alves, A.R., Dos Reis Coutinho, A., 2015. The evolution of the niobium production in Brazil. Mater. Res. 18, 106–112. https://doi.org/10.1590/1516-1439.276414

Amini, M.M., Mirzaee, M., 2009. Effect of solvent and temperature on the preparation of potassium niobate by hydrothermal-assisted sol-gel processing. Ceram. Int. 35, 2367–2372. https://doi.org/10.1016/j.ceramint.2009.01.009

Antonio, M.R., Nyman, M., Anderson, T.M., 2009. Direct observation of contact ion-pair formation in aqueous solution. Angew. Chemie - Int. Ed. 48, 6136–6140. https://doi.org/10.1002/anie.200805323

Bai, S., Zhang, F., Karaki, T., Adachi, M., 2011. Effect of surfactants on morphology of niobate hydrate particles in hydrothermal synthesis. Jpn. J. Appl. Phys. 50, 1–5. https://doi.org/10.1143/JJAP.50.09ND12

Bai, S., Zhang, J., Chen, Z., Wang, Y., Hong, M., Karaki, T., 2017a. Near-room-

temperature synthesis of niobate hydrate particles with hexagonal-platelike morphologies. Mater. Chem. Phys. 199, 230–238. https://doi.org/10.1016/j.matchemphys.2017.06.048

Bai, S., Zhang, J., Chen, Z., Wang, Y., Hong, M., Karaki, T., 2017b. Near-room-temperature synthesis of niobate hydrate particles with hexagonal-platelike morphologies. Mater. Chem. Phys. 199, 230–238. https://doi.org/10.1016/j.matchemphys.2017.06.048

Bakry, M., Li, J., Zeng, X., 2023. Evaluation of global niobium flow modeling and its market forecasting. Front. Energy 17, 286–293. https://doi.org/10.1007/s11708-022-0823-y

Baktash, A., Amiri, O., Saadat, M., 2020. High efficient perovskite solar cells base on niobium doped TiO2 as a buffer layer. J. Nanostructures 10, 119–127. https://doi.org/10.22052/JNS.2020.01.013

Brandão, R.F., Quirino, R.L., Mello, V.M., Tavares, A.P., Peres, A.C., Guinhos, F., Rubim, J.C., Suarez, P.A.Z., 2009. Synthesis, characterization and use of Nb2O5 based catalysts in producing biofuels by transesterification, esterification and pyrolysis. J. Braz. Chem. Soc. 20, 954–966. https://doi.org/10.1590/S0103-50532009000500022

Bruziquesi, C.G.O., Balena, J.G., Pereira, M.C., Silva, A.C., Oliveira, L.C.A., 2019. Niobium: A strategic chemical element for brazil. Quim. Nova 42, 1184–1188. https://doi.org/10.21577/0100-4042.20170442

C. K. Gupta & A. K. Suri, 1994. Extractive Metallurgy of Niobium. Taylor & Francis Group.

Cao, Y., Zhu, K., Qiu, J., Pang, X., Ji, H., 2012. Sol-gel processing and characterization of potassium niobate nano-powders by an EDTA/citrate complexing method. Solid State Sci. 14, 655–660. https://doi.org/10.1016/j.solidstatesciences.2012.03.011

Čekerevac, M., Simičić, M., Bujanović, L.N., Popović, N., 2012. The influence of silicate and sulphate anions on the anodic corrosion and the transpassivity of iron and silicon-rich steel in concentrated KOH solution. Corros. Sci. 64, 204–212. https://doi.org/10.1016/j.corsci.2012.07.019

Chan, X., Pu, T., Chen, X., James, A., Lee, J., Parise, J.B., Kim, D.H., Kim, T., 2017. Effect of niobium oxide phase on the furfuryl alcohol dehydration. Catal. Commun. 97, 65–69. https://doi.org/10.1016/j.catcom.2017.04.019

Chandel, R., Jindal, S., 2023. Fabrication technique of smart ferroelectric materials and its applications. AIP Conf. Proc. 2735. https://doi.org/10.1063/5.0140223

Chen, Y., Wang, Z., Liu, S., Zhang, G., 2022. Modified niobic acid via acidification by various liquid acids for dehydration of succinic acid to succinic anhydride. Colloids Surfaces A Physicochem. Eng. Asp. 650, 129644. https://doi.org/10.1016/j.colsurfa.2022.129644

Cheng, X., Zhu, H., Yu, H., Ye, W., Zheng, R., Liu, T., Peng, N., Shui, M., Shu, J., 2018. K2Nb8O21 nanotubes with superior electrochemical performance for ultrastable lithium storage. J. Mater. Chem. A 6, 8620–8632. https://doi.org/10.1039/c8ta01411f

De Andrade, J.S., Pinheiro, A.G., Vasconcelos, I.F., De Araújo, M.A.B., Valente, M.A., Sombra, A.S.B., 2000. Structural studies of KNbO3 in niobate glass-ceramics. J. Phys. Chem. Solids 61, 899–906. https://doi.org/10.1016/S0022-3697(99)00387-X

De Cock, B., Delaunay, N., Deblonde, G., Bosi, V., Pasti, L., Mangelings, D., Vander Heyden, Y., 2017. Kinetic study of niobium and tantalum hexameric forms and their substituted ions by capillary electrophoresis in alkaline medium. Talanta 175, 127–134. https://doi.org/10.1016/j.talanta.2017.07.025

Deblonde, G.J.P., Bengio, D., Beltrami, D., Bélair, S., Cote, G., Chagnes, A., 2019. A fluoride-free liquid-liquid extraction process for the recovery and separation of niobium and tantalum from alkaline leach solutions. Sep. Purif. Technol. 215, 634–643. https://doi.org/10.1016/j.seppur.2019.01.052

Deblonde, G.J.P., Chagnes, A., Bélair, S., Cote, G., 2015a. Solubility of niobium(V) and tantalum(V) under mild alkaline conditions. Hydrometallurgy 156, 99–106. https://doi.org/10.1016/j.hydromet.2015.05.015

Deblonde, G.J.P., Chagnes, A., Roux, M.A., Weigel, V., Cote, G., 2016a. Extraction of Nb(v) by quaternary ammonium-based solvents: toward organic hexaniobate systems. Dalt. Trans. 45, 19351–19360. https://doi.org/10.1039/C6DT03873E

Deblonde, G.J.P., Chagnes, A., Weigel, V., Cote, G., 2016b. Direct precipitation of niobium and tantalum from alkaline solutions using calcium-bearing reagents. Hydrometallurgy 165, 345–350. https://doi.org/10.1016/j.hydromet.2015.12.009

Deblonde, G.J.P., Coelho-Diogo, C., Chagnes, A., Cote, G., Smith, M.E., Hanna, J. V., Iuga, D., Bonhomme, C., 2016c. Multinuclear Solid-State NMR Investigation of Hexaniobate and Hexatantalate Compounds. Inorg. Chem. 55, 5946–5956. https://doi.org/10.1021/acs.inorgchem.6b00345

Deblonde, G.J.P., Delaunay, N., Lee, D., Chagnes, A., Cote, G., Gareil, P., 2015b. First investigation of polyoxoniobate and polyoxotantalate aqueous speciation by capillary zone electrophoresis. RSC Adv. 5, 64119–64124. https://doi.org/10.1039/c5ra11521c

Deblonde, G.J.P., Moncomble, A., Cote, G., Bélair, S., Chagnes, A., 2015c. Experimental and computational exploration of the UV-visible properties of hexaniobate and hexatantalate ions. RSC Adv. 5, 7619–7627. https://doi.org/10.1039/c4ra14866e

Deblonde, G.J.P., Weigel, V., Bellier, Q., Houdard, R., Delvallée, F., Bélair, S., Beltrami, D., 2016d. Selective recovery of niobium and tantalum from low-grade concentrates using a simple and fluoride-free process. Sep. Purif. Technol. 162, 180–187. https://doi.org/10.1016/j.seppur.2016.02.025

Dolganova, I., Bosch, F., Bach, V., Baitz, M., Finkbeiner, M., 2020. Life cycle assessment of ferro niobium. Int. J. Life Cycle Assess. 25, 611–619. https://doi.org/10.1007/s11367-019-01714-7

Etxebarria, N., Fernandez, L.A., Madariaga, J.M., 1994. On the hydrolysis of niobium(V) and tantalum(V) in 3mol/dm3 KCl at 25ºC. PART 1: Construction of a thermodynamic model for Nb(V). J. Chem. Soc. Dalt. Trans. 3055–3059.

Eysseltová, J., Bouaziz, R., 2012. IUPAC-NIST Solubility Data Series. 93. Potassium Sulfate in Water. J. Phys. Chem. Ref. Data 41. https://doi.org/10.1063/1.3679678

Fan, W., Zhang, Q., Deng, W., Wang, Y., 2013. Niobic acid nanosheets synthesized by a simple hydrothermal method as efficient Brønsted acid catalysts. Chem. Mater. 25, 3277–3287. https://doi.org/10.1021/cm400192q

Feizpour, M., Barzegar Bafrooei, H., Hayati, R., Ebadzadeh, T., 2014. Microwave-

assisted synthesis and sintering of potassium sodium niobate lead-free piezoelectric ceramics. Ceram. Int. 40, 871–877. https://doi.org/10.1016/j.ceramint.2013.06.081

Filella, M., May, P.M., 2020. The aqueous solution thermodynamics of niobium under conditions of environmental and biological interest. Appl. Geochemistry 122, 104729. https://doi.org/10.1016/j.apgeochem.2020.104729

Galutskiy, V. V., Ivashko, S.S., Stroganova, E. V., 2020. Growth of lithium niobate and potassium niobate single crystals using the Czochralski method with liquid and ceramic charging. Solid State Sci. 108, 106355. https://doi.org/10.1016/j.solidstatesciences.2020.106355

Gasik, M., Bizhanov, V., Dashevskii, A., 2020. Ferroalloys - Theory and Practice.

Guo, C., Qian, Z., 1993. Acidic and catalytic properties of niobic acid crystallized at low temperature. Catal. Today 16, 379–385. https://doi.org/10.1016/0920-5861(93)80077-E

Guo, Z., Liu, L., Hou, Z., Wang, Y., Yu, J., Jiang, H., 2020. Fabrication of K2Nb8O21 microcrystalline with good dispersion by molten salt synthesis. Ferroelectrics 554, 197–203. https://doi.org/10.1080/00150193.2020.1705111

Hagelüken, C., 2014. Recycling of (critical) metals, 1st ed, Critical Metals Handbook. John Wiley & Sons, Ltd. https://doi.org/10.1002/9781118755341.ch3

Hajdara, I., Lengyel, K., Kovács, L., Péter, Á., Szaller, Z.S., 2012. Effect of alkali doping on the Raman spectra of potassium lithium niobate crystals. Ferroelectrics 428, 57–63. https://doi.org/10.1080/00150193.2012.675271

Hayashi, H., Hakuta, Y., & Kurata, Y., 2004. Hydrothermal synthesis of potassium niobate photocatalysts under subcritical and supercritical water conditions. Mater. Chem. 14, 2046–2051. https://doi.org/10.1039/b400130n

Heisterkamp, F., Carneiro, T., 2001. Niobium: Future possibilities - Technology and the market place. Niobium, Sci. Technol. 1109–1159.

Hughes, M.A., 1964. Thermal studies on niobium compounds. I. Niobic acid and some niobic acid/amine derivatives. J. Less-Common Met. 6, 232–238. https://doi.org/10.1016/0022-5088(64)90104-3

Jehng, J. -M, Wachs, I.E., 1991. Niobium oxide solution chemistry. J. Raman Spectrosc. 22, 83–89. https://doi.org/10.1002/jrs.1250220207

Jo, Y., Garbev, K., Çevirim-Papaioannou, N., Blanco, O.D., de Blochouse, B., Altmaier, M., Gaona, X., 2022. Solubility of niobium(V) in cementitious systems relevant for nuclear waste disposal: Characterization of the solubility-controlling solid phases. J. Hazard. Mater. 440, 129810. https://doi.org/10.1016/j.jhazmat.2022.129810

Kanie, K., Numamoto, Y., Tsukamoto, S., Takahashi, H., Mizutani, H., Terabe, A., Nakaya, M., Tani, J., Muramatsu, A., 2011. Hydrothermal synthesis of sodium and potassium niobates fine particles and their application to lead-free piezoelectric material. Mater. Trans. 52, 2119–2125. https://doi.org/10.2320/matertrans.M2011148

Kaseda, K., Takesue, M., Aida, T.M., Watanabe, M., Hayashi, H., Smith, R.L., 2011. Restructuring mechanism of NbO6 octahedrons in the crystallization of KNbO3 in supercritical water. J. Supercrit. Fluids 58, 279–285. https://doi.org/10.1016/j.supflu.2011.06.009

Klemperer, W.G., Marek, K.A., 2013. An 17O NMR study of hydrolyzed NbV in weakly acidic and basic aqueous solutions. Eur. J. Inorg. Chem. 28, 1762–1771. https://doi.org/10.1002/ejic.201201231

Kong, X., Hu, D., Wen, P., Ishii, T., Tanaka, Y., Feng, Q., 2013. Transformation of potassium Lindquist hexaniobate to various potassium niobates: Solvothermal synthesis and structural evolution mechanism. Dalt. Trans. 42, 7699–7709. https://doi.org/10.1039/c3dt00062a

Korzhinskaya, V.S., Kotova, N.P., Shapovalov, Y.B., 2017. Experimental study of natural pyrochlore and niobium oxide solubility in Alkaline hydrothermal solutions. Dokl. Earth Sci. 475, 793–796. https://doi.org/10.1134/S1028334X17070157

Kotova, N.P., 2012. Experimental study of concentration dependence of niobium oxide solubility in fluoride solutions at T=550oC, P=500 bar and low oxygen fugacity (Co–CoO buffer). Vestn. Otd. Nauk Zemle 4, 1–3. https://doi.org/10.2205/2012NZ

Kotova, N.P., 2011. Experimental study of concentration dependence of Ta2O5 and Nb2O5 solubility in the alkaline and carbonate solutions at T=550oC, P=500 bar and

low oxygen fugacity (Co-CoO buffer). Vestn. Otd. Nauk o Zemle RAN 3, 1–7. https://doi.org/10.2205/2011nz000185

Kudo, K., Kakiuchi, K., Mizutani, K., Fukami, T., Hoshikawa, K., 2004. Non-stoichiometry in potassium niobate crystals grown by directional solidification. J. Cryst. Growth 267, 150–155. https://doi.org/10.1016/j.jcrysgro.2004.03.032

Labinger, J.A., 1982. Niobium and Tantalum, in: Niobium and Tantalum. pp. 705–782.

Leal Marchena, C., Saux, C., Dinamarca, R., Pecchi, G., Pierella, L., 2016. Alkaline niobates ANbO3 (A = Li, Na, K) as heterogeneous catalysts for dipropyl sulfide oxidation. RSC Adv. https://doi.org/10.1039/c6ra21749d

Lebarbier, V., Houalla, M., Onfroy, T., 2012. New insights into the development of Bronsted acidity of niobic acid. Catal. Today 192, 123–129. https://doi.org/10.1016/j.cattod.2012.02.061

Lothenbach, B., Ochs, M., Wanner, H., Mikazu, Y., 1999. Thermodynamic Date for the Speciation and Solubility of Pd,Pb,Sn,Sb,Nb,and Bi in Aqueous Solution.

Lü, X., Mou, X., Wu, J., Zhang, D., Zhang, L., Huang, F., Xu, F., Huang, S., 2010. Improved-Performance Dye-Sensitized solar cells using Nb-Doped TiO 2 electrodes: Efficient electron Injection and transfer. Adv. Funct. Mater. 20, 509–515. https://doi.org/10.1002/adfm.200901292

Lübke, M., Sumboja, A., Johnson, I.D., Brett, D.J.L., Shearing, P.R., Liu, Z., Darr, J.A., 2016. High power nano-Nb2O5 negative electrodes for lithium-ion batteries. Electrochim. Acta 192, 363–369. https://doi.org/10.1016/j.electacta.2016.01.226

Mackay, D.A.R., Simandl, G.J., 2014. Geology, market and supply chain of niobium and tantalum—a review. Miner. Depos. 49, 1025–1047. https://doi.org/10.1007/s00126-014-0551-2

Mączka, M., Ptak, M., Majchrowski, A., Hanuza, J., 2011. Raman and IR spectra of K4Nb6O17and K 4Nb6O17·3H2O single crystals. J. Raman Spectrosc. https://doi.org/10.1002/jrs.2668

Maiorov, V.G., Nikolaev, A.I., Kopkov, V.K., 2013. Preparation of alkaline Nb(V) solutions using K(I) compounds. Russ. J. Appl. Chem. 86, 108–111.

https://doi.org/10.1134/S1070427213010199

Masoud, M., 2005. Diffusivity and Ionic Conductivity in Lithium Niobate and Related Glasses and Glass Composites. Arbeit.

Nakajima, K., Baba, Y., Noma, R., Kitano, M., N. Kondo, J., Hayashi, S., Hara, M., 2011. Nb2O5•nH2O as a heterogeneous catalyst with water-tolerant lewis acid sites. J. Am. Chem. Soc. 133, 4224–4227. https://doi.org/10.1021/ja110482r

Nico, C., Monteiro, T., Graça, M.P.F., 2016. Niobium oxides and niobates physical properties: Review and prospects. Prog. Mater. Sci. 80, 1–37. https://doi.org/10.1016/j.pmatsci.2016.02.001

Nikolaev, A.I., Kirichenko, N. V., Maiorov, V.G., 2009. Niobium, tantalum, and titanium fluoride solutions. Russ. J. Inorg. Chem. 54, 505–511. https://doi.org/10.1134/S0036023609040032

Nikolay, T., Larina, L., Shevaleevskiy, O., Ahn, B.T., 2011. Electronic structure study of lightly Nb-doped TiO2 electrode for dye-sensitized solar cells. Energy Environ. Sci. 4, 1480–1486. https://doi.org/10.1039/c0ee00678e

Niu, J., Pengtao, M., Niu, H., Li, J., Zhao, J., Song, Y., Wang, J., 2007. Giant polyniobate clusters based on [Nb7O22] 9- Units derived from a Nb6O19 precursor. Chem. - A Eur. J. 13, 8739–8748. https://doi.org/10.1002/chem.200700612

Noseck, U., Becker, D., Flügge, J., Fah-, C., Herbert, H., Kull, H., Meleshyn, A., Wolf, J., 2021. Scientific basis for a safety case of deep geological repositories.

Nyman, M., 2011. Polyoxoniobate chemistry in the 21st century. Dalt. Trans. 40, 8037–8248.

Nyman, M., Alam, T.M., Bonhomme, F., Rodriguez, M.A., Frazer, C.S., Welk, M.E., 2006. Solid-state structures and solution behavior of alkali salts of the [Nb6O19]8- Lindqvist ion. J. Clust. Sci. 17, 197–219. https://doi.org/10.1007/s10876-006-0049-x

Ozmen, O., Ozsoy-Keskinbora, C., Suvaci, E., 2018. Chemical stability of KNbO3, NaNbO3, and K0.5Na0.5NbO3 in aqueous medium. J. Am. Ceram. Soc. 101, 1074–1086. https://doi.org/10.1111/jace.15291

Park, G., Gunawardhana, N., Lee, C., Lee, S.M., Lee, Y.S., Yoshio, M., 2013. Development of a novel and safer energy storage system using a graphite cathode and Nb2O5 anode. J. Power Sources 236, 145–150. https://doi.org/10.1016/j.jpowsour.2012.10.102

Patat, S., Rahman, S., Dokan, F.K., 2022. The effect of sodium and niobium co-doping on electrochemical performance of Li4Ti5O12 as anode material for lithium-ion batteries. Ionics (Kiel). 28, 3177–3185. https://doi.org/10.1007/s11581-022-04579-3

Peiffert, C., Nguyen-Trung, C., Palmer, D.A., Laval, J.P., Giffaut, E., 2010. Solubility of B-Nb2O5 and the hydrolysis of niobium(V) in aqueous solution as a function of temperature and ionic strength. J. Solution Chem. 39, 197–218. https://doi.org/10.1007/s10953-010-9495-z

Petrus, E., Segado-Centellas, M., Bo, C., 2022. Computational Prediction of Speciation Diagrams and Nucleation Mechanisms: Molecular Vanadium, Niobium, and Tantalum Oxide Nanoclusters in Solution. Inorg. Chem. 1–13. https://doi.org/10.1021/acs.inorgchem.2c00925

Philip A. Schweitzer, P.E., 2003. METALLIC MATERIALS: Physical, mechanical and corrosion properties, Marcel Dekker, Inc. https://doi.org/10.1201/9781315177281-4

Piskin, C., Karacasulu, L., Bortolotti, M., Vakifahmetoglu, C., 2021. Synthesis of potassium–sodium niobate (KNN) from NbO2. Open Ceram. 7, 100159. https://doi.org/10.1016/j.oceram.2021.100159

Prasetyoko, D., Ramli, Z., Endud, S., Nur, H., 2008. Characterization and catalytic performance of niobic acid dispersed over titanium silicalite. Res. Lett. Mater. Sci. 2008. https://doi.org/10.1155/2008/345895

Qiu, J., Li, X., Qi, X., 2019. Raman Spectroscopic Investigation of Sulfates Using Mosaic Grating Spatial Heterodyne Raman Spectrometer. IEEE Photonics J. 11, 1. https://doi.org/10.1109/JPHOT.2019.2939222

Santandrea, R., Brasil, S.L.D.C., Reznik, L.Y., Carvalho, L.J., 2018. Estudo dos diagramas E-pH aplicados a revestimentos à base de pentóxido de nióbio. Intercorr

2018 10.

Santos, I.C.M.S., Loureiro, L.H., Silva, M.F.P., Cavaleiro, A.M.V., 2002. Studies on the hydrothermal synthesis of niobium oxides. Polyhedron 21, 2009–2015. https://doi.org/10.1016/S0277-5387(02)01136-1

Sasidharan, M., Gunawardhana, N., Yoshio, M., Nakashima, K., 2012. Nb2O5 hollow nanospheres as anode material for enhanced performance in lithium ion batteries. Mater. Res. Bull. 47, 2161–2164. https://doi.org/10.1016/j.materresbull.2012.06.004

Souza, C. R., da Silva, L. M., Penha, F. M., Rocha, S. D. F. Crystallization-based recovery of niobium compounds from alkaline liquor, Sep. & Purif. Tech., v. 360 (2), 2025, 131085, https://doi.org/10.1016/j.seppur.2024.131085.

Souza, R.M.F. de, Fernandes, L.E., Guerra, W., 2013. Nióbio. Química Nov. na Esc. 35, 68–69.

Tanabe, K., 1987. Niobic acid as an unusual acidic solid material. Mater. Chem. Phys. 17, 217–225. https://doi.org/10.1016/0254-0584(87)90057-5

Theresa Von Rennenberg, 2359. Towards a circular economy of critical raw materials: The case of niobium.

Timofeev, A., 2018. Department of Earth and Planetary Sciences, McGill University, The Solubility, Speciation, and Transport of the High Field Strength Elements (HFSE) Niobium, Tantalum, and Uranium. Montreal, Canada.

Uekawa, N., Kudo, T., Mori, F., Wu, Y.J., Kakegawa, K., 2003. Low-temperature synthesis of niobium oxide nanoparticles from peroxo niobic acid sol. J. Colloid Interface Sci. 264, 378–384. https://doi.org/10.1016/S0021-9797(03)00460-0

USGS, 2017. Zirconium and Hafnium Chapter V of Critical Mineral Resources of the United States — Economic and Environmental Geology and Prospects for Future Supply Professional Paper 1802 – V U . S . Department of the Interior. U.S. Geol. Surv. Prof. Pap. 1802, Prep. by Jones, J.V., Piatak, N.M., Bedinger, G.M. V1–V26, Reston, Virginia.

Wang, X., Jia, Y., Ma, S., Zheng, S., Sun, Q., 2018. Effect of mechanical activation on

the leaching kinetics of niobium-bearing mineralisation in KOH hydrothermal system. Hydrometallurgy 181, 123–129. https://doi.org/10.1016/j.hydromet.2018.08.012

Wang, X., Zheng, S., Xu, H., Zhang, Y., 2009. Leaching of niobium and tantalum from a low-grade ore using a KOH roast-water leach system. Hydrometallurgy 98, 219–223. https://doi.org/10.1016/j.hydromet.2009.05.002

Wang, Y., Yi, Z., Li, Y., Yang, Q., Wang, D., 2007. Hydrothermal synthesis of potassium niobate powders. Ceram. Int. 33, 1611–1615. https://doi.org/10.1016/j.ceramint.2006.07.013

Yang, D., Wang, Y., Chen, C., Su, Y., Li, L., Miao, L., Gu, H., Zhao, W., Ding, L., Hu, D., 2023. Oriented Plate-like KNbO3 Polycrystals: Topochemical Mesocrystal Conversion and Piezoelectric and Photocatalytic Responses. Inorg. Chem. 62, 10408–10419. https://doi.org/10.1021/acs.inorgchem.3c01286

Ye, Y., Chen, C., Feng, H., Zhou, J., Ma, J., Chen, J., Yuan, J., Kong, L., Qian, Z., 2013. Visible photoluminescence of polyoxoniobates in aqueous solution and their high electrocatalytic activities for water oxidation. Open J. Inorg. Chem. 03, 59–69. https://doi.org/10.4236/ojic.2013.33009

Yi, T.F., Sari, H.M.K., Li, Xuezhong, Wang, F., Zhu, Y.R., Hu, J., Zhang, J., Li, Xifei, 2021. A review of niobium oxides based nanocomposites for lithium-ion batteries, sodium-ion batteries and supercapacitors. Nano Energy 85, 105955. https://doi.org/10.1016/j.nanoen.2021.105955

Zhou, H., Zheng, S., Zhang, Y., 2005. Leaching of a low-grade niobium-tantalum ore by highly concentrated caustic potash solution. Hydrometallurgy 80, 83–89. https://doi.org/10.1016/j.hydromet.2005.07.006

Zhou, H.M., Yi, D.Q., Zhang, Y., Zheng, S.L., 2005a. The dissolution behavior of Nb2O5, Ta2O5 and their mixture in highly concentrated KOH solution. Hydrometallurgy 80, 126–131. https://doi.org/10.1016/j.hydromet.2005.07.010

Zhou, H.M., Zheng, S.L., Zhang, Y., Yi, D.Q., 2005b. A kinetic study of the leaching of a low-grade niobium-tantalum ore by concentrated KOH solution. Hydrometallurgy 80, 170–178. https://doi.org/10.1016/j.hydromet.2005.06.011

CHAPTER 5 – COOLING CRYSTALLIZATION OF POTASSIUM NIOBATE IN AQUEOUS MEDIUM UNDER MILD CONDITION OF TEMPERATURE AND PRESSURE

5.1 Introduction

Crystallization is one of the major unit operations of a chemical process in which a dispersed solid phase is formed from a continuous homogeneous phase. It involves a complex variety of conditions such as nucleation, crystal growth, fluid dynamics, agglomeration, mass transfer, supersaturation and diverse solid and liquid properties (Nývlt et al., 2001; Lewis et al., 2015; Chabanon et al., 2016). Due to its versatility, crystallization is frequently used in industry, in many sectors, to obtain high-purity products, to recover raw materials and to maximise water reuse (Souza et al., 2021; Ibis et al., 2021; Penha et al., 2018, 2019, 2020 2021a, 2021b; Zago et al., 2019; Rocha et al., 1995, 2004).

It is a process governed by the creation of a driving force in solution – the supersaturation – which is based on the concentration of the solute in the medium and its solubility in the prevailing temperature and pressure. Supersaturation is the most important variable in the crystallization and affects all the mechanisms of the process and the rate in which they occur. Crystals are created when nuclei are formed and grow, and kinetics play a role important in this process. The system must be supersaturated for nucleation and crystal growth happen. This supersaturation can be generated by diverse forms, mainly a change the temperature, removing a solvent and/or by adding a precipitant agent.

In this chapter the cooling crystallization of potassium niobate was studied. The saturated solution subjected to cooling induces the nucleation and growth of crystallites of the dissolved substances. Different variables such as initial concentration of liquor and rate of cooling were evaluated. Moreover, the crystallization of potassium niobate from an alkaline liquor was carried out at atmospheric pressure, distinct of the majority studies in literature.

Potassium niobate in its most stable phase – $KNbO_3$ – is a perovskite-type compound and its crystalline structure, cubic, tetragonal, orthorhombic, and rhombic, depend on the

temperature of synthesis. At atmospheric temperature and pressure, potassium niobate has an orthorhombic structure, being tetragonal at 225 °C and cubic near 435 °C (Wood, 1951). These properties may influence the behaviour of this compound in aqueous media.

Due to its piezoelectric and photorefractive properties, potassium niobate has several applications. Associated to its structure, potassium niobate is an interesting material for the study of ferroelectric phase transitions, because it undergoes a cubic–tetragonal–orthorhombic–rhombohedral phase change sequence (Hewat, 1973), where the orthorhombic crystals have piezoelectric properties (Komatsu et al., 2001); and as a material to substitute lead zirconate titanate (PZT) (Kanie et al., 2011) – currently the main material used for piezoelectric applications. There are also considerable applications for potassium niobate in ceramics and glasses (Amini and Sacks, 1991; Bai et al., 2017; De Andrade et al., 2000).

Besides this, potassium niobate oxides have been studied for their photocatalytic properties, especially the $K_4Nb_6O_{17}$ due to their anisotropic structure (Zhou et al., 2014). However, due to large bandgap, the potassium niobate has no photocatalytic activity under visible light irradiation (Zhou et al., 2014). The $K_4Nb_6O_{17}$ structure is composed of significantly distorted octahedra with N=O bonds that is oriented toward the interior of the lamellar region and slightly distorted octahedra with Nb-O bonds deformed toward the interior of the lamellar region, producing distinct characteristics.

Alkaline Leaching of the niobium ores, soluble potassium niobate can be obtained. According to Reisman and Holtzberg, (1955), the study of equilibrium interactions of the M_2O-Nb_2O_5 (M=K, Na) has problems that involves the metastable fields formation and the dissimilarity between the aqueous (aq) and anhydrous (s) systems. Depending on the synthesis path of niobate, its crystallization could involve the formation of metastable phases which are later changed to the most stable phase.

A soluble metastable phase may be formed before the final stable phase is founded. For example, K_2NbO_4 can be hydrolyzed to $K_8Nb_6O_{19}.nH_2O$ followed by the formation of the more stable and insoluble $KNbO_3$ (Wang et al., 2009; H. Zhou et al., 2005; H. M. Zhou et al., 2005) . According to Hayashi et al., (2004) and Magrez et al. (2006), $K_4Nb_6O_{17}$ is a metastable phase which processes a layered structure consisting of $(Nb_6O_{17})^{-4}$ layers and interlayers of K^+ ions. The KNb_3O_8 structure is formed by two Nb_2O_{10} octahedra units

separated by NbO_6 octahedra that is connected by its vertices and by K ions with distinct K-O distances.

The synthesis of potassium niobate particles has been studied by many methods, such as the sol-gel method, microwave-assisted method and the hydrothermal method, as shown in Table 5.1. The sol-gel method needs complex chemicals and the microwave-assisted method has interesting advantages, especially regarding lower energy consumption and control of reaction time. Nevertheless, the hydrothermal method is better understood and commonly used. In general, wet chemical methods such as hydrothermal, sol-gel and solvothermal can produce small particles.

Table 5.1. Studies about the synthesis of potassium niobate.

Author	*Method*	*Reagents*			*Product*			
Yang et al., 2023	Solvothermal	Nb_2O_5	KOH		$KNbO_3$	$K_4Nb_6O_{17}$		
Kong et al., 2013	Solvothermal	Nb_2O_5	KOH		$KNbO_3$	$K_4Nb_6O_{17}$	KNb_3O_8	$K_2Nb_2O_6$
You et al., 2021	Hydrothermal	Nb_2O_5	KOH		$KNbO_3$			
Duarte et al., 2015	Hydrothermal	Nb_2O_5	KOH		$KNbO_3$	$K_4Nb_6O_{17}$	KNb_3O_8	
Vuttivong and Vittayakorn, 2015	Hydrothermal	Nb_2O_5	KOH		$KNbO_3$			
Feizpour et al., 2014	Hydrothermal	Nb_2O_5	K_2CO_3	Na_2CO_3	$(K,Na)NbO_3$			
Ma et al., 2014	Hydrothermal	Nb_2O_5	KOH		$K_4Nb_6O_{17}$			
Bai et al., 2011	Hydrothermal	Nb_2O_5	KOH	NaOH	$KNbO_3$	$NaNbO_3$	$(K,Na)NbO_3$	
Kanie et al., 2011	Hydrothermal	$NbCl_5$	KOH	NaOH	$KNbO_3$	$(K,Na)NbO_3$		
Handoko and Goh, 2010	Hydrothermal	Nb_2O_5	KOH	NaOH	$(K,Na)NbO_3$			
Han et al., 2008	Hydrothermal	Nb_2O_5	KOH		$KNbO_3$	$K_4Nb_6O_{17}$		
Wang et al., 2007	Hydrothermal	Nb_2O_5	KOH		$KNbO_3$			
Magrez et al., 2006	Hydrothermal	Nb_2O_5	KOH		$KNbO_3$			
Simões et al., 2004	Hydrothermal	Nb_2O_5	$C_8H_5KO_4$		KNbO3	$KNbO_3$		
Hayashi et al., 2004	Hydrothermal	Nb_2O_5	KOH	K_2CO_3	$KNbO_3$	$K_4Nb_6O_{17}$		
Liu et al., 2002	Hydrothermal	Nb_2O_5	KOH		$KNbO_3$	$K_4Nb_6O_{17}$	KNb_3O_8	
Lu et al., 1998	Hydrothermal	Nb_2O_5	KOH		$KNbO_3$			
Uchida et al., 1998	Hydrothermal	Nb_2O_5	KOH		$KNbO_3$	$K_4Nb_6O_{17}$		

Cheng et al., 2005	Precipitation	Nb_{ETOX}	K_{ETOX}	H_2O_2	$KNbO_3$	$K_4Nb_6O_{17}$	
Komatsu et al., 2001	Precipitation	Nb_2O_5	K_2CO_3	K_2NbO_3F	$KNbO_3$	K_2NbO_3F	
Vlazan et al., 2017	Sol-gel	NbOxalate	KOH		$KNbO_3$		
Khorrami et al., 2015	Sol-gel	NbOxalate	KNO_3	$NaNO_3$	$KNbO_3$	$NaNbO_3$	$(K,Na)NbO_3$
Cao et al., 2012	Sol-gel	Nb_2O_5	K_2CO_3	EDTA	$KNbO_3$		
Amini and Mirzaee, 2009	Sol-gel	Nb_{ETOX}	K_{ETOX}	Ethanol	$KNbO_3$	$K_4Nb_6O_{17}$	
Tanaka et al., 2007	Sol-gel	Nb_{ETOX}	K_{ETOX}		$KNbO_3$	$K_4Nb_6O_{17}$	
Amini and Sacks, 1991	Sol-gel	Nb_{ETOX}	K_{ETOX}		$KNbO_3$	$K_4Nb_6O_{17}$	$K_2Nb_3O_8$
Raja et al., 2017	Solid-state	Nb_2O_5	K_2CO_3	Ethanol	$KNbO_3$		
Su et al., 2010	Solid-state	Nb_2O_5	K_2CO_3 KNO_3	CH_3COOK HCOOK	$KNbO_3$	$K_4Nb_6O_{17}$	
Lee et al., 2009	Solid-state	Nb_2O_5	K_2CO_3		$K_4Nb_6O_{17}$		

Despite the large amounts of methods to produce potassium niobate, the variation in the structure phase and morphology of the solids, even if the same reagents were used, is a challenging issue. In this sense, the main advantage of the hydrothermal method is the potential to obtain highly purified and homogenized metal oxide powders by controlling the stoichiometry of reagents, temperature, and time of reaction (Kanie et al., 2011).

Han et al. (2008) studied the hydrothermal synthesis of the stable phase of potassium niobate ($KNbO_3$) and the stability of the system K-Nb-H_2O. This study shows the dependence of $KNbO_3$ formation on the temperature, in which the stable phase stabilizes at 250 °C. According to these authors, a high alkaline concentration may promote the formation of $KNbO_3$, while the stability of hexaniobate ion in solution increases in lower KOH concentration medium and temperature. Magrez et al. (2006) also synthesized potassium niobate hydrothermally at 150 °C for 6 days and presented a structural transformation of $Nb_6O_{19}^{8-}$ hexaniobate ions to the perovskite structure of $KNbO_3$, explained by the following reactions. The first one is related to the dissolution of niobium pentoxide (Nb_2O_5) forming $Nb_6O_{19}^{8-}$ hexaniobate Lindqvist ion, where NbO_6 octahedrons share edges. Subsequently, this complex changes into a single octahedron NbO_6^{7-} anions, which function as elementary specie with a NbO_3^- corner-sharing octahedron network for potassium niobate perovskite, according to the reactions (Equation 5.1 – 5.6):

Nb_2O_5 dissolution:

$$Nb_2O_5 + OH^- = Nb_6O_{19}^{8-} + 4\ H_2O \quad (5.1)$$

$KNbO_3$ formation:

$$Nb_6O_{19}^{8-} + 34OH^- = 6NbO_6^{7-} + 17H_2O \quad (5.2)$$

$$NbO_6^{7-} + K^+ + 3H_2O = KNbO_3 + 6OH^- \quad (5.3)$$

$K_4Nb_6O_{17}$ formation:

$$Nb_6O_{19}^{8-} + 2H_2O = Nb_6O_{17}^{4-} + 4OH^- \quad (5.4)$$

$$Nb_6O_{17}^{4-} + K^+ = K_4Nb_6O_{17} \quad (5.6)$$

Several studies show the importance of KOH concentration in the hydrothermal synthesis, that involves heterogeneous chemical reactions in aqueous medium at temperatures higher than 100 ºC and under pressure greater than 1 atm (Kanie et al., 2011; Kong et al., 2013; Uchida et al., 1998; Vuttivong and Vittayakorn, 2015; Wang et al., 2007). These studies have shown that higher KOH concentrations promote the $KNbO_3$ formation and that controlling the KOH concentration influences the particle size distribution. One limitation of this method is the long synthesis time for the complete reaction and formation of the potassium niobate crystals.

Liu et al. (2002) identified that both the KOH concentration and reaction temperature are key factors influencing the final products, with $KNbO_3$ formed in strongly alkaline media (6 – 10 mol/L KOH) and at 120 ºC for 7 days, while $K_4Nb_6O_{17}$ and KNb_3O_8 were produced in moderately and slightly alkaline media (0.5 – 4 mol/L KOH), at 180 ºC for 4 days. In contrast, Vuttivong and Vittayakorn (2015) produced only the KNbO3 via hydrothermal method using 15 mol/L KOH at 150 and 200 ºC for 24 hours. Lu et al. (1998) showed that the amount of Nb_2O_5 used also affects the final product - at higher concentrations of Nb in the aqueous solution the solids present a pseudo cubic crystalline structure.

Bai et al. (2011) explored the hydrothermal synthesis of potassium and sodium niobates and the effect of the use of surfactants on the morphology of the particles. The results show that the use of surfactants like sodium dodecyl benzene sulfonate improved particle growth without altering their strip-like shape. In another study, Bai et al. (2017) produced potassium niobate at lower temperature synthesis (40 to 70 ºC) with the addition of sodium dodecyl benzene sulfonate enhancing the hexagonal morphology of the particles.

Ma et al. (2004) produced $K_4Nb_6O_{17}{\cdot}4.5H_2O$ via hydrothermal method and the increasing the KOH concentration enhances the crystallinity of this phase, which also demonstrated a promising adsorption capacity for Cr (III) ions.

Microwave-assisted synthesis is another effective method for producing potassium niobates, offering shorter reaction times and precise control over the phases formed. Feizpour et al. (2014) evaluated different heating temperatures by this method and showed that higher temperatures increase the crystallinity of niobate solids and increase the particle size. Duarte et al. (2015) also used a microwave-assisted solvothermal

method. They observed that the higher K/Nb ratio could favour the formation of the $KNbO_3$ phase and the adjusted of pH with acetic acid to less basic values promote the formation of metastable phases, such as $K_4Nb_6O_{17}$ and KNb_3O_8.

The sol-gel is a method used to produce inorganic oxides by a preparation of a colloidal dispersion – sol. The gel is characterized as a substance that contains a solid network formed by the establishment of bonds between the particles or the molecular species of the sol (Alves, 2019). Amini and Sacks (1991) synthesized $KNbO_3$ through the hydrolysis of alkoxides at low temperatures and a stable gel was obtained controlling the water concentration. Crystalline phases such as $K_2Nb_3O_8$ and $K_4Nb_6O_{17}$ appear at temperatures higher than 600 °C and $KNbO_3$ formation above 750 °C. Cheng et al. (2005) used potassium and niobium ethoxide solutions with the addition of H_2O_2 under stirring in air and, followed by reflux at 100 °C, to synthesize $KNbO_3$ thin film. It was observed the presence of $K_4Nb_6O_{17}$ with the increase of H_2O_2 addition.

Additionally, Amini and Mirzaee (2009) synthesized $KNbO_3$ and $K_4Nb_6O_{17}$ by hydrothermal-assisted sol–gel processing. They identified a potassium deficient phase formation ($K_4Nb_6O_{17}$) due to the volatility of K_2O during the process in different temperatures. Tanaka et al. (2007), observed that the formation $K_4Nb_6O_{17}$ was related to the existence of the remained dimer in the precursor solutions that became the nuclei of this phase rather than volatilization of K_2O during the heat treatment.

Hayashi et al. (2004) used supercritical and subcritical water conditions to produce potassium niobate, finding that the metastable phase $K_4Nb_6O_{17}$ is formed under subcritical conditions (< 300 °C), and that higher temperatures and longer heating times promote $KNbO_3$ formation. Simões et al. (2004) synthesized thin films of potassium niobate hydrothermally, using potassium biftalate and niobium oxide, achieving acceptable electrical characteristics for applications in switches, non-volatile memories, and surface acoustic wave devices.

The solid-state method was used by Lee et al. (2009), Su et al., (2010) and Raja et al. (2017) to produce potassium niobate as $K_4Nb_6O_{17}$ and $KNbO_3$. This method offers the advantage of high yield quantity and easier processing. However, to successfully produce the potassium niobate, it is necessary to use high temperatures (200 to 1000 ºC) and reaction time.

Among these methods, crystallization by cooling is generally used for substances with moderate to high solubility, when the solubility-temperature curve shows a positively steep and the final crystallizer temperature must be as low as possible to avoid loss of the product in the mother liquor. In addition, a lower rate of crystal growth and heat transfer must be considered for higher liquid viscosity at lower temperatures (Lewis et al., 2015).

By decreasing in the temperature, the supersaturation is created and reduced by the growth of crystals in the solution. Supersaturated solutions are thermodynamically unstable. However, in some specific conditions, their properties can be stable for some time, and the metastable phases may be formed. The main limitation of this method is that the yield is limited by the solubility of the compound at lowest temperature. The control of nucleation is also an issue to achieve the crystal properties and high-quality product.

To improve purity, thermal treatment can be applied to crystallized potassium niobate aiming to remove volatile phases, thermal decomposition and changing the structure into crystalline substances (Campos et al., 2018). Calcination plays a crucial role in determining the structure of the crystal and physicochemical properties of the potassium niobate. The temperature has an important influence in the phase formation, and the structure transition of potassium niobate is related to crystalline transformation in the range of 50 to 500 ºC. The phase transition may occurs following from rhombohedrum or triclinic to orthorrombic, orthorrombic to tetragonal and tetragonal to cubic – from low temperature to high temperature (Wen et al., 2005; You et al., 2021; Zhang et al., 2013).

Several studies also have shown that calcination step favour the formation of crystalline structure of alkali niobates (Amini and Mirzaee, 2009; Cao et al., 2012; Khorrami et al., 2015; Lente, 2015; Pecchi et al., 2013; Raja et al., 2017; Su et al., 2010; Tanaka et al., 2007; Vlazan et al., 2017; Yang et al., 2023; You et al., 2021). Some of these studies found that from 500 ºC a powder of pure $KNbO_3$ can be produced via different approaches wet-chemical methods (Khorrami et al., 2014; Pecchi et al., 2013, Raja et al., 2017, Vlazan et al., 2017, Cao et al., 2012). Khorrami et al (2014) shows by the thermogravimetric analysis of alkali niobates that potassium niobate needs a higher calcination temperature than sodium niobate solids due to the lower chemical reactivity of potassium in comparison with sodium.

Furthermore, one of the difficulties when crystallizing potassium niobate is to control the stoichiometry of potassium and niobium, since the potassium tends to volatilize with the increase of the temperature in the heating process. In case of low temperature of calcination and volatilization of K_2O, the secondary phase $K_4Nb_6O_{17}$ can appear and prevent the crystallization of single-phase $KNbO_3$ (Tanaka et al., 2007, Cao et al., 2012).

In the present study, potassium niobate was crystallized by cooling the alkaline liquor from Fe-Nb alloy fines alkaline leaching (Chapter 3). In this context, this chapter aims to investigate the parameters for cooling crystallization of potassium niobate in atmospheric pressure, and the chemical composition and morphology of the obtained solids. To this end, the initial concentration of the alkaline liquor was evaluated, and different cooling rates were carried out (0.1, 0.5 and 1 ºC/min) to understand their influence on the chemical composition, morphology and kinetic in potassium niobate crystallization. Characterization of all obtained solids was also performed.

5.2 Materials and methods

5.2.1 Reagents

Fe-Nb alloy fines (< 106 μm) were used as the starting material to produce the alkaline liquor. The alkaline liquor was produced according to experimental procedure presented in Chapter 3, section 3.3.2. Analytical-grade $KOH_{(s)}$ (85%, CAS: 1310-58-3) was used without further purification in all experiments. Solutions were prepared with distilled or Milli Q water.

5.2.2 Potassium niobate crystallization from alkaline liquor

The initial concentration of Nb and K in the alkaline liquor was evaluated at different temperatures by removal of water of the liquor. The alkaline liquor was evaporated at 100 °C and kept in boiling until 60, 40 and 20 wt% removal of water from the initial volume, and the liquor was cooled until 15 and 30 °C for each concentration, as shown in Figure 5.1:

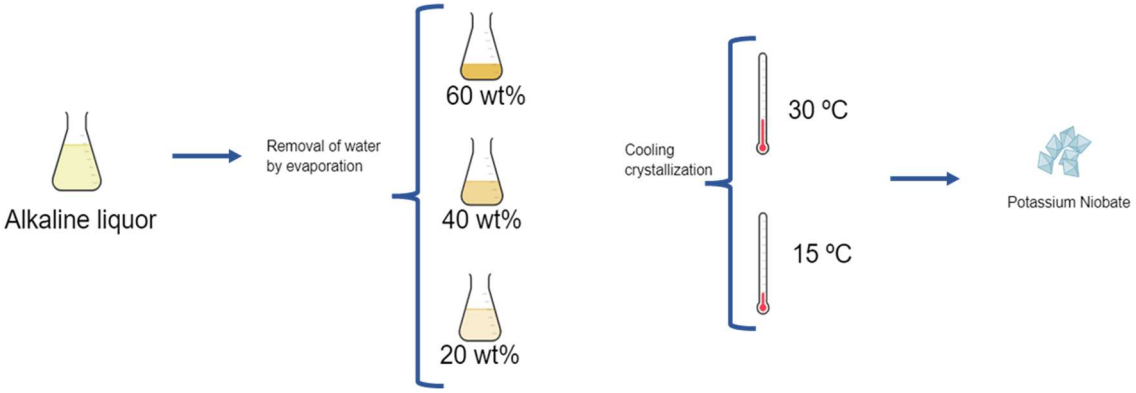

Figure 5.1. Crystallization of potassium niobate steps from removal of water by evaporation and cooling crystallization in different conditions.

The experimental apparatus for the crystallization of potassium niobate was described in Chapter 3, section 3.2.3. The temperature was controlled with the circulation of water into the jacketed reactor with a thermostatic bath (Solid Steel SSD). The liquor was kept under stirring at 300 rpm at a cooling rate of 0.45 ± 0.05 °C/min. The initial temperature of the liquor was 100 ºC and when the final temperature was achieved, the solution was kept at constant temperature and stirring for 1 hour. The solids obtained were vacuum filtered on a quantitative strip filter paper and dried at 60 ºC for 12 hours prior to analysis.

5.2.3 Evaluation cooling rate in the crystallization of potassium niobate

Table 5.2 shows the conditions used to investigate the influence of cooling rate on crystallization of potassium niobate. An aqueous solution was prepared using the previously crystallized potassium niobate. The concentration was determined according to the solubility data from Crystal 16 (see Chapter 4).

Table 5.2. Experimental conditions used for cooling crystallization of potassium niobate.

Experimental conditions	
Cooling rate	0.1, 0.5 and 1.0 °C/min
Initial temperature	80 ºC
Final temperature	30 ºC
Solubility of potassium niobate in water – Crystal 16 data	
Concentration	338.5 g/L
Temperature	70 ºC

The crystallization was carried out by cooling the solution of potassium niobate in a reactor with 250 mL of capacity. The temperature was controlled with the circulation of water into the jacketed reactor with a thermostatic bath (Julabo FP 50). The solution was heated at 80 ºC for 1 hour to the dissolution of potassium niobate and then cooled at the desired cooling rate until 30 °C. When the temperature of 30 ºC was achieved, the crystallization process was maintained for 24 hours. The solution was kept under stirring at 200 rpm. Samples were taken during the experiments to monitor the concentration of Nb and K. The solids were centrifuged and dried at 60 ºC for 12 hours prior to analysis.

5.2.4 Supersaturation index

The supersaturation of the system during the crystallization was calculated from the chemical solution composition measurements using the Equation 5.7:

$$S = \frac{c}{c_{eq}} \tag{5.7}$$

Where S is the supersaturation, c the concentration in the solution and c_{eq} the equilibrium concentration (solubility), with 1 representing the saturation state. The solubility data was given by OLI and Crystal 16 curves.

5.2.5 Thermal conversion

Potassium niobate was calcined in a furnace (Carbolite CWF1200) at 500 to 900 ºC for 2 hours in a heating rate of 5 ºC/min to evaluate the thermal conversion in the crystalline structure of the solids, as presented in Table 5.3.

Table 5.3. Calcination of crystallized potassium niobate (Rate of heating: 5ºC/min for 2 hours).

Temperature (°C)	Initial mass (g)	Final mass (g)	Loss (%)
500	0.6355	0.6135	3
600	0.7686	0.7177	7
700	0.6458	0.6013	7
800	0.6070	0.5574	8
900	0.7281	0.6523	10

5.2.6 Physico-chemical characterization

The chemical composition of the aqueous solutions was determined by ICP-OES (Perkin Elmer - Optima 7300DV and Thermo Scientific - iCAP 7000 Series). The detection limits were < 0.005 mol/L.X-ray diffraction was carried out to identify the crystalline phases in solids using the PHILIPS equipment (XRD PANalytical and PANalytical, X'Pert Pro) both with a Cu (Kα) radiation.

The chemical composition of the solids was analysed by X-ray fluorescence spectrometer with wavelength dispersion (WDXRF - ARL PERFORM'X - Thermo Scientific GEN-X 4200W) and Rd tube (5GNf Rh 50u).

To analyse the structural characteristics the Fourier Transform Infrared (FTIR) spectroscopy was used and performed in a spectrometer at a resolution of 4 cm^{-1} and scanned from 4000 to 400 cm^{-1} (Bruker Alpha and Perkin Elmer UATR Two).

Scanning Electron Microscopy (SEM) (APREO 2C – Thermo Ficher) coupled with Energy-Dispersive X-ray Spectroscopy (EDS) (Bruker Xflash 60-30) was perfomed to investigate particle morphology and chemical composition. The solids produced were

also analysed by using optical microscopy (NOVEL-BM2100POL). The samples were fixed on a glass slide and the images were captured using the camera with coupled objective lenses.

The size of suspended particles was measured by dynamic light scattering (DLS) (Zeta Sizer Pro, Malvern PANalytical) using a polypropylene cuvette.

The thermal stability of the solids was evaluated by thermogravimetric analysis (Netzsch STA 449 F3 Jupiter) under an inert atmosphere with nitrogen at a flow rate of 80 mL/min.

5.3 Results and Discussions

5.3.1 Cooling crystallization of potassium niobate

5.3.2.1 Evaluation of the initial concentration of the alkaline liquor

The crystallization of potassium niobate was evaluated by changing the initial concentration of the leached alkaline liquor and, as consequence, changing the supersaturation of the solution. The initial concentration of niobium and potassium were monitored based on pre-concentration steps of 60, 40 and 20 wt% of water removal by evaporation at 100 ºC, respectively. The crystallization of potassium niobate was carried out in a cooling rate of 0.45 ± 0.5 ºC/min from 100 ºC to 30 and from 100 °C to 15 ºC. The variation in the initial concentration of the alkaline liquor and temperature was proposed to evaluate how the change in the supersaturation of the liquor could influence in the potassium niobate crystallization. No crystallization occurred during the pre-concentration step.

Figure 5.2 shows the theoretical and experimental concentration of Nb and K in the alkaline liquor, after the pre concentration by removal of water and post crystallization steps.

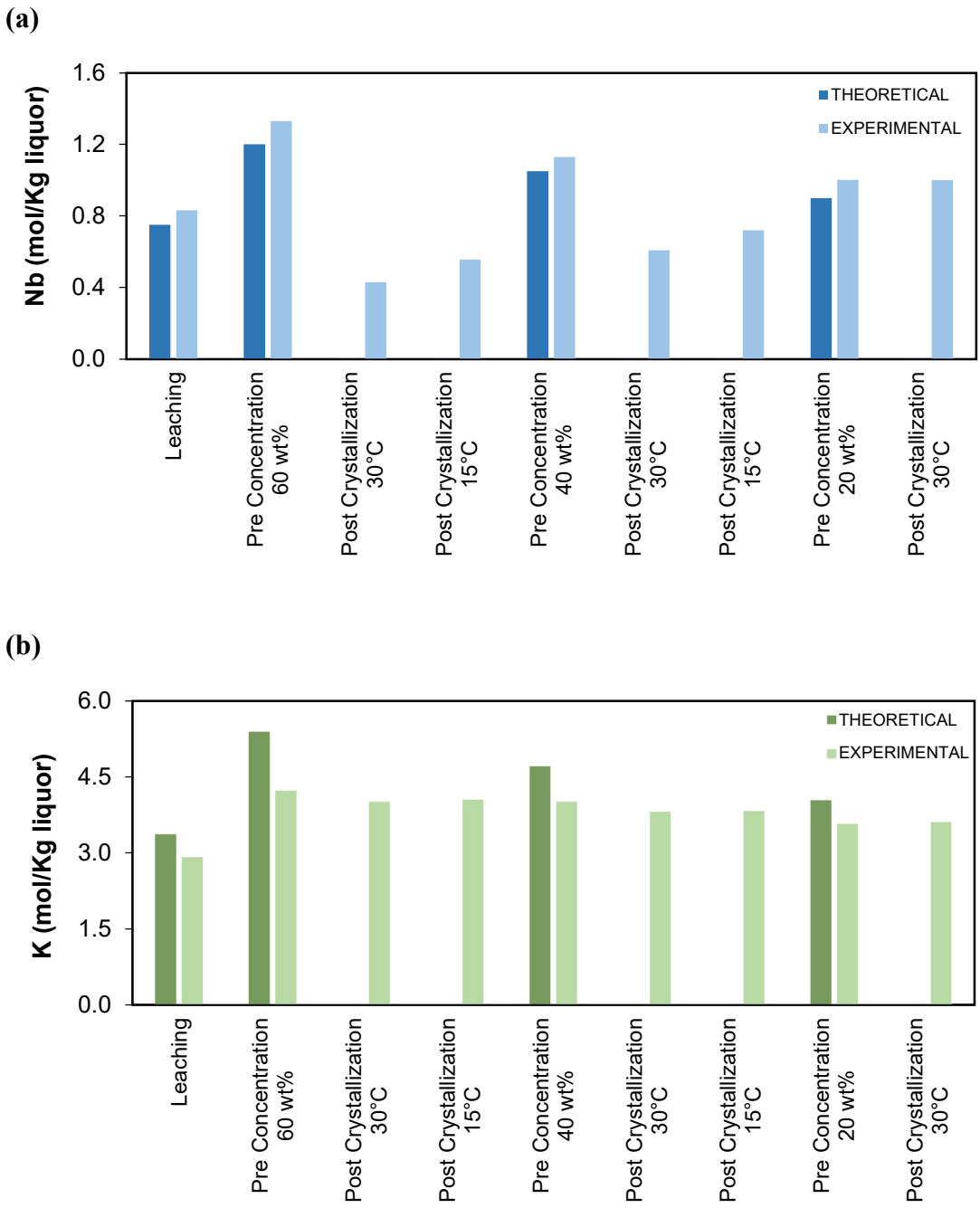

Figure 5.2. Concentration of (a) Nb and (b) K during alkaline leaching, pre concentration of liquor and post crystallization steps of the crystallized potassium niobate at 30 and 15 ºC.

From the Figure 5.2 it is possible to observe the consumption of niobium and potassium in each step of the potassium niobate crystallization. The Nb consumption during the crystallization of potassium niobate (Figure 5.2 (a)) declines with the decreases in the

wt% removal of water from the alkaline liquor and in whole crystallization. Counterintuitively, the Nb consumption for the 60 % water removal at 15 °C was not the highest. When 60 wt% of the water removed from the liquor and the final temperature of crystallization of 30 ºC was reached, the Nb consumption was the highest. The situation of 20 wt% removal of water at 15 ºC was not evaluated, once the crystallization yield was lower than expected (Figure 5.3).

Table 5.4 shows the supersaturation of each condition in potassium niobate crystallization, calculated based on the experimental concentration of niobium using the Equation 5.7. The supersaturation reaches a maximum value in the pre concentrated liquors and decrease after the crystallization process. This behaviour is expected, since the concentration of liquor rise after the evaporation step by removal of water and decrease after Nb and K are consumed by the crystallization of potassium niobate solids.

Table 5.4. Supersaturation index of experimental data of crystallization of potassium niobate from the alkaline liquor.

Steps	60 wt%		40 wt%		20 wt%
	30 °C*	**15 °C***	**30 °C***	**15 °C***	**30 °C***
Leaching	8.24	8.24	8.24	8.24	8.24
Pre concentration	22.38	28.47	18.99	24.17	16.86
Post crystallization	7.22	11.9	10.23	15.41	16.82

* The solubility limit was based on $KNbO_3$ phase from OLI Studio modeling at 30 ºC = 0.059 mol/L and 15 ºC = 0.047 mol/L.

In the pre concentrated liquors with 60 and 40 wt% of removal of water from the alkaline liquor, the highest values of supersaturation were observed when 15 ºC was the final temperature of cooling crystallization. However, the crystallization yield of potassium niobate had better performance at 30 ºC than at 15 ºC, as presented in Figure 5.3.

The cooling crystallization yield of potassium niobate was monitored in each condition – pre-concentrated 60, 40 and 20 wt% at 30 and 15 ºC (Figure 5.3). The amount of solids formation decreases with decreasing initial concentration of Nb in liquor (1.33, 1.13 and 1.00 mol/kg_{liquor}, respectively), which is expected, since the supersaturation also decreases. Furthermore, decreases in the final temperature of the system also reduced the

formation of solids at the end of the crystallization although a high yield was expected according to theoretical calculation by mass balance. This difference could be related to the kinetics of the mix of phases of potassium niobate during the crystallization and the presence of impurities in the liquor.

Due to the low crystallization yield when the potassium niobate was crystallized until 30 ºC with the liquor pre-concentrated 20 wt%, the final temperature of 15 ºC was not evaluated. According to the theoretical calculations, the highest yield was expected at 30 ºC and was obtained only 11% of the predicted value. When the liquor was pre concentrated with 40 wt% water removal and potassium niobate crystallized until 30 ºC, the yield reached 96 % while 60 wt% of water removal from the liquor presented 86 % of yield.

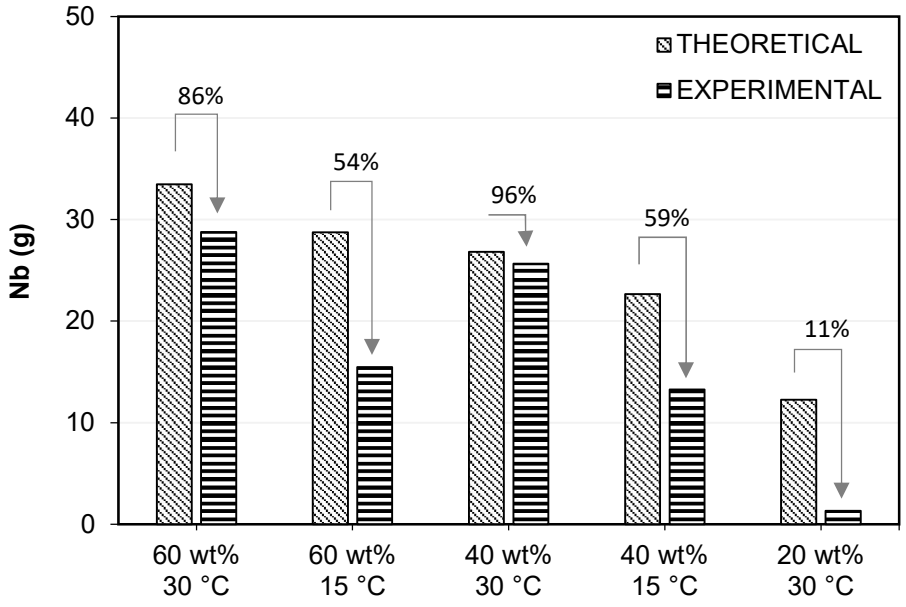

Figure 5.3. Theoretical and experimental crystallization yield of potassium niobate solids after the cooling crystallization at 30 and 15 ºC in 60, 40 and 20 wt% pre concentrated alkaline liquor and the extent of reaction.

The produced solids were characterized by XRF analysis and Table 5.5 shows the chemical composition of crystallized potassium niobate. There is no significant difference between the samples of potassium niobate, that present approximately 44 % of Nb and 26 % of K. With the exception of the potassium niobate crystallized from 20 wt% pre

concentrated liquor which shows 10 % more Nb and K in its composition – probably related to a formation of a different phase.

Table 5.5. Chemical composition of potassium niobate crystallized at 30 and 15 ºC in 60, 40 and 20 wt% pre concentrated alkaline liquor.

SAMPLE	Nb (%)	K (%)
60 wt% 30ºC	43.38	27.29
60 wt% 15 ºC	44.77	26.20
40 wt% 30 ºC	44.89	25.07
40 wt% 15 ºC	43.98	26.33
20 wt% 30 ºC	55.28	20.57

The relative amounts of Nb and K can also be compared to identify potassium niobate phases. The stable phase $KNbO_3$ exhibits a chemical composition of 34.95 % of Nb and 41.51 % of K, whereas the intermediate phase $K_4Nb_6O_{17}$, for instance, presents 41.94 % of Nb and 33.20 % of K. Based on the chemical composition showed in Table 5.5, it can be inferred that $K_4Nb_6O_{17}$ could be the predominant phase of the crystallized potassium niobate.

A mix of potassium niobate phases were identified in the crystallized solids as shown by the XRD analysis (Figure 5.4). It is possible to observe that the increase of the initial concentration of the liquor, i.e., higher supersaturation, results in more crystalline structures of potassium niobate solids, with well-defined peaks.

According to Figure 5.4, two majoritary phases are present in the solids: the metastable phase $K_4Nb_6O_{17}$ and the stable phase $KNbO_3$. The unknown peaks may be related to the soluble intermediate hexaniobate phase $K_8Nb_6O_{19}.nH_2O$ (Bai et al., 2011, 2017; Kanie et al., 2011). The limited of crystallography data on potassium niobate phases hinders the accurate identification of all peaks in the crystallized solid. Some studies report that mixtures of these two phases ($K_4Nb_6O_{17}$ and $KNbO_3$) were observed using different methodologies such as hydrothermal, solvothermal, precipitation, sol-gel and solid state, as presented in Table 5.1. Most of these studies use Nb_2O_5 as source of niobium to produce

potassium niobates. As far as we know, this is the first study that presents the cooling crystallization of these phases from a recovered alkaline liquor from a secondary source of niobium. Kong et al. (2013) and Yang et al. (2023) produced Lindqvist type hexaniobates from solvothermal reaction with Nb_2O_5 and $K_4Nb_6O_{17}$ predominates in the solids were predominantly, as a product with K-rich phase. Han et al (2008), shows that these two phases can coexist under a wide pH range and specific hydrothermal conditions of temperature from a Nb_2O_5 solution. They also show the effect of KOH concentration on the phase to be formed– higher concentration of KOH leads to the formation of the stable phase $KNbO_3$, while the amount of $Nb_6O_{17}^{4-}$ ions is reduced. In addition, Kudo et al. (2004) observed that the metastable phase $K_4Nb_6O_{17}$ was firstly formed and enabled the formation of the stable phase $KNbO_3$ under directional solidification of the starting materials at higher temperature (800 ºC). Here, a solid phase with similar profile was produced under much milder conditions of temperature and pressure.

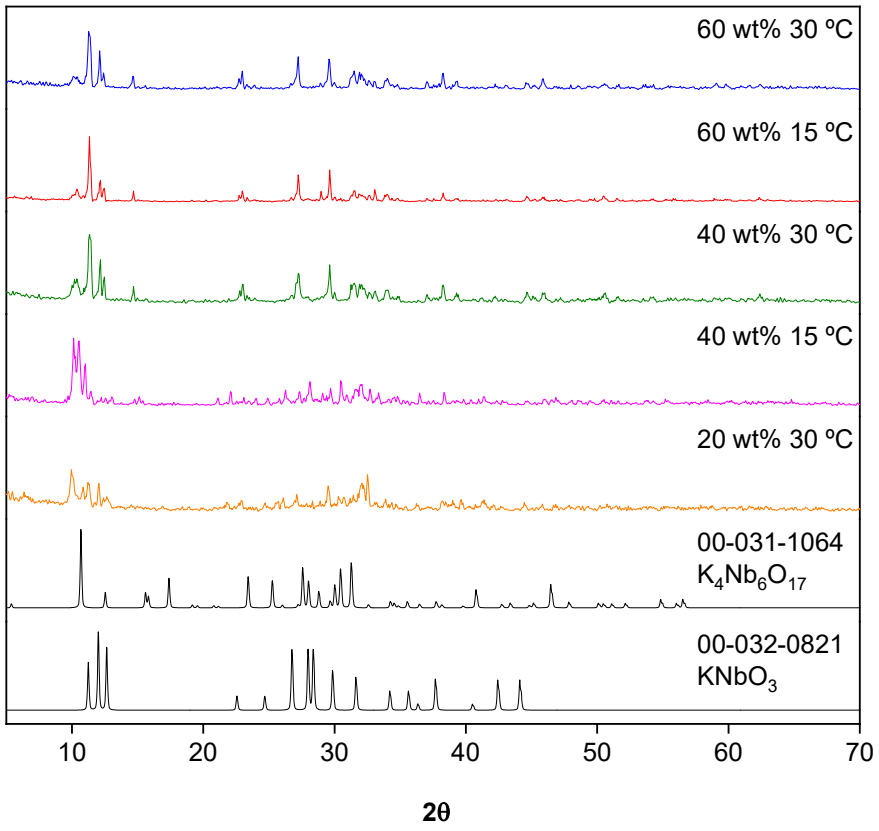

Figure 5.4. XRD of potassium niobate solids obtained by cooling crystallization from pre concentrated liquors until 30 and 15 ºC.

Figure 5.5 shows the FT-IR spectra obtained for all crystallized potassium niobate solids from pre concentrated liquors. The bands observed around 3500 to 2500 cm^{-1} are characteristic to the O-H vibrations and -OH groups, confirming the presence of water molecules in the surface of the solids (Vlazan et al., 2017). The bands of potassium niobate obtained from 20 wt% pre concentrated liquor shows a higher intensity in this region, which may imply a more hydrated solid. The bands in the range of 2000 to 1000 cm^{-1} are attributed to adsorbed water on the surfaces of the samples (Feizpour et al., 2014; Zhang et al., 2013). The bands from 1000 to 500 cm^{-1} corresponding to the vibrations of metal-oxygen bonds: Nb-O from NbO_6 octahedron, reveals the formation of potassium niobate. Additionally, $KNbO_3$ has related bands in the region of 500 cm^{-1}, suggesting different crystalline structure such as orthorhombic, cubic or tetragonal (Zhang et al., 2013).

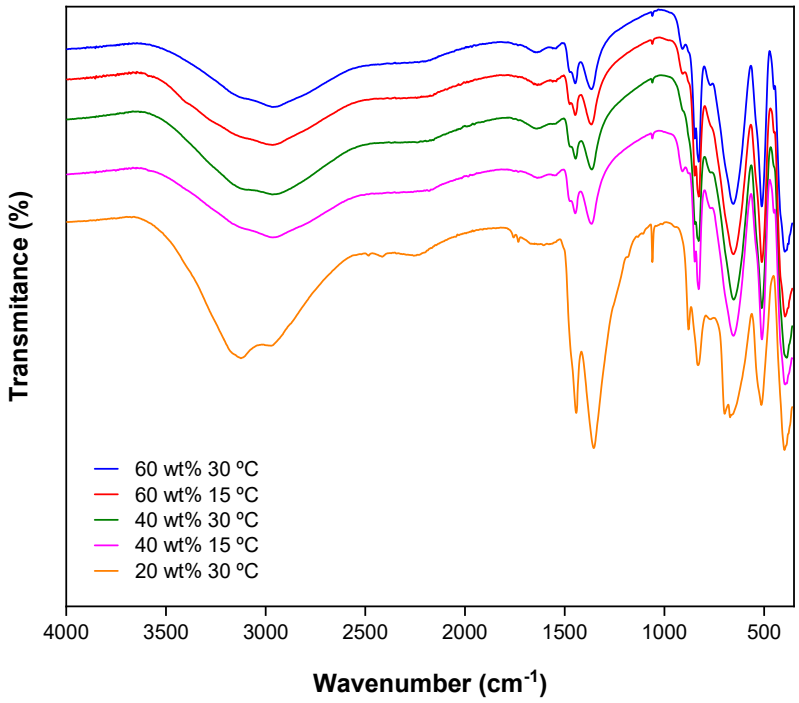

Figure 5.5. FT-IR spectra of potassium niobate solids obtained by cooling crystallization from pre concentrated liquors until 30 and 15 ºC.

Optical microscopies in Figure 5.6 reveal that potassium niobate crystallized from pre concentrated alkaline liquor at different conditions of concentration and temperature

shows mostly isolated single crystals with a rectangular shape and long-side lengths. In the Figures 5.6 (a) and (b) it is possible to observe particles with more distinct morphology and size, with the presence of small agglomerates, formed from the solutions pre-concentrated by 60 % water removal. Figures 5.6 (c) and (d) show the potassium niobate that was crystallized from the liquor with 40 wt% of removal of water, which presented more homogeneously sized crystals, with an improved hexagonal morphology. And the solids crystallized at lower concentration - 20 wt% at 30 ºC shows the presence of agglomerated particles, Figure 5.6 (e), comprised mostly by crystals in the same size range. It is also noteworthy that, despite the lower yield, crystals observed in Figure 5.6 (e) are the largest ones. Liu et al. (2002) also found particles with a hexagonal shape by hydrothermal synthesis at lower temperature and reaction time (120 ºC for 2 days). They related the formation of the hexagonal particle as an intermediate form of potassium niobate before the formation of the stable phase $KNbO_3$ (rodlike shape).

As mentioned in Chapter 3, section 3.4.2, the low temperatures of crystallization when compared to hydrothermal methods allowed that fewer defective particle were formed with more homogeneous structures and the lower cooling rate favouring the formation of the crystalline particles. The supersaturation was driven by the different initial concentration of the pre concentrated alkaline liquor. Hence, as expected, the higher concentration, i.e., higher supersaturation, favours the formation of smaller crystals by enhancing the nucleation rates.

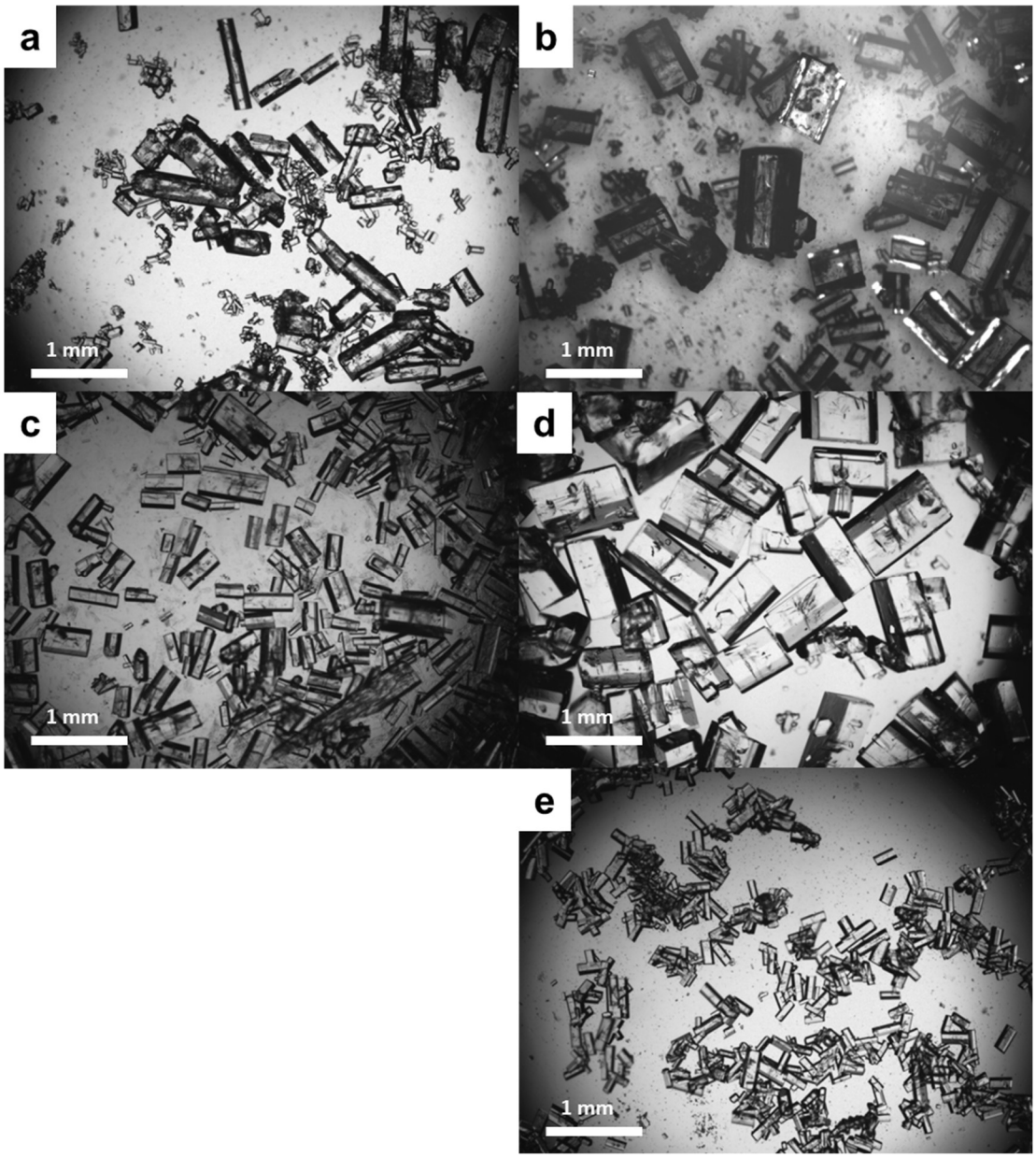

Figure 5.6. Optical Microscopy of potassium niobate crystallized from pre concentrated alkaline liquor (a) 60 wt% at 15 ºC, (b) 60 wt% at 30 ºC, (c) 40 wt% at 15 ºC, (d) 40 wt% at 30 ºC and (e) 20 wt% at 30 ºC.

5.3.2.2 The influence of cooling rate in the crystallization of potassium niobate

Three different cooling rates – 0.1, 0.5 and 1 ºC/min – were evaluated in order to find out their influence on the cooling crystallization of potassium niobate in a temperature range of 80 to 30 ºC. According to the crystallization yield seen in Figure 5.3, the final temperature was set as 30 ºC. Hence, a solution was prepared with the previously crystallized potassium niobate, as a mix of metastable and stable phase – $K_4Nb_6O_{17}$ and $KNbO_3$, respectively. Table 5.6 shows the initial concentration of niobium and potassium in the start solution.

Table 5.6. Initial concentration of Nb and K in the potassium niobate solution to crystallization at different cooling rates (0.10, 0.50 and 1.00 ºC/min) in a temperature range of 80 to 30 ºC.

Rate (°C/min)	0.10	0.50	1.00
Nb (mol/L)	1.80	1.88	1.79
K (mol/L)	0.22	0.23	0.21

Figure 5.7 shows the consumption of niobium during the crystallization of potassium niobate at different cooling rates. The concentration of Nb was normalized to standardize the initial Nb concentration in all solutions. Thus, the initial Nb concentration was set as 100 % to be used for comparison between the samples during the cooling crystallization. It is observed that the Nb consumption during the potassium niobate crystallization was different for each cooling rate. The lower cooling rate (0.10 ºC/min) and, as consequence, longer residence time led to a higher consumption of Nb. This behaviour should not be expected if the equilibrium was achieved in all conditions of cooling rate and temperature, once the initial concentration of niobium had no significant variation (Table 5.6), the final Nb concentration was expected to be the same, i.e. the same crystallization yield should be achieved at the end of the crystallization in all cooling rates. However, the extent of crystallization was very low when compared to the theoretical calculations. The crystallization yield was only 10.7, 8.3, 4.4 % to 0.10, 0.50 and 1.00 ºC/min cooling rate, respectively. Since the crystallization yield was different from that predicted for the different cooling rates, it can be inferred that the equilibrium was not reached. Therefore,

the lowest cooling rate and the longest cooling time (0.10 ºC/min - 500 minutes) provide more time for growth kinetics compared to the other conditions (100 and 40 minutes for 0.50 and 1.00 ºC/min, respectively). Due to the low growth kinetic of the crystals, crystallization at 0.10 ºC/min resulted in a higher yield at the end of the process. Moreover, although very low, the yield is much lower than it was anticipated from the remaining Nb in solution seen in Figure 5.7. The predicted solid yield was 10.2, 7.6 and 4.1 g to 0.10, 0.50 and 1.00 ºC/min cooling rate, respectively.

A higher crystallization yield obtained at lower cooling rate can be related to the residence time. The decreasing in the cooling rate increases the residence time, since the final temperature to be reached is the same in all experiments, and may increase the effects of secondary nucleation caused by friction and breakage of crystals, as well as due to impeller collision in the reactor, thus increasing the overall yield.

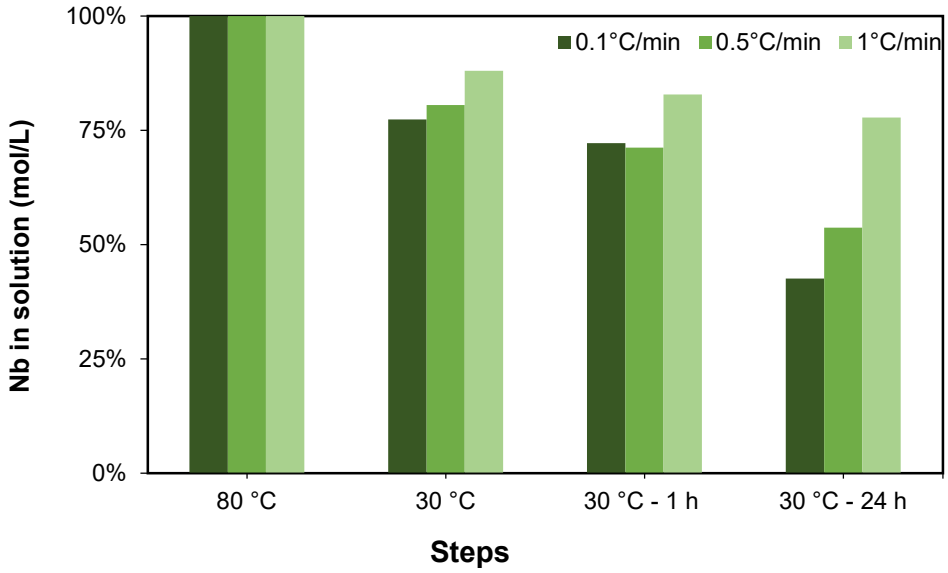

Figure 5.7. Niobium consumption during the crystallization of potassium niobate in the different rates of cooling.

Supersaturation is achieved by uniformly reducing the temperature of the solution. The control of the cooling rates is directly related to the diffusion of solution and the supersaturation, which is very important to control the growth of the crystals. Table 5.7 shows the maximum supersaturation of the system.

Table 5.7. Supersaturation of experimental data of cooling crystallization from a potassium niobate solution at 80 and 30 ºC based on OLI Studio modeling and Crystal 16 experimental solubility curve.

Supersaturation	**80 ºC**	**30 ºC**
OLI Studio[*]		
1.00 ºC/min	0.27	1.85
0.50 ºC/min		
0.10 ºC/min		
Crystal 16[**]		
1.00 ºC/min	0.37	3.75
0.50 ºC/min	0.38	3.93
0.10 ºC/min	0.37	3.74

* The solubility limit was based on $KNbO_3$ phase from OLI Studio modeling at 80 ºC = 0.35 mol/L and 30 ºC = 0.05 mol/L.
** The solubility limit was based on Nb concentration from Crystal 16 solubility curve at 80 ºC = 0.49 mol/L and 30 ºC = 0.48 mol/L.

In the supersaturation calculations carried out from OLI Studio data only the stable phase of the system ($KNbO_3$) was considered, since no other phase of Nb-K-H_2O is present on its the database. The initial mass of crystallized potassium niobate for the start solution of 16.92 g, containing approximately 44.5 % of Nb, was considered. However, for the supersaturation from solubility curves obtained from Crystal 16, the presence of the major phase ($K_4Nb_6O_{17}$) was also considered.

It is possible to verify a variation on the supersaturation values calculated for both methods, OLI Studio and Crystal 16. The supersaturation of the system was calculated considering that the solid was crystallized only after the solution achieved 30 ºC. According to the supersaturation results, the system was undersaturated at 80 ºC, as expected, with S values < 1. By cooling the system, the solution becomes supersaturated allowing the crystal formation - in the end of the cooling crystallization, at 30 ºC the supersaturation was > 1 for both the $KNbO_3$ only (OLI values) and > 3 for the mix (Crystal 16 values). Using OLI Studio solubility data, the presence of $K_4Nb_6O_{17}$ phase was not considered in the supersaturation calculation and because of this, the results may be underestimated. However, Crystal 16 solubility data was obtained from the crystallized potassium niobate as a mix of phases and, as discussed previously in this chapter, the

crystallization of both metastable and stable phases in the same system may affect the formation of crystals. Additionally, to the supersaturation calculation by Crystal 16 data, only the Nb concentration was considered while OLI Studio considered the phase $KNbO_3$ concentration.

Figure 5.8 shows the XRD of potassium niobate crystallized in 0.10, 0.50 and 1.00 ºC/min in a temperature range of 80 to 30 ºC. The two major phases of initial potassium niobate used in the start solution – $KNbO_3$ and $K_4Nb_6O_{17}$ – are still present in the crystallized solids at the different cooling rates. The unidentified peaks could be related to minor intermediate phases of potassium niobate (e.g., KNb_3O_8, $K_8Nb_6O_{19}.nH_2O$).

It can be observed that by lowering the cooling rates, the peaks of XRD analysis become better-defined. Due to the low kinetics of potassium niobate formation, the lower cooling rate can favour the formation of well-formed crystals with smoother surfaces (Souza et al., 2024) and improve the crystalline structure of potassium niobate. Similarly, other synthesis conditions have also showed the influence on phase formation and crystallinity. Bai et al. (2017) showed the formation of intermediate phases at lower hydrothermal synthesis of potassium niobate. They produced a hydrated potassium niobate phase at 40 to 70 ºC by adding the surfactant SDBS (Sodium dodecyl benzene sulfonate) in a high KOH concentration (9 mol/L).

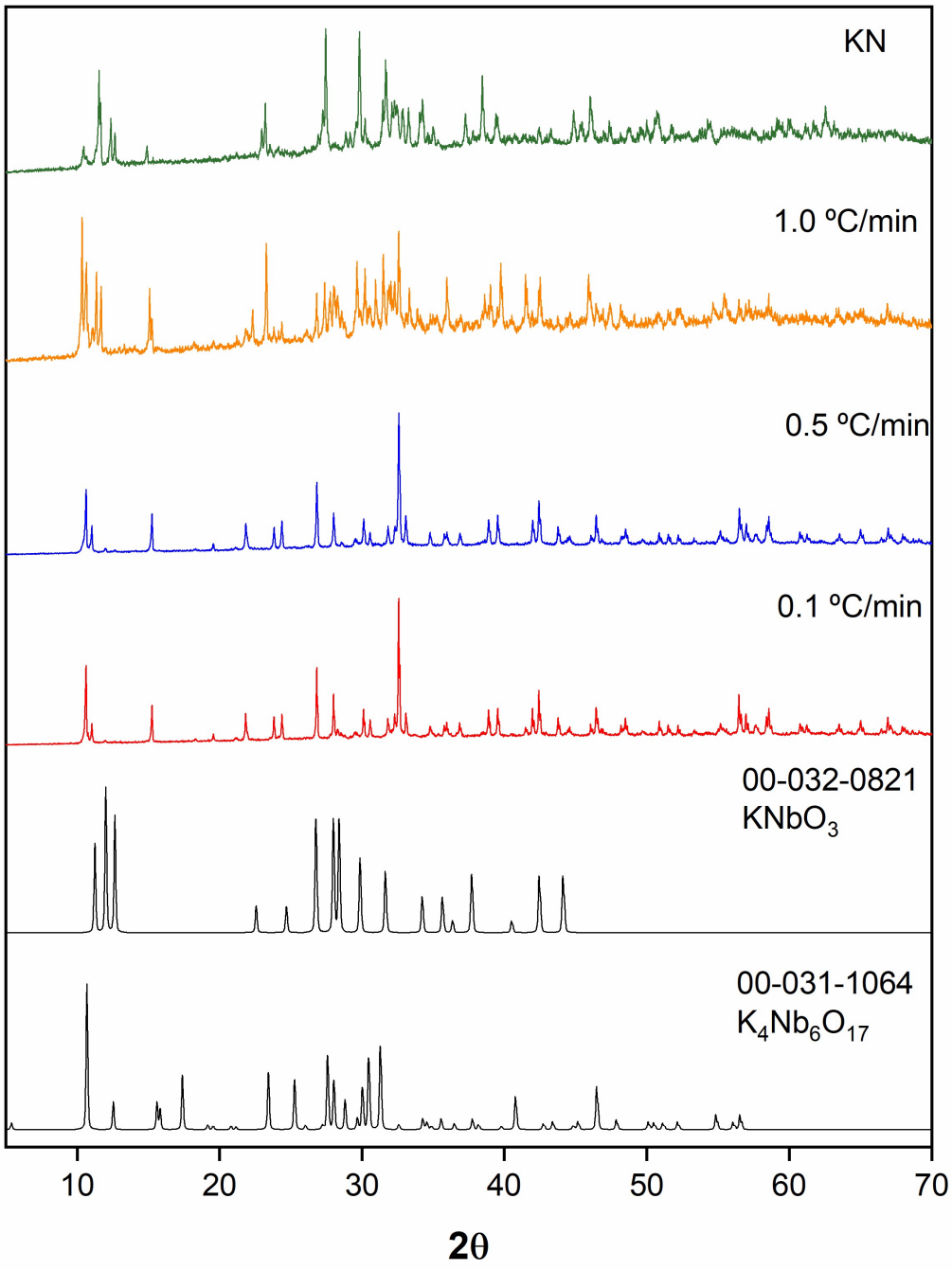

Figure 5.8. XRD of potassium niobate crystallized at different cooling rates – 0.10, 0.50 and 1.00 ºC/min, in a temperature range of 80 to 30ºC. KN: crystallized potassium niobate used in the start solution

The FTIR analysis was also conducted in the crystallized solids, as showed by Figure 5.9. The potassium niobate crystallized at lower cooling rates presented less water in its

structure, as we can observe between the bands around 3500 – 2500 cm^{-1} and in the bands related to the O-H bonds between 1800 – 1000 cm^{-1}. And similar to the FTIR of crystallized potassium niobate presented by the Figure 5.9, the bands at wavenumber smaller than 1000 cm^{-1} are associated to vibrations of NbO_6 octahedron, related to the vibrations of Nb-O in the structure of the solids.

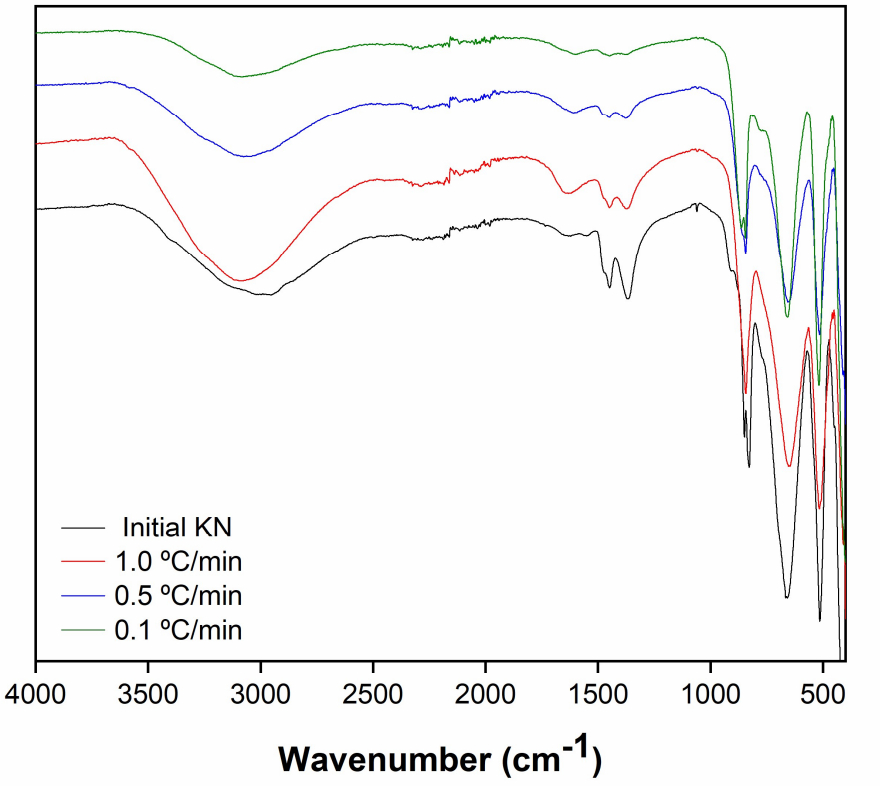

Figure 5.9. FTIR spectra of potassium niobate crystallized at different cooling rates in a temperature range of 80 to 30ºC.

Figure 5.10 shows SEM images of potassium niobate crystallized at (a, b) 1.00, (c, d) 0.50 and (e, f) 0.10 ºC/min. The solids obtained by cooling at 1.00 ºC/min were small agglomerated of particles without a defined shape (more amorphous particles), which corroborates with the low crystallinity seen on the diffractogram. The lower cooling rates improved the shape of the hexagonal crystals. This behaviour was also reported by Bai et al. (2017) at 40 to 70 ºC. Liu et al. (2002) also found an intermediate phase of potassium niobate with hexagonal shape at relatively low temperature (120 ºC) by hydrothermal reaction.

Tong et al., (2025) observed that lower cooling rates in hydrothermal synthesis of potassium niobate can also improve the crystallinity of the crystals and the crystal growth can be accelerated by reducing the cooling rate. However, in crystallization from a supersaturated solution under stirring, a lower cooling rate leads to a higher residence time, and also may lead to higher degree of particle breakage.

The spontaneous nucleation from a supersaturated solute solution is uncontrolled, which can lower quality of the crystals (less well-defined morphologies and lower crystallinity). In addition, spontaneous nuclei can produce different shape and size of solids, resulting in non-uniform crystal growth, defect formation, and crystal size distributions (Tong et al., 2025).

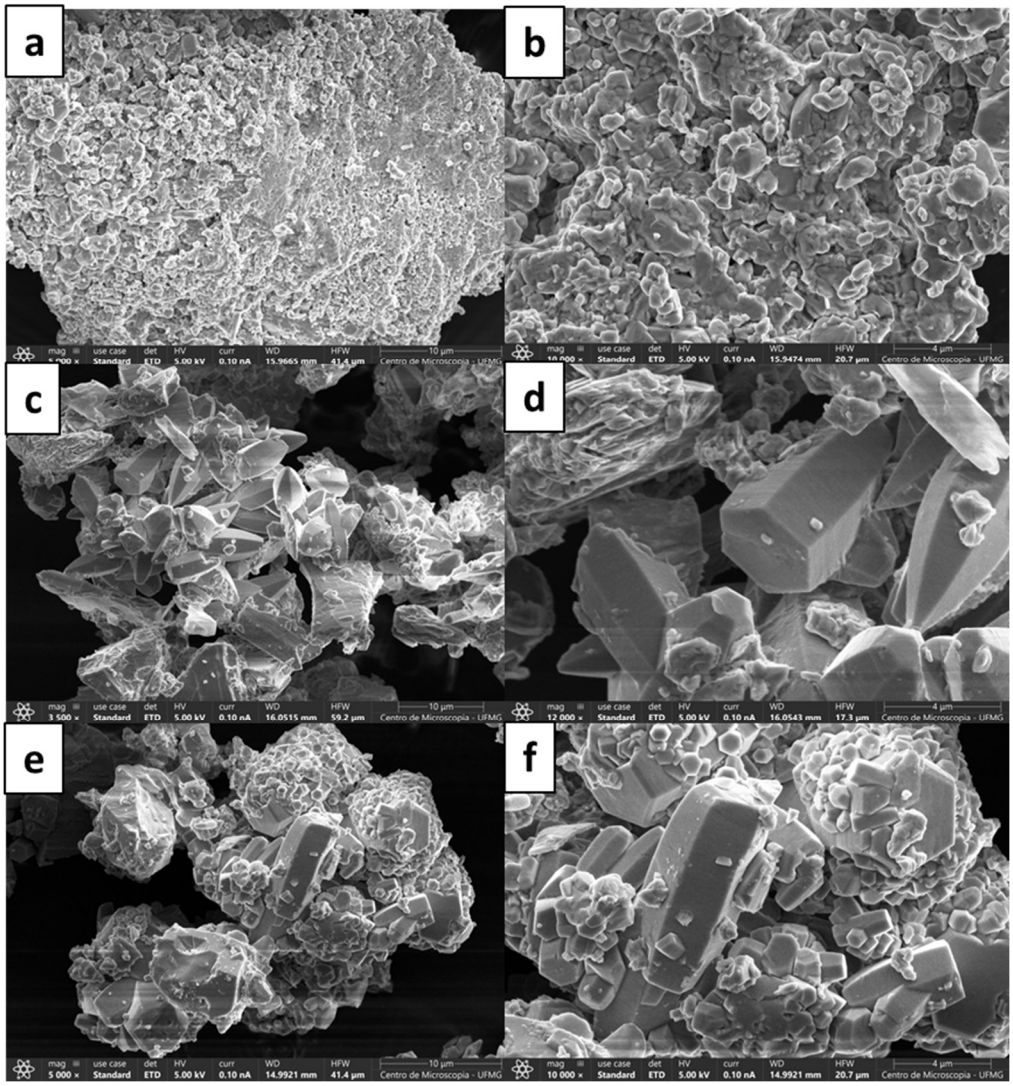

Figure 5.10. SEM images of potassium niobate crystallized at (a-b) 1.00 ºC/min, (c-d) 0.50 ºC/min and (e-f) 0.10 ºC/min.

The chemical elemental mapping confirms the uniform composition of niobium, potassium and oxygen in the solids (Figure 5.11). Punctual EDS analysis of two distinct regions shows a consistent chemical composition of 41 % of Nb, 19 % of K and 8 % of O for all samples of potassium niobate cooled crystallized in the three evaluated cooling rates.

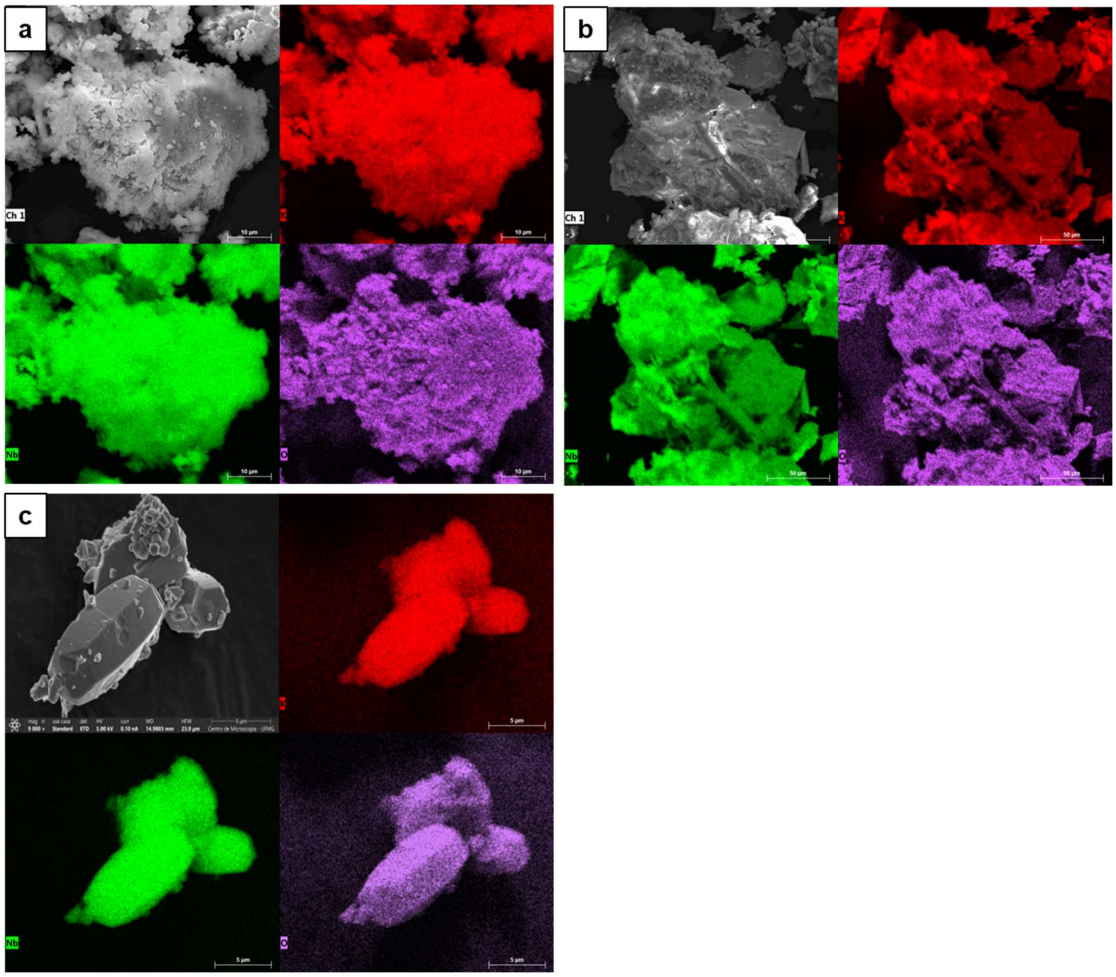

Figure 5.11. Chemical mapping of crystallized potassium niobate in the cooling rate of (a) 1.00, (b) 0.50 and (c) 0.10 ºC/min in a temperature range of 80 to 30 ºC. Images grey: background, green: Nb, red: K, and purple: O.

5.3.2.3 Kinetics of potassium niobate crystallization

It is speculated that the low crystallization yield, and the disparity between the niobium consumption and the yield, may be related to the low kinetics of potassium niobate formation. To evaluate the formation of small particles of potassium niobate during the

cooling crystallization, a potassium niobate solution was prepared and a Crystal 16 experiment was performed at 0.50 ºC/min in a temperature range of 70 to 30 ºC. The solution was left stirring at 30 °C and the solutions were analyzed for small particles using the dynamic light scattering. The results for particle populations are shown in Figure 5.12.

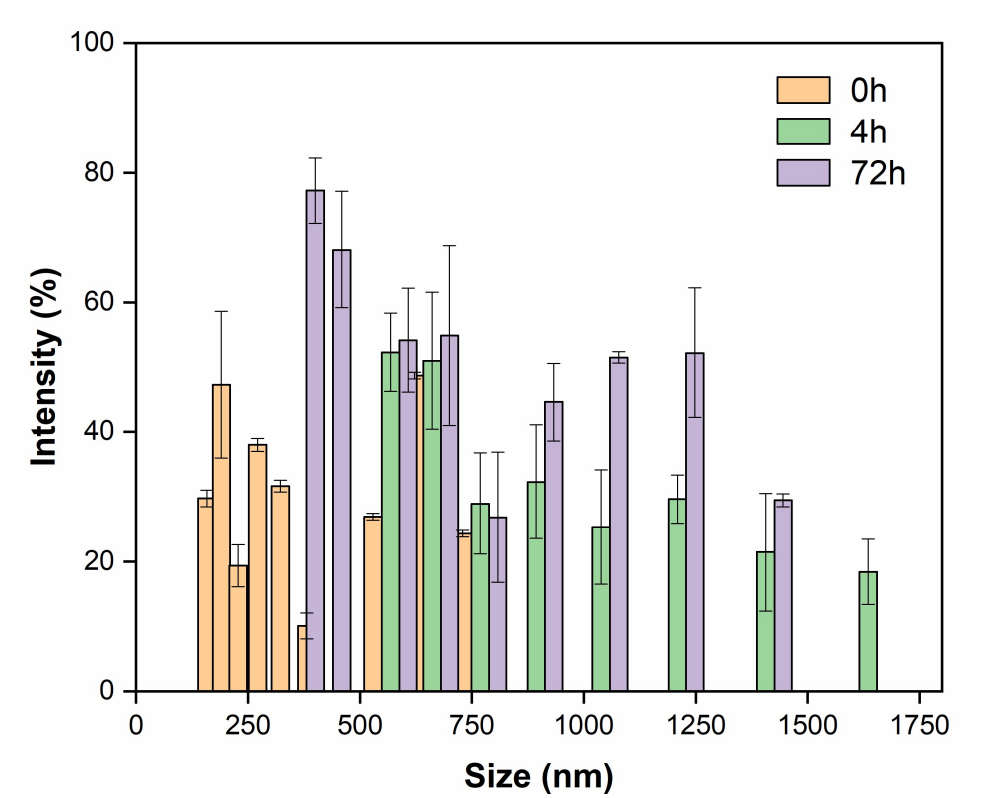

Figure 5.12. Investigation of particle size during the cooling crystallization of potassium niobate by Crystal 16 in a range of 70 to 30 ºC and 700 rpm with a cooling rate of 0.50 ºC/min.

From the Figure 5.12 it is possible to observe the presence of small particles is majority in a range of 150 – 300 nm, with a maximum intensity of 50 % at 200 nm particles. The solution was kept under stirring and after 4 hours at 30 ºC the particless grown to 600 – 1400 nm. When the crystallization achived 72 hours at 30 ºC the intensity of bigger particles had a significant increase. This results evidence the low kinetics of potassium niobate crystallization, since it was necessary 72 hours for the particules to achieve 300 - 500 nm with 80 % of intensity and 50 % with particles between 600 – 1200 nm.

The presence of these very small particles can explain the discrepancy from the Nb found in solution and the solid yield. Since the liquid samples from the previous experiments were all filtered (PVDF syringe filter – 0.22 μm) prior to ICP analysis for Nb content, and the solids were filtered using quantitative strip filter paper, these particles were large enough to be filtered out for the ICP analysis, but not for the solid yield.

In each step of the investigation, the solution was analyzed and the crystallized potassium niobate was filtrated in a PVDF membrane. The FTIR analysis was performed to evaluate the produced solids, as shown in Figure 5.13.

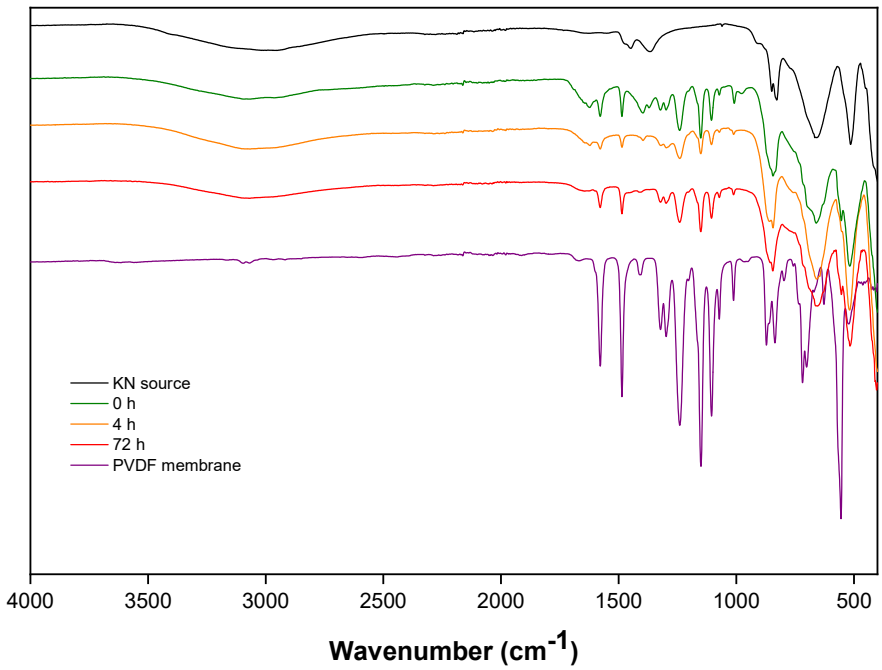

Figure 5.13. FTIR spectrum of crystallized potassium niobate by Crystal 16 in a range of 70 to 30 ºC and 700 rpm with a cooling rate of 0.50 ºC/min.

From the FTIR spectra it is possible to observe the presence of crystallized potassium niobate on PVDF membrane, in accordance with the previous potassium niobate FTIR analysis shown in Figure 5.9. Weak bands around 3500 to 2500 cm^{-1} related to the presence of water and O-H bonds can be seen in the sample of potassium niobate crystallized in the cooling rate of 0.5 ºC/min from 80 to 30 ºC and kept under stirring to 4 and 72 hours from 80 to 30ºC. Bands between 1800 to 1000 cm^{-1} can be associated to the PVDF membrane, attributed to carbon-oxygen-fluorine bonds (Da Silva et al., 2024).

Due to the presence of empty spaces between the solid and the membrane, the membrane bands appear in the analysis results. The increase of the crystallization time led to a improve in the IR spectra, due to the presence of more crystallized particles, where some bands related to the PVDF membrane disappear. The bands at wavenumber smaller than 1000 cm^{-1} are associated to vibrations of NbO_6 octahedron, related to the vibrations of Nb-O in the structure of the solids.

5.3.2 Thermal conversion of crystallized potassium niobate

Thermal treatment of crystallized potassium niobate was conducted to assess the progressive stages of the exothermic reaction and the changes on the crystalline structure from 500 to 900 ºC. Figure 5.14 shows the TG/DSC curve of the solid.

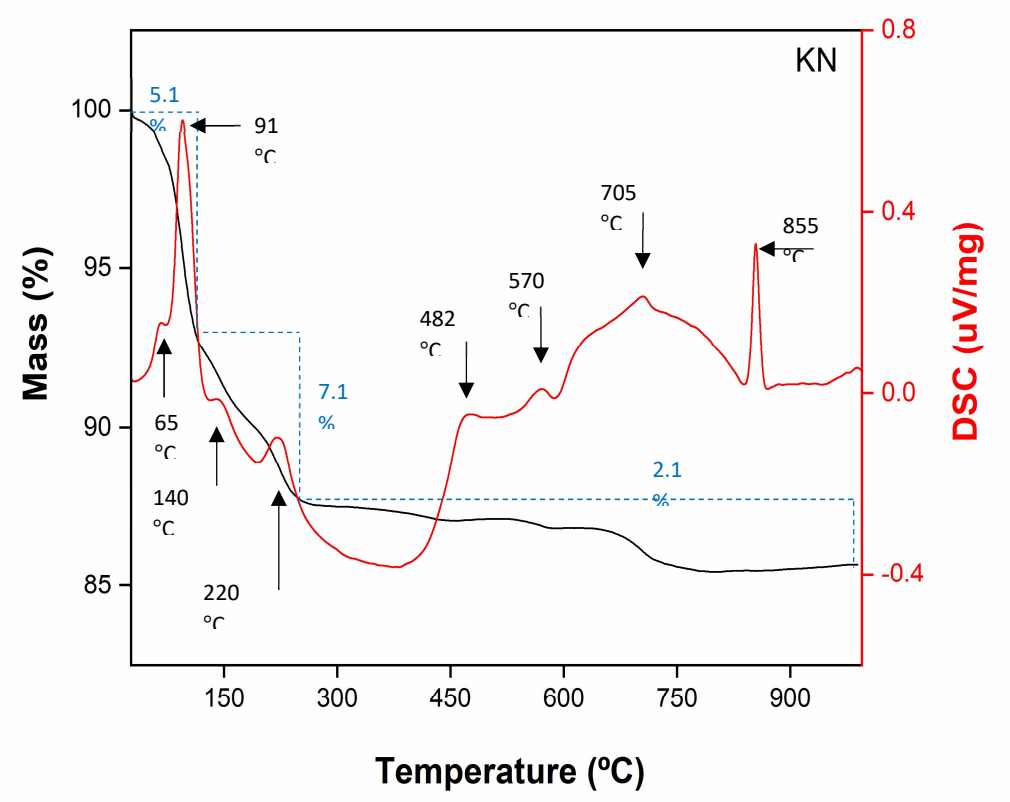

Figure 5.14. TG/DSC of crystallized potassium niobate at 30 ºC in 40 wt% pre concentrated alkaline liquor in nitrogen atmosphere.

A significant weight loss is observed until 200 ºC with three exothermic peaks that are related to the dehydration of adsorbed water from the crystallized potassium niobate. Several peaks in the range of 200 to 900 ºC appear in the TG/DSC curve. Tanaka et al (2017) described the exothermic peaks at 500 and 620 ºC as the crystallization of two phases: $K_4Nb_6O_{17}$ and $KNbO_3$ and Feizpour et al. (2014) as phase transition phenomena. In this study, these peaks could be seen at 482 and 570 ºC and could be associated to the both cases, as the crystallized potassium niobate is a mix of phases. The peak and loss of mass between 600 and 750 ºC could be related to the volatilization of K_2O (Tanaka et al., 2017). A very sharp peak at 855 ºC accompanied with no mass loss can be observed in the curve, which may be attributed to the liberation of heat caused by the formation of a perovskite phase (Cao et al., 2012; Yao et al., 2009, Vlazan et al., 2017). This suggest that the calcination temperature to obtain a $KNbO_3$ phase should be above 855 ºC, which can be confirmed by the XRD analysis. The total mass loss of the potassium niobate sample was 14.3 %.

The temperature of calcination was explored for the phase transition of the calcined solids, as shown by the XRD analysis in Figure 5.15. When the temperature was 500 ºC the obtained product had no significant change in its structure, with low intensity peaks. The crystallinity of the potassium niobate increased with the increase of calcination temperature – higher temperatures lead to the formation of the stable phase $KNbO_3$. However, the potassium can volatilize at higher calcination temperature and this factor may also lead to phase changes (Yang et al., 2023). Moreover, at different temperatures of calcination, potassium niobate can show a different crystalline structure. Only at 900 ºC the product of calcination presented the orthorhombic structure (PDF 00-077-1098). This imply that the calcination temperature affects the crystallinity of the solids and its crystalline structure.

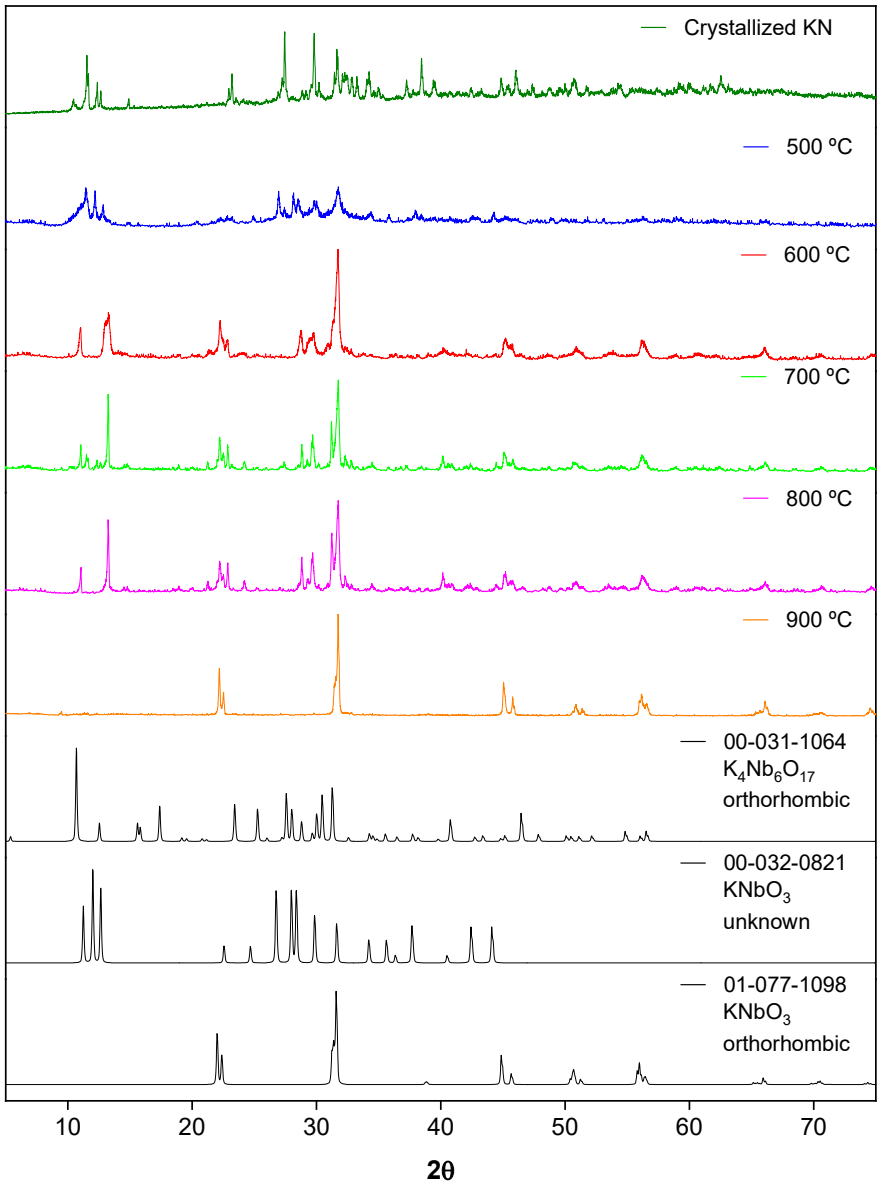

Figure 5.15. XRD of calcined potassium niobate crystallized at 30 ºC in 40 wt% pre concentrated alkaline liquor.

The FT-IR analysis of the calcined potassium niobate was also conducted and is shown in Figure 5.16. Weak bands related to the presence of water and O-H bonds (3500 to 2500 cm^{-1}) can be observed in the calcined at 500 ºC, however they are not present in the samples that were calcined at 600 to 900 ºC. The bands around 2000 to 1000 cm^{-1} drop with the increase of calcination temperature and are attributed to water on the surface of the solids and H-bonds (Feizpour et al., 2014). The increase of calcination temperature

leads to a significant change in the IR spectra, and the bands at wavenumber smaller than 1000 cm^{-1} disappear. These bands are related to the vibrations of oxygen-metal – Nb-O. One strong and broad band at 500 cm^{-1} is formed and it is associated to vibrations of NbO_6 octahedron in the perovskite structure, confirming the formation of stable phase of potassium niobate (Vittivong and Vittayakorn, 2015).

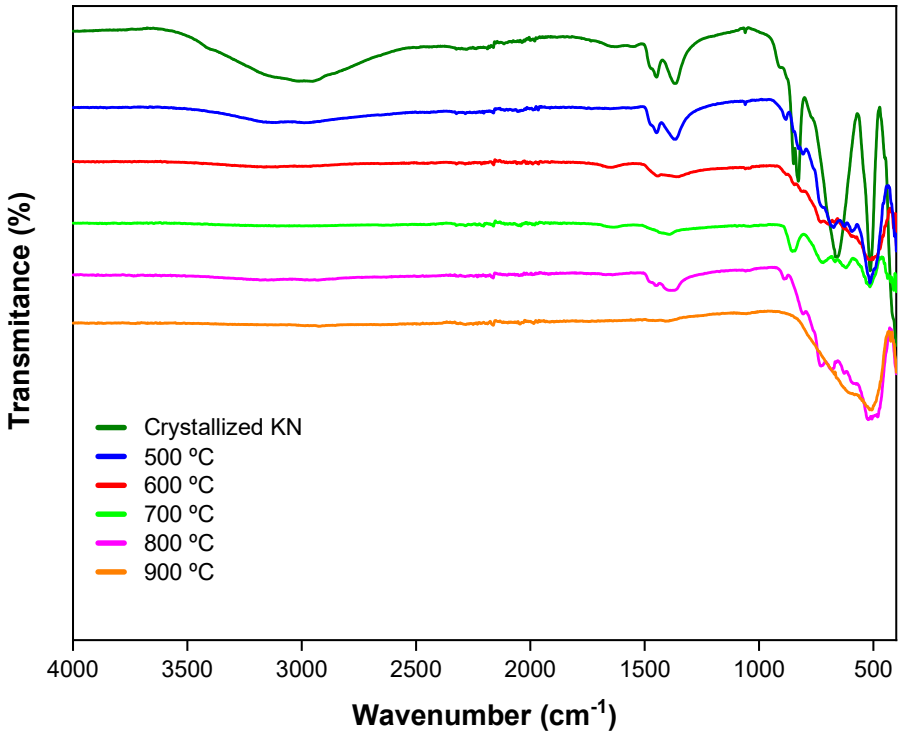

Figure 5.1612. FTIR of calcined potassium niobate crystallized at 30 ºC in 40 wt% pre concentrated alkaline liquor.

5.4 Conclusions

Cooling crystallization of potassium niobate was investigated from an alkaline liquor from Fe-Nb alloy fines leached with KOH. Different initial concentration Nb and K were obtained after evaporation step with 60, 40 and 20 wt% of removal of water of the leached liquor. It was observed that the crystallization yield was higher for the 40 wt % pre concentrated solution (1.6 times more concentrated than the initial liquor) was cooled from 100 to 30 ºC (95 % yield). The produced solids were identified as a mix of $KNbO_3$ and $K_4Nb_6O_{17}$.

Three different cooling rates (1.00, 0.50 and 0.10 ºC/min) from the potassium niobate solution were also evaluated–to study its influence on shape and morphology of the crystals. Lower cooling rates contributed to improvement of crystallinity of the solids and the final product was a mix of phases. Additionally, the lower cooling rate improved the shape of the hexagonal crystals. Punctual EDS shows a chemical composition of 41 % of Nb, 19 % of K and 8 % of O for potassium niobate obtained at cooling rates of 1.00, 0.50 and 0.10 ºC/min in a temperature range of 80 to 30 ºC.

The crystallization yield varied for distinct initial condition and cooling rates. This variation was related to the low kinetic of potassium niobate formation, evidenced by the particle size development measured with dynamic light scattering. When the system was maintained under agitation, an increase in the particle size was observed with time. The median particle size was 230, 568, and 1039 nm at 0, 4 and 72 h, respectively.

The thermal treatment conducted on potassium niobate showed that the variation on temperature of calcination has a significant impact on the structure of the crystallized solids. The crystallinity of the potassium niobate increases with the increase of calcination temperature in the range of 500 to 900 ºC and higher temperatures lead to the formation of the stable phase $KNbO_3$.

5.5 References

Alves, A. K., 2019. Nanomaterials for Ecofriendly Applications. Engineering Materials. Springer Cham. https://doi.org/10.1007/978-3-030-26810-7

Amini, M.M., Mirzaee, M., 2009. Effect of solvent and temperature on the preparation of potassium niobate by hydrothermal-assisted sol-gel processing. Ceram. Int. 35, 2367–2372. https://doi.org/10.1016/j.ceramint.2009.01.009

Amini, M.M., Sacks, M.D., 1991. Synthesis of Potassium Niobate from Metal Alkoxides. J Am Ceram Soc 74, 53–59.

Bai, S., Zhang, F., Karaki, T., Adachi, M., 2011. Effect of surfactants on morphology of niobate hydrate particles in hydrothermal synthesis. Jpn. J. Appl. Phys. 50, 1–5. https://doi.org/10.1143/JJAP.50.09ND12

Bai, S., Zhang, J., Chen, Z., Wang, Y., Hong, M., Karaki, T., 2017. Near-room-temperature synthesis of niobate hydrate particles with hexagonal-platelike morphologies. Mater. Chem. Phys. 199, 230–238. https://doi.org/10.1016/j.matchemphys.2017.06.048

Cao, Y., Zhu, K., Qiu, J., Pang, X., Ji, H., 2012. Sol-gel processing and characterization of potassium niobate nano-powders by an EDTA/citrate complexing method. Solid State Sci. 14, 655–660. https://doi.org/10.1016/j.solidstatesciences.2012.03.011

Campos, A. R., Luz, A. B., Bastos, F. F., Nogueira, I. Tratamento De minérios Capítulo 16: Calcinação. 6ª ed., Rio de Janeiro, CETEM/MCTI, 2018.

Chabanon, E., Mangin, D., Charcosset, C., 2016. Membranes and crystallization processes: State of the art and prospects. J. Memb. Sci. 509, 57–67. https://doi.org/10.1016/j.memsci.2016.02.051

Cheng, Z.X., Ozawa, K., Miyazaki, A., Kimura, H., 2005. Potassium niobate derived from a novel chemical solution. J. Cryst. Growth 275, 971–975. https://doi.org/10.1016/j.jcrysgro.2004.11.150

Da Silva, I. P., Maged, A., Pinheiro Lima Abreu, V., Luisa Quintanilha Candido, A., Denise Ferreira Rocha, S., Coutinho de Paula, E., 2024. Transfiguration of discarded PVDF ultrafiltration membranes: Optimization of pyrolysis parameters for high-value char production. Waste Manag. 190, 360–369. https://doi.org/10.1016/j.wasman.2024.09.033

De Andrade, J.S., Pinheiro, A.G., Vasconcelos, I.F., De Araújo, M.A.B., Valente, M.A., Sombra, A.S.B., 2000. Structural studies of KNbO3 in niobate glass-ceramics. J. Phys. Chem. Solids 61, 899–906. https://doi.org/10.1016/S0022-3697(99)00387-X

Duarte, T.M., Honorio, L.M.C., Brito, A.S., Souza, J.K.D., Longo, E., Tranquilin, R.L., Souza, A.G., Santos, I.M.G., Maia, A.S., 2015. Synthesis of potassium niobates by the microwave-assisted solvothermal method. IOP Conf. Ser. Mater. Sci. Eng. 97, 1–7. https://doi.org/10.1088/1757-899X/97/1/012001

Feizpour, M., Barzegar Bafrooei, H., Hayati, R., Ebadzadeh, T., 2014. Microwave-assisted synthesis and sintering of potassium sodium niobate lead-free piezoelectric ceramics. Ceram. Int. 40, 871–877. https://doi.org/10.1016/j.ceramint.2013.06.081

Han, X., Zhang, D., Zhong, Z., Yang, F., Wei, N., Zheng, K., Li, Z., Gao, Y., 2008. Theoretical design and experimental study of hydrothermal synthesis of KNbO3. J. Phys. Chem. Solids 69, 193–198. https://doi.org/10.1016/j.jpcs.2007.08.053

Handoko, A.D., Goh, G.K.L., 2010. Hydrothermal synthesis of sodium potassium niobate solid solutions at 200 °C. Green Chem. 12, 680–68. https://doi.org/10.1039/b923840a

Hayashi, H., Hakuta, Y., & Kurata, Y., 2004. Hydrothermal synthesis of potassium niobate photocatalysts under subcritical and supercritical water conditions. Mater. Chem. 14, 2046–2051. https://doi.org/10.1039/b400130n

Hayashi, H., Hakuta, Y., Kurata, Y., 2004. Hydrothermal synthesis of potassium niobate photocatalysts under subcritical and supercritical water conditions. J. Mater. Chem. 14, 2046–2051. https://doi.org/10.1039/b400130n

Hewat, A.W., 1973. Solid State Physics Related content ferroelectric transitions in perovskite potassium niobate : neutron powder profile refinement of the structures. Phys. C 6.

Ibis F., Yu T.W., Penha F.M., Ganguly D., Nuhu M.A., Van Der Heijden A.E.D.M., Kramer H.J.M., Eral H.B. (2021) Nucleation kinetics of calcium oxalate monohydrate as a function of pH, magnesium, and osteopontin concentration quantified with droplet microfluidics. Biomicrofluidics, 15 (6).

Kanie, K., Numamoto, Y., Tsukamoto, S., Takahashi, H., Mizutani, H., Terabe, A., Nakaya, M., Tani, J., Muramatsu, A., 2011. Hydrothermal synthesis of sodium and potassium niobates fine particles and their application to lead-free piezoelectric material. Mater. Trans. 52, 2119–2125. https://doi.org/10.2320/matertrans.M2011148

Khorrami, G.H., Kompany, A., Khorsand Zak, A., 2015. Structural and optical properties of (K,Na)NbO3 nanoparticles synthesized by a modified sol-gel method using starch media. Adv. Powder Technol. 26, 113–118. https://doi.org/10.1016/j.apt.2014.08.013

Komatsu, R., Adachi, K., Ikeda, K., 2001. Growth and characterization of potassium niobate (KNbO3) crystal from an aqueous solution. Japanese J. Appl. Physics, Part

1 Regul. Pap. Short Notes Rev. Pap. 40, 5657–5659. https://doi.org/10.1143/jjap.40.5657

Kong, X., Hu, D., Wen, P., Ishii, T., Tanaka, Y., Feng, Q., 2013. Transformation of potassium Lindquist hexaniobate to various potassium niobates: Solvothermal synthesis and structural evolution mechanism. Dalt. Trans. 42, 7699–7709. https://doi.org/10.1039/c3dt00062a

Kudo, K., Kakiuchi, K., Mizutani, K., Fukami, T., Hoshikawa, K., 2004. Non-stoichiometry in potassium niobate crystals grown by directional solidification. J. Cryst. Growth 267, 150–155. https://doi.org/10.1016/j.jcrysgro.2004.03.032

Lee, S., Teshima, K., Niina, Y., Suzuki, S., Yubuta, K., Shishido, T., Endo, M., Oishi, S., 2009. Highly crystalline niobium oxide converted from flux-grown K 4Nb6O17 crystals. CrystEngComm 11, 2326–2331. https://doi.org/10.1039/b905870b

Lente, M.H., 2015. Influence of niobium pentoxide phase and calcination route on the formation of potassium sodium niobate powders. Ferroelectrics 479, 15–21. https://doi.org/10.1080/00150193.2015.1008377

Lewis, A. E., Seckler, M. M., Kramer, H., & Van Rosmalen, G. (2015). Industrial crystallization: Fundamentals and applications. In Industrial Crystallization: Fundamentals and Applications. https://doi.org/10.1017/CBO9781107280427.

Liu, J.F., Li, X.L., Li, Y.D., 2002. Novel Synthesis of Polymorphous Nanocrystalline KNbO3 by a Low Temperature Solution Method. J. Nanosci. Nanotechnol. 2, 617–619. https://doi.org/10.1166/jnn.2002.152

Lu, C.H., Lo, S.Y., Lin, H.C., 1998. Hydrothermal synthesis of nonlinear optical potassium niobate ceramic powder. Mater. Lett. 34, 172–176. https://doi.org/10.1016/S0167-577X(97)00170-5

Ma, Y., Liu, X., Li, Y., Su, Y., Chai, Z., Wang, X., 2014. K4Nb6O17·4.5H2O: A novel dual functional material with quick photoreduction of Cr(VI) and high adsorptive capacity of Cr(III). J. Hazard. Mater. 279, 537–545. https://doi.org/10.1016/j.jhazmat.2014.07.046

Magrez, A., Vasco, E., Seo, J.W., Dieker, C., Setter, N., Forro, L., 2006. Growth of

Single-Crystalline KNbO 3 Nanostructures. . ChemInform 37, 58–61. https://doi.org/10.1002/chin.200615221

Nývlt, J., Hostmomský, J., Giuliietti, M. (2001). Cristalização. São Carlos: EdUFSCar/IPT, 2001. 160p.

Pecchi, G., Cabrera, B., Delgado, E.J., García, X., Jimenez, R., 2013. Activity of KNbO3 as catalyst for soot combustion: Effect of the preparation method. Appl. Catal. A Gen. 453, 341–348. https://doi.org/10.1016/j.apcata.2012.12.030

Penha, F. M., Zago, G. P.; Nariyoshi, Y. N.; Bernardo, A.; Seckler, M. M. (2018). Simultaneous Crystallization of NaCl and KCl from Aqueous Solution: Elementary Phenomena and Product Characterization. Crystal Growth & Design, v. 18, n. 3, p. 1645-1656, 7 mar. 2018. DOI: 10.1021/acs.cgd.7b01603.

Penha F.M., Zago G.P., Seckler M.M. (2019). Strategies To Control Product Characteristics in Simultaneous Crystallization of NaCl and KCl from Aqueous Solution: Seeding with KCl. Crystal Growth and Design, 19 (2), pp. 1257 - 1267, DOI: 10.1021/acs.cgd.8b01670.

Penha, F. M., Zago, G. P.; Seckler, M. M. (2020). Strategies To Control Product characteristics in simultaneous crystallization of NaCl and KCl from aqueous solution: seeding with NaCl and KCl. CrystEngComm, p. 75900-7600.

Penha F.M., Andrade F.R.D., Lanzotti A.S., Moreira Junior P.F., Zago G.P., SECKLER M.M. (2021). In situ observation of epitaxial growth during evaporative simultaneous crystallization from aqueous electrolytes in droplets. Crystals, 11 (9), art. no. 1122, DOI: 10.3390/cryst11091122.

Penha F.M., Gopalan A., Meijlink J.C., Ibis F., Eral H.B. (2021). Selective crystallization of D-Mannitol polymorphs using surfactant self-assembly. Crystal Growth and Design, 21 (7), pp. 3928 – 3935.

Raja, S., Babu, R.R., Ramamurthi, K., 2017. Structural and ferromagnetic properties of KNbO3 microrods. AIP Conf. Proc. 1832, 1–4. https://doi.org/10.1063/1.4980827

Reisman, A., Holtzberg, F., 1955. Phase Equilibria in the System K2CO3-Nb2O5 by the

Method of Differential Thermal Analysis. J. Am. Chem. Soc. 77, 2115–2119. https://doi.org/10.1021/ja01613a025

Rocha, S. D. F., Mansur, M. B., Ciminelli, V. S. T. (2004). Kinetics and mechanistic analysis of caustic magnesia hydration. Chem. Techon. Biotech., v. 79, n. 8, p. 816-821, 2004.

Rocha, S.D.F., Ciminelli, V.S.T. (1995). Effect of surfactants on calcium sulfate crystallization in phosphoric acid solutions. Mining, Metallurgy & Exploration 12, 166–171. https://doi.org/10.1007/BF03403098.

Simões, A.Z., Ries, A., Riccardi, C.S., Gonzalez, A.H., Zaghete, M.A., Stojanovic, B.D., Cilense, M., Varela, J.A., 2004. Potassium niobate thin films prepared through polymeric precursor method. Mater. Lett. 58, 2537–2540. https://doi.org/10.1016/j.matlet.2004.03.025

Souza, C. R., Vaughan, J. Rocha, S. D. F., Birchal, V. Manufacturing Reactive magnesia from nickel laterite waste solution via nesquehonite precipitation. Hydrometallurgy, v. 204, 105725, 2021, doi: 10.1016/j.hydromet.2021.105725.

Su, T., Jiang, H., Gong, H., Zhai, Y., 2010. An alternative approach of solid-state reaction to prepare nanocrystalline KNbO3. J. Mater. Sci. 45, 3778–3783. https://doi.org/10.1007/s10853-010-4431-6

Tanaka, K., Kakimoto, K. ichi, Ohsato, H., 2007. Morphology and crystallinity of KNbO3-based nano powder fabricated by sol-gel process. J. Eur. Ceram. Soc. 27, 3591–3595. https://doi.org/10.1016/j.jeurceramsoc.2007.02.070

Tong, J., Zhou, H., Yu, H., Wu, W., Song, X., Zhao, W., Zhang, C., Wang, X., 2025. Hydrothermal growth of potassium tantalate niobate crystals. J. Cryst. Growth 650, 127983. https://doi.org/10.1016/j.jcrysgro.2024.127983

Uchida, S., Inoue, Y., Fujishiro, Y., Sato, T., 1998. Hydrothermal synthesis of K4Nb6O17. J. Mater. Sci. 33, 5125–5129. https://doi.org/10.1023/A:1004411315906

Vlazan, P., Stoia, M., Poienar, M., S, P., 2017. Phase transition behaviour and

physicochemical properties of KNbO 3 ceramics. Ceram. Int. 43, 5963–5967. https://doi.org/10.1016/j.ceramint.2017.01.120

Vuttivong, S., Vittayakorn, N., 2015. Synthesis and Morphology of KNbO 3 Powders via Hydrothermal Method. Integr. Ferroelectr. 149, 25–31. https://doi.org/10.1080/10584587.2013.852915

Wang, X., Zheng, S., Xu, H., Zhang, Y., 2009. Leaching of niobium and tantalum from a low-grade ore using a KOH roast-water leach system. Hydrometallurgy 98, 219–223. https://doi.org/10.1016/j.hydromet.2009.05.002

Wang, Y., Yi, Z., Li, Y., Yang, Q., Wang, D., 2007. Hydrothermal synthesis of potassium niobate powders. Ceram. Int. 33, 1611–1615. https://doi.org/10.1016/j.ceramint.2006.07.013

Wen, C.H., Chu, S.Y., Juang, Y. Der, Wen, C.K., 2005. New phase transition of erbium-doped KNbO3 polycrystalline. J. Cryst. Growth 280, 179–184. https://doi.org/10.1016/j.jcrysgro.2005.03.033

Wood, E.A., 1951. Polymorphism in potassium niobate, sodium niobate, and other AB O 3 compounds . Acta Crystallogr. 4, 353–362. https://doi.org/10.1107/s0365110x51001112

Yang, D., Wang, Y., Chen, C., Su, Y., Li, L., Miao, L., Gu, H., Zhao, W., Ding, L., Hu, D., 2023. Oriented Plate-like KNbO3 Polycrystals: Topochemical Mesocrystal Conversion and Piezoelectric and Photocatalytic Responses. Inorg. Chem. 62, 10408–10419. https://doi.org/10.1021/acs.inorgchem.3c01286

Yang, Q., Furigay, M.H., Chaudhuri, S., Gau, M.R., Schatz, G.C., Schelter, E.J., 2024. Toward Redox- and Photoredox-Based Niobium/Tantalum Separations. ACS Sustain. Chem. Eng. 12, 8503–8511. https://doi.org/10.1021/acssuschemeng.4c01840

You, J., Li, G., Zhang, S., Zhang, X., Luo, J., Rao, M., Peng, Z., 2021. Synthesis, characterization and thermodynamic properties of KNbO3. J. Alloys Compd. 882, 3–10. https://doi.org/10.1016/j.jallcom.2021.160641

Zago, G. P.; Penha, F. M.; Seckler, M. M. (2019). Product Characteristics In simultaneous crystallization of NaCl and CaSO4 from aqueous solution under different evaporation rates. Desalination, v. 457, n. February, p. 85-95.

Zhang, T., Zhao, K., Yu, J., Jin, J., Qi, Y., Li, H., Hou, X., Liu, G., 2013. Photocatalytic water splitting for hydrogen generation on cubic, orthorhombic, and tetragonal KNbO3 microcubes. Nanoscale 5, 8375–8383. https://doi.org/10.1039/c3nr02356g

Zhou, C., Zhao, Y., Shang, L., Cao, Y., Wu, L.Z., Tung, C.H., Zhang, T., 2014. Facile preparation of black Nb4+ self-doped K4Nb6O17 microspheres with high solar absorption and enhanced photocatalytic activity. Chem. Commun. 50, 9554–9556. https://doi.org/10.1039/c4cc04432k

Zhou, H., Zheng, S., Zhang, Y., 2005. Leaching of a low-grade niobium-tantalum ore by highly concentrated caustic potash solution. Hydrometallurgy 80, 83–89. https://doi.org/10.1016/j.hydromet.2005.07.006

Zhou, H.M., Zheng, S.L., Zhang, Y., Yi, D.Q., 2005. A kinetic study of the leaching of a low-grade niobium-tantalum ore by concentrated KOH solution. Hydrometallurgy 80, 170–178. https://doi.org/10.1016/j.hydromet.2005.06.011

CHAPTER 6 – PRECIPITATION OF NIOBIC ACID FROM POTASSIUM NIOBATE AND SULFURIC ACID SOLUTIONS AND ITS CONVERSION THROUGH CALCINATION

6.1 Introduction

Niobium oxides have a great potential of practical applications as individual compounds or as components of solid solution. Among the niobium oxide compounds, niobic acid has shown interesting properties as a catalytic material due to its high activity, selectivity and stability (Brandão et al., 2009; Ushikubo et al., 1993).

Niobic acid ($Nb_2O_5.nH_2O$) is an amorphous hydrated form of niobium pentoxide (Nb_2O_5) composed mainly of distorted NbO_6 octahedra and NbO_4 tetrahedra (Hara, 2014; Nakajima et al., 2011). The Nb–O bonds are highly polarized in distorted polyhedrons and this part of the surface OH group acts as Brønsted acid sites, while the NbO_4 tetrahedra act as a Lewis-acidic sites, due to its positive charge (Siddiki et al., 2019; Takagaki et al., 2013). When calcined at 100 – 300ºC, the amorphous niobic acid surface acquires high acidity with a strong Brønsted acidity – H_0: 5.6, which decreases with increasing the calcination temperature due to the conversion of amorphous niobic acid into niobium oxide polymorphous (Carniti et al., 2006; Lebarbier et al., 2012).

Hydrous niobium oxide is usually applied as a solid acid catalyst for several reactions such as esterification, hydration, dehydration, condensation, hydrolysis (Brandão et al., 2009; Tanabe and Okazaki, 1995). Niobic acid is a catalytic solid stable even in the presence of water (Tanabe, 2003; Tanabe and Okazaki, 1995). The use of solid acid catalyst is an environmentally friendly alternative to liquid acids and has been studied to the development of green chemical process (Hara, 2014; Nakajima et al., 2010; Takagaki et al., 2013).

Niobic acid can be produced by different ways based on precipitation process that can occur by decomposition of niobates in acidic solution or by hydrolysis process. The method of synthesis has an important influence in the properties of this oxides such as the particles size, the chemical and phase composition, and degree of defects and

incorporation of impurities (Brandão et al., 2009; Deblonde et al., 2019; Fan et al., 2013; Ushikubo et al., 1993).

Precipitation is a process where a product is formed through a chemical reaction, also known as reactive crystallization. This definition introduces several factors that impart various characteristics to precipitation. One of them is the low solubility of the solids formed, allowing for high supersaturation levels, which in turn promotes very high primary nucleation rates. Another important factor is that high nucleation rate produces a large number of nuclei, which limits the average size of the crystals (Söhnel & Garside, 1992).

In the precipitation process, to form a low-solubility product, in the range of 0.001 to 1 kg/m³ (solute/solvent), two soluble reagents are mixed. Aiming at high recovery, solutions with high concentrations – very high supersaturation – are used to increase the conversion of the formed species into solid particles, typically making this a very rapid process. However, high levels of supersaturation may lead to the formation of low-quality products (small primary crystals and agglomerates) and other undesirable phases, such as polymorphs or amorphous phases (Lewis et al., 2015). Since the degree of supersaturation is one of the primary factors for achieving the desired precipitation rates, uniform degree of mixture is essential, as homogeneous supersaturation in the reactor is critical for the quality of the final product.

The amorphous niobic acid is formed in the beginning of precipitation process and has a high degree of disorder. During the aging of hydrated niobium oxide several processes occurs such as recrystallization, aggregation, and Ostwald ripening, which involve gradual transformation of the precipitates. Metastable forms transition into more stable structures, and dehydration of the precipitates also take place, resulting in denser and more stable compounds with reduced water content (Nikishina et al., 2012).

The anhydrous form of niobium pentoxide (Nb_2O_5) – a white solid, is air stable and insoluble in water. The use of niobium pentoxide as an electronic material has attracted attention because of its resistance to acid and base, stability in aqueous medium and high refractive index (Xiao et al., 2008). It has been used with great potential as anode material for lithium-ion batteries, solar cells, photocatalytic conversion, sensors and optical devices (Su et al., 2010; Xiao et al., 2008; Yun Zhao et al., 2012). The electronic

properties of Nb_2O_5 depends on its crystalline structure and stoichiometry (Jun Park et al., 2022).

According to Ody (2018), niobium oxide is obtained through the thermal treatment of niobic acid ($Nb_2O_5.nH_2O$), an endothermic process that involves a thermal decomposition of the hydrated niobium oxide ($Nb_2O_5.nH_2O$) into niobium pentoxide (Nb_2O_5). In this process, the temperature is the parameter that most influence the crystallinity of the solid. Niobium pentoxide exhibits many polymorphic forms, such as TT-Nb_2O_5 (pseudohexagonal), T-Nb_2O_5 (orthorhombic) and H-Nb_2O_5 (monoclinic) as the most common phases.

The Figure 6.1 summarize the structure of Nb_2O_5 as function of calcination temperature. The transition from one structure to another depends on the initial material, impurities and temperature. At lower temperatures the Nb_2O_5 is an amorphous phase and converted into a crystalline phase with increase in temperature.

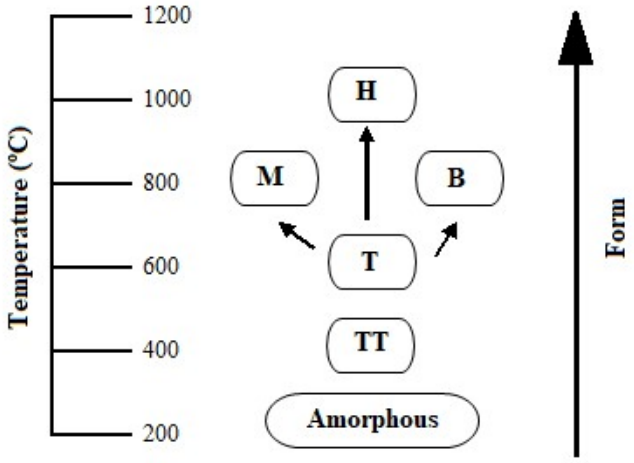

Figure 6.1. Modification of Nb_2O_5 structure – H, M, B: monoclinic; T: orthorhombic; TT: pseudohexagonal. Source: Adapted from Ko and Weissman, 1990.

The difference between T and TT phases are that some oxygen atoms in T-phase are replaced by monovalent species or vacancies (reported as impurities in TT phase) while Nb atoms occupy a range of positions between the sites (Nowak & Ziolek, 1999). The most thermodynamic stable structure is the monoclinic phase (H) and the

pseudohexagonal (TT) is the least stable one (Zhao et al., 2012). The phases B- and M- are medium-temperatures transition group.

6.2 Materials and methods

6.2.1 Reagents

Potassium niobate crystallized from Fe-Nb alloy fines alkaline liquor was used as source of niobium to niobic acid precipitation (Chapter 5). Analytical-grade sulphuric acid (H_2SO_4 - CAS 7664-93-9) was used without further purification. All solutions were prepared with Milli Q water.

6.2.2 Modeling

The PHREEQC version 3.4.12927 (Parkhurst and Appelo, 2013) was used to model and evaluate the speciation of the niobium system. The SIT (Specific ion Interaction Theory) database (sit.dat) was used as aqueous model to obtain the solution description parameters, such as composition data, saturation index, distribution of the species in the solution and possible solid phases formed.

To obtain the solution description parameters, a thermodynamic modelling was also performed using OLI Studio Stream Analyser (version 11). The thermodynamic framework AQ (aqueous model) and MSE (Mixed Solvent Electrolyte) were used in OLI. The AQ thermodynamic framework includes both stable phases – $KNbO_3$ and Nb_2O_5 – and is applied to electrolytes dissolved in water, using the Bromley-Zemaitis activity model. In contrast, the MSE framework contains only the Nb_2O_5 and utilizes the MSE activity model, which uses (i) the extended Debye-Huckel term that accounts for long-range interactions, (ii) an UNIQUAC term that accounts for short-range interactions, and a middle-range term that includes the ionic interactions.

6.2.3 Niobic acid precipitation

Niobic acid was precipitated with H_2SO_4 solution addition to a potassium niobate solution. The initial solution was prepared dissolving 5 g of previously crystallized potassium niobate into 50 mL of distilled water at 90 ± 0.50 ºC in a beaker. Two different

concentrations of H_2SO_4 solution were used as precipitant agent - 0.25 and 0.50 mol/L, slowly added to the niobium solution until pH 3. The system was maintained under stirring at 200 rpm for 30 minutes after the pH 3 was achieved.

The obtained solids were washed – after a first step of filtration – with 50 mL of Milli-Q water under agitation for 20 minutes at 40 ºC, to remove the impurities. The solids were vacuum filtered on a quantitative strip filter paper and later dried at 60 ºC for 12 hours prior to analysis.

6.2.4 Supersaturation index

The supersaturation of the system during the crystallization was calculated from the chemical solution composition measurements using the Equation 6.1:

$$S = \frac{c}{c_{eq}} \tag{6.1}$$

Where S is the supersaturation, c the concentration in the solution and c_{eq} the equilibrium concentration (solubility). The solubility data was given by OLI Studio.

6.2.5 Calcination

The thermal conversion of niobic acid ($Nb_2O_5.nH_2O$) to Nb_2O_5 was carried out in a furnace (CARBOLITE CWF1200) at 900 ºC for 5 hours. The solids obtained were subsequently characterized.

6.2.6 Physico-chemical characterization

The chemical composition of the aqueous solutions was determined by ICP-OES (Thermo Scientific - iCAP 7000 Series). The detection limit was < 0.005 mol/L.X-ray diffraction was carried out to identify the crystalline phases in solids using the PHILIPS equipment (XRD PANalytical and PANalytical, X'Pert Pro) both with a Cu (Kα) radiation.

The solids were analysed by X-ray fluorescence spectrometer with wavelength dispersion (WDXRF - ARL PERFORM'X - Thermo Scientific GEN-X 4200W) and Rd tube (5GNf Rh 50u) to determine their chemical composition.

To analyse the structural characteristics, such as chemical composition and intermolecular interactions, the Fourier Transform Infrared (FTIR) spectroscopy was used and performed in a spectrometer at a resolution of 4 cm^{-1} and scanned from 4000 to 400 cm^{-1} (Bruker Alpha and Perkin Elmer UATR Two).

Scanning Electron Microscopy (SEM) (APREO 2C – Thermo Ficher) coupled with Energy-Dispersive X-ray Spectroscopy (EDS) (Bruker Xflash 60-30) was used to provide information about the solids surface morphology and composition.

The niobic acid particles size distribution was measured by laser diffraction particle size analyzer (Shimadzu SALD-2300) in water and glycerine. The thermal stability of the solids was evaluated by thermogravimetric analysis (Netzsch STA 449 F3 Jupiter) under an inert atmosphere with nitrogen at a flow rate of 80 mL/min.

6.3 Results and Discussions

6.3.1 Niobic acid precipitation

From the initial solution of potassium niobate, the niobic acid was precipitated by adding H_2SO_4 solution. Two different concentrations were used – 0.25 and 0.50 mol/L H_2SO_4, to investigate the influence of supersaturation on the final product.

As the crystallized potassium niobate was used as source of niobium and precursor to other niobium compounds, a simulation in OLI Studio and PHREEQC was conducted and its behaviour in acid media was evaluated through the addition of 0.25 and 0.50 mol/L H_2SO_4. The addition of the acid solution promotes the formation of niobium oxide due to the decrease in the solution's pH. pH 3 was considered the optimal condition for niobic acid precipitation, since at this pH value all the potassium niobate was dissolved. Moreover, both PHREEQC and OLI show that niobic acid achieves the highest supersaturation index at pH 3, as shown in Figure 6.2.

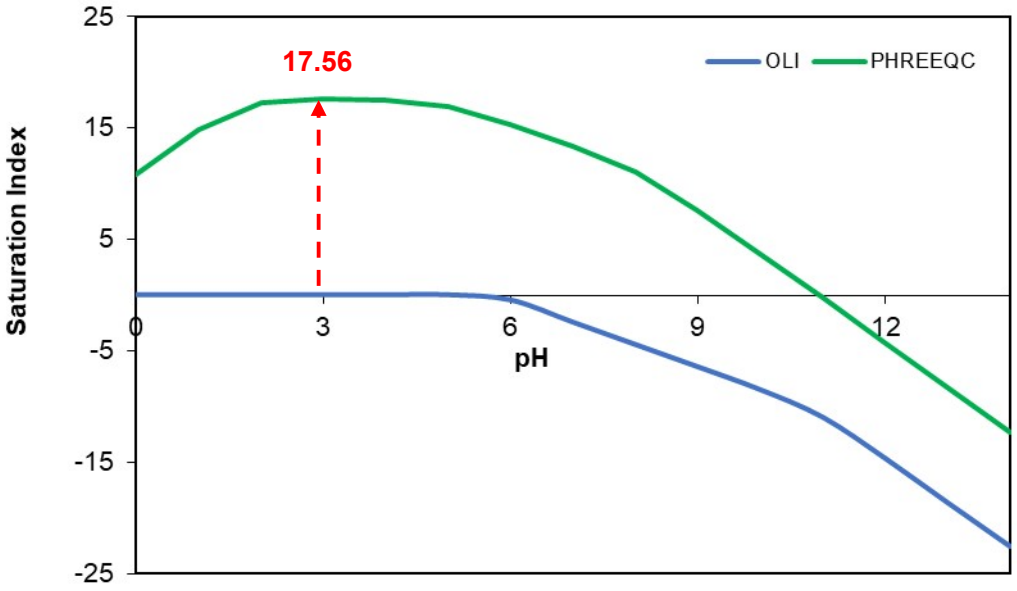

Figure 6.2. Saturation index of $Nb_2O_5.nH_2O$ as function of the pH by PHREEQC and OLI Studio.

Figure 6.3 shows the concentration of niobium, potassium and sulfate (as Sulfur) in the start and final solution of precipitation compared to the values obtained by theoretical calculations (based on the chemical composition of dissolved potassium niobate solid in the start solution) and simulated by PHREEQC and OLI Studio.

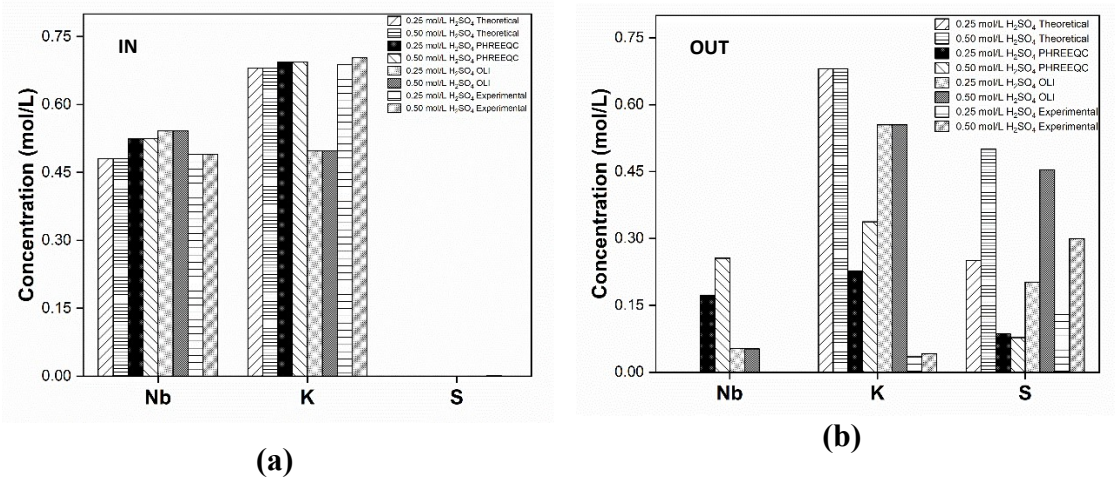

(a) **(b)**

Figure 6.3. Concentration of Nb, K and S (as sulfate) in the start and final solution to niobic acid precipitation with 0.25 and 0.50 mol/L H_2SO_4 at 90±0.50 ºC and 200 rpm.

Figure 6.3 (a) shows the initial concentration of the start solution to niobic acid precipitation. It is possible to observe a small fluctuation from the modeled data for Nb concentration. Notably, for K concentration a significant deviation is only seen between the OLI Studio and others. This could be explained by the fact that only the $KNbO_3$ was used as source of Nb in the simulations on OLI to precipitation of niobic acid, and, experimentally and on PHREEQC simulations, the intermediate phase $K_4Nb_6O_{17}$ was present. No sulfate was present in the start solution.

At the end of niobic acid precipitation very low concentration of Nb in solution was measured for both H_2SO_4 concentrations used (0.25 and 0.50 mol/L), as seen in Figure 6.3 (b). However, to the PHREEQC and OLI Studio simulations a remaining Nb was still present in solution at the end of the reaction. The simulations also showed a pronounced decrease in K and S concentration, indicating its consumption during the precipitation. This indicates secondary phases of K and S can be precipitated together with niobic acid. For both PHREEQC and OLI Studio simulations, secondary phases were allowed to be formed, since a consumption in K and S was observed experimentally, and the formation of K_2SO_4 was predicted only by OLI Studio. According to Souza et al. (2021), the complexation of sulfate affects the supersaturation index calculation, since only free sulfate was considered in the equilibrium expression in PHREEQC simulations.

The supersaturation of the system was calculated (Table 6.1) based on the aqueous Nb concentration in the solution from experimental data and OLI Studio simulations, considering the amounts of potassium niobate initially dissolved, according to the Equation 6.1 The equilibrium concentration of Nb that was taken from OLI Studio simulations was considered the addition of 0.50 and 0.25 mol/L H_2SO_4 in the solution to niobic acid precipitation.

Table 6.1 Supersaturation from experimental data of precipitation of niobic acid with 0.50 and 0.25 mol/L H_2SO_4 at 90±0.50 ºC and 200 rpm.

Supersaturation*	**0.50 mol/L H_2SO_4**	**0.25 mol/L H_2SO_4**
Initial solution	9.33	9.11
Final solution	1.87×10^{-2}	6.83×10^{-3}

* The solubility limit was based on aqueous Nb^{5+} from experimental data and OLI Studio modeling at 90 ºC of 0.0525 and 0.535 mol/L with 0.50 and 0.25 mol/L H_2SO_4, respectively.

The supersaturation was evaluated based on the concentration ratio, with the H_2SO_4 solution being gradually added and maintained at constant pH= 3. The calculated supersaturation would have reached its maximum if the addition of H_2SO_4 had been added instantaneously. However, since the addition was conducted in steps during the precipitation process, the supersaturation was lower than the reference value (Table 6.1). Furthermore, the supersaturation on the final solution represents the real value of residual supersaturation.

The chemical composition of the product by XRF analysis confirms that potassium and sulphur were also consumed during the precipitation (Table 6.2). Due to the presence of them in the solids, a washing protocol to the precipitated solids was implemented to improve the quality of niobic acid and further niobium oxide.

Table 6.2. Chemical composition of niobic acid precipitate with 0.25 and 0.50 mol/L H_2SO_4 at 90 ± 0.50 ºC and 200 rpm compared to commercial niobic acid HY-340.

Samples	**Nb (%)**	**S (%)**	**K (%)**
Commercial HY-340	69.36	-	-
0.25 mol/L H_2SO_4			
unwashed	56.65	3.23	7.73
washed	61.47	0.15	2.49
0.50 mol/L H_2SO_4			
unwashed	56.72	3.53	7.78
washed	64.38	0.07	2.04

From the Table 6.2, after washing the precipitated solids 68% of K and 95% of S were removed from the precipitated niobic acid. Additionally, the washed niobic acid precipitated with addition of 0.25 mol/L H_2SO_4 has an Nb composition of 89% when compared to the commercial one while the precipitated with 0.50 mol/L H_2SO_4 has 93%. The concentration of niobium, potassium and sulfur and pH were evaluated during the washing of the solids, as shown Figure 6.4.

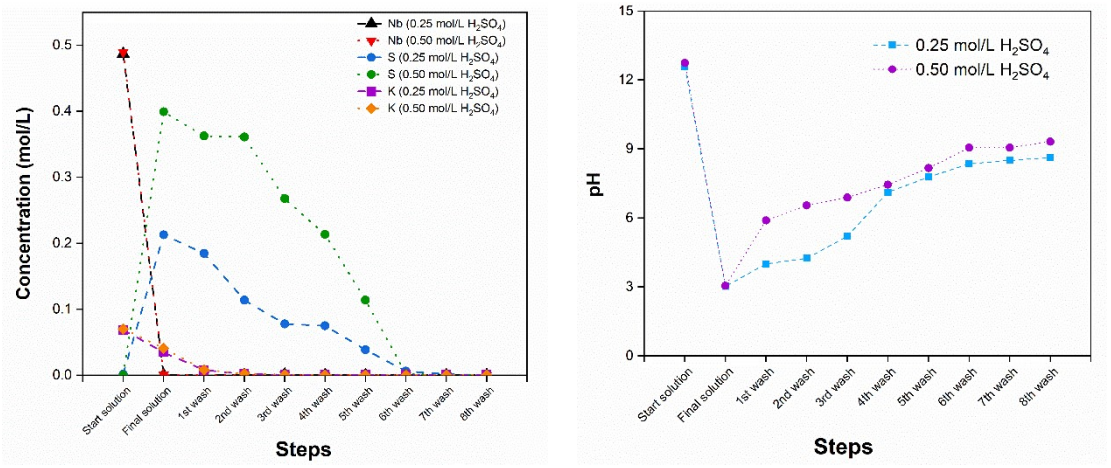

Figure 6.4. (a) Concentration of Nb, K and S and (b) pH during the washing protocol of the niobic acid precipitated using 0.25 and 0.50 mol/L H_2SO_4 addition at 90±0.50 ºC and 200 rpm.

Figure 6.4 (a) shows the concentration of niobium, potassium and sulfur during the washing protocol of precipitated solids. Niobium was not detected in the solutions from washing of the solids. However, it is possible to verify the decreasing in the concentration of potassium and sulfur through the washing steps. After the 2nd wash, potassium was no longer present in the washing solution and soluble S (sulfate) was not detectable after the 6th wash. To ensure the maximum removal of K and S, the precipitated solids were washed 8 times for both concentration of H_2SO_4 solution used during the precipitation. Figure 6.4 (b) shows the increase in the pH of the solution during the washing step, confirming the removal of the impurities K and S from the solids.

Through the XRD (Figure 6.5), it is seen that the solids presented an amorphous structure, similar to the commercial niobic acid HY-340 from CBMM and in agreement with the literature (Brandão et al., 2009; Chan et al., 2017a; Chen et al., 2022; Guo and Qian, 1993; Lebarbier et al., 2012; Luisa Marin et al., 2014; Rodrigues and da Silva, 2010; Tanabe, 1987). The amorphous phase of niobic acid is mostly used in catalysis, which has relevant, yet underexplored, properties for environmental applications (Fillela and May, 2020). As expected, diffraction peaks related to the presence of potassium sulphate were detected in all samples of unwashed niobic acid. This result corroborates with the chemical composition of solids in Table 6.2 and with the excess solid yield.

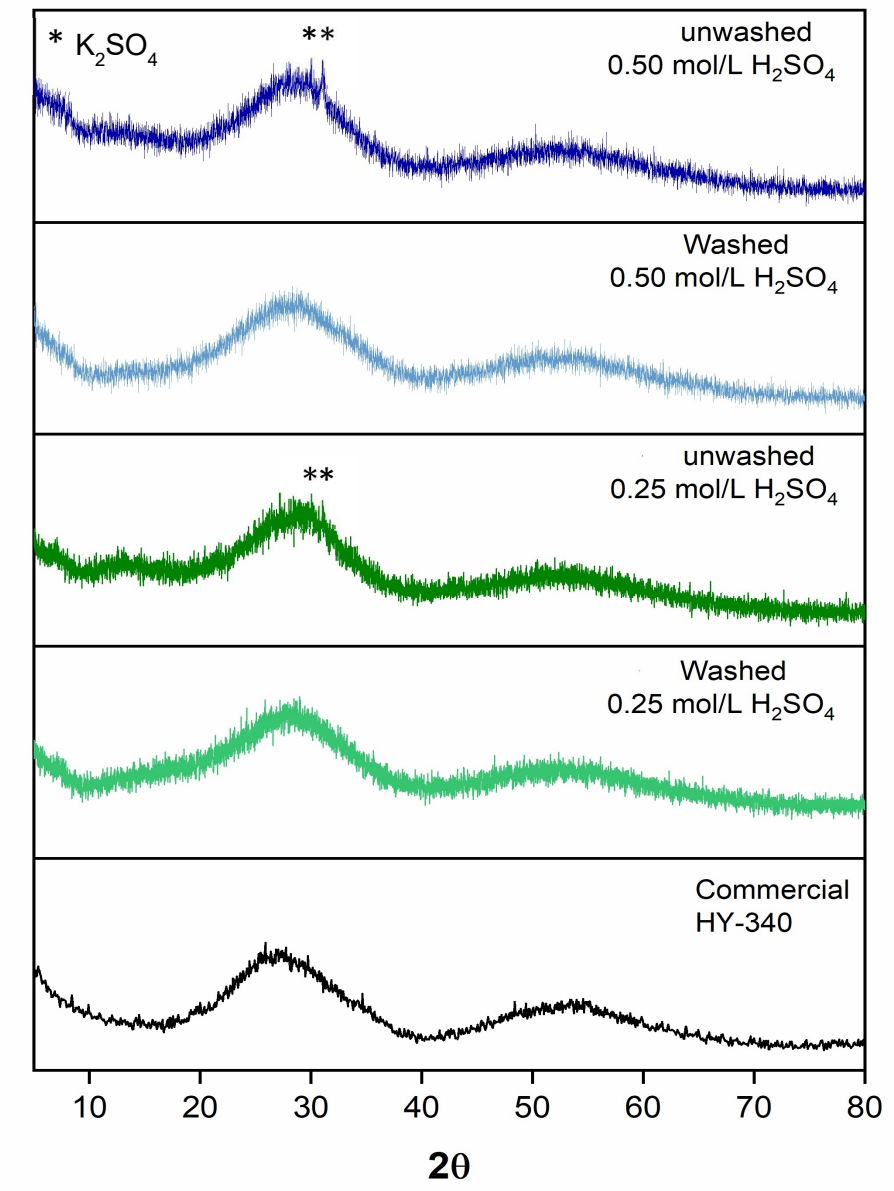

Figure 6.5. XRD of precipitated niobic acid with 0.25 and 0.50 mol/L H_2SO_4 addition at 90±0.50 ºC and 200 rpm before and after the washing protocol.

The Raman analysis (Figure 6.6) also indicates the presence of potassium sulphate in the precipitate. The unwashed solids precipitated by addition of 0.50 mol/L H_2SO_4 shows higher intensity bands related to the impurities at 450, 620, 624, 980, 981 1100 and 1145 cm^{-1}. According to Qiu et al. (2019), these bands are related to K_2SO_4. For the solid precipitated by addition of 0.25 mol/L H_2SO_4, only a weak band was attributed to the presence of potassium sulphate in the solids. The spectrum obtained to the washed precipitated solids shows only broad bands, characteristic of niobic acid (Chan et al.,

2017b; Lebarbier et al., 2012) which confirms the removal of impurities with the implementation of a washing protocol.

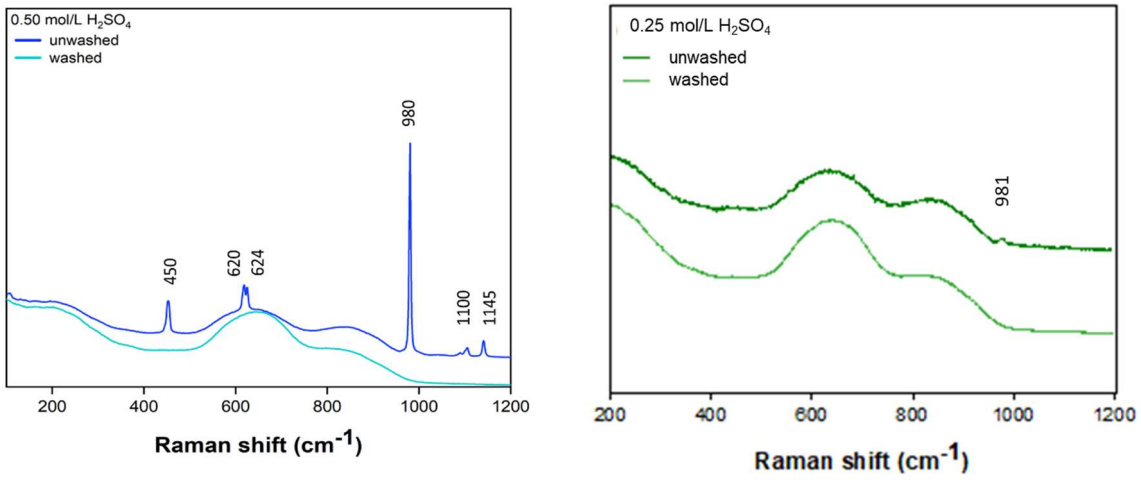

Figure 6.6. RAMAN of potassium niobate with (a) 0.50 and (b) 0.25 mol/L H_2SO_4 addition at 90±0.50 ºC and 200 rpm before and after the washing protocol.

The FTIR spectra (Figure 6.7) of precipitated niobic acid presented bands around 4000 and 2400 cm^{-1} which are related to the presence of water in the solids and O-H bonds. The band at 1600 cm^{-1} is due to absorbed water and hydroxyl (Nb-OH) on $Nb_2O_5.nH_2O$. The number of Brønsted and acid-Lewis sites, which corresponds to the OH group associated with Nb-O bonds, on the surface of the solid could be attributed at this band (Fan et al., 2013; Siddiki et al., 2019). Weak bands between 1000 and 800 cm^{-1} present in the unwashed solids could be associated to the presence of potassium and sulfate bonds in the solids (Chen et al., 2022). Bands around 800 and 400 cm^{-1} are related to vibration of Nb=O and Nb-O groups, characteristic of hydrated niobium oxides (Chen et al., 2022; Rodrigues and Silva, 2010). From the analysis, the spectra obtained for the washed niobic acid solid precipitated with 0.50 mol/L H_2SO_4 was similar to the commercial one.

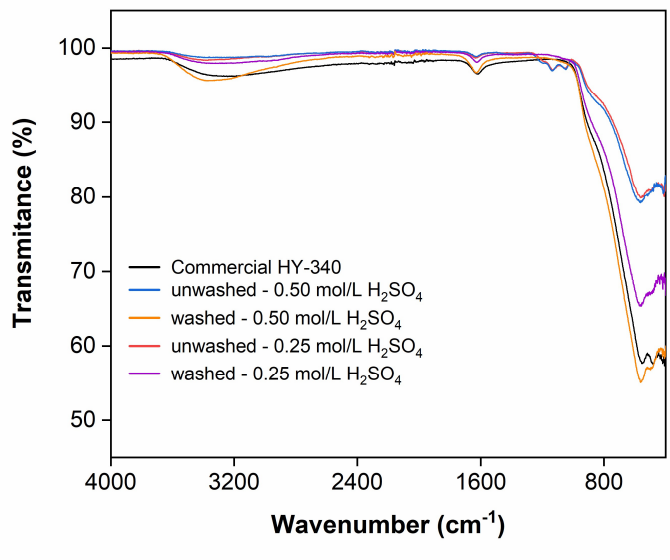

Figure 6.7. FTIR spectrum of potassium niobate with 0.25 and 0.50 mol/L H_2SO_4 addition at 90±0.50 ºC and 200 rpm before and after the washing protocol.

The results of TG-DSC analysis of all samples of precipitated niobic acid are presented in Figure 6.8, alongside the commercial sample. According to the TG, the niobic acid weight loss between 25 and 300 ºC for all samples is attributed to removal of adsorbed and structural water. These results are in agreement with the literature (Foo et al., 2014; Nikishina et al., 2012; Rade et al., 2018; Tokio Iizuka, 1983). The niobic acid precipitated under both conditions of H_2SO_4 addition presents a second weight loss at ~ 700 ºC that could be related to the presence of a potassium and sulfate in the solids. The dehydration of sulphuric acid groups occurs when the solids are heated at higher temperatures (> 700 º) (Brandão et al., 2009; Chen et al., 2022). The washing the precipitated solids removed the sulfate, and as expected the peaks related to the presence of sulphate in the solids disappeared (Figure 6.8 (a-d)). As a residual of potassium still is present in the washed solids, the peaks at ~ 500 and 600 ºC (Figure 6.8 (b-d) may be related to a formation of a potassium niobate phase during the heating process. The commercial niobic acid (Figure 6.8 (e)) presents a peak at 556 ºC that are related to transformation of crystalline phase. According to Brayner and Bozon-Verduraz (2003), at 600 ºC the pseudo-hexagonal – orthorhombic transformation of commercial niobic acid can occur.

With the increase of temperature, exothermic peaks can be observed in Figure 6.8 (a-e). The exoeffect corresponds to phase transformation of niobic acid, the transition from the amorphous to a crystalline structure.

According to the TG analysis the degree of hydration of the final niobium pentoxide – *n* in $Nb_2O_5 \cdot nH_2O$ – could be estimated. The compositional formula for all samples is presented in Table 6.3.

Table 6.3. Compositional formula of precipitated niobic acid with 0.25 and 0.50 mol/L H_2SO_4 addition at 90±0.50 ºC and 200 rpm before and after the washing protocol and commercial HY-340.

Sample	Compositional formula
0.50 mol/L H_2SO_4	
Unwashed	$Nb_2O_5 \cdot 0.67H_2O$
Washed	$Nb_2O_5 \cdot 0.98H_2O$
0.25 mol/L H_2SO_4	
Unwashed	$Nb_2O_5 \cdot 0.73H_2O$
Washed	$Nb_2O_5 \cdot 0.78H_2O$
Commercial	
HY-340	$Nb_2O_5 \cdot 1.19H_2O$

It is noteworthy that the hydration degree estimations shown in Table 6.4 may deviate from reality, since previous analysis have shown residual potassium in the solid samples. There is a difference in the hydration degree between the precipitated niobic acid in this study and the commercial solid. This difference is significant for catalytic applications, as the hydration degree directly influences the number of O-H groups, which are related to acidic sites in the solid (Fan et al., 2013; Nikishina et al., 2012; Siddiki et al., 2019).

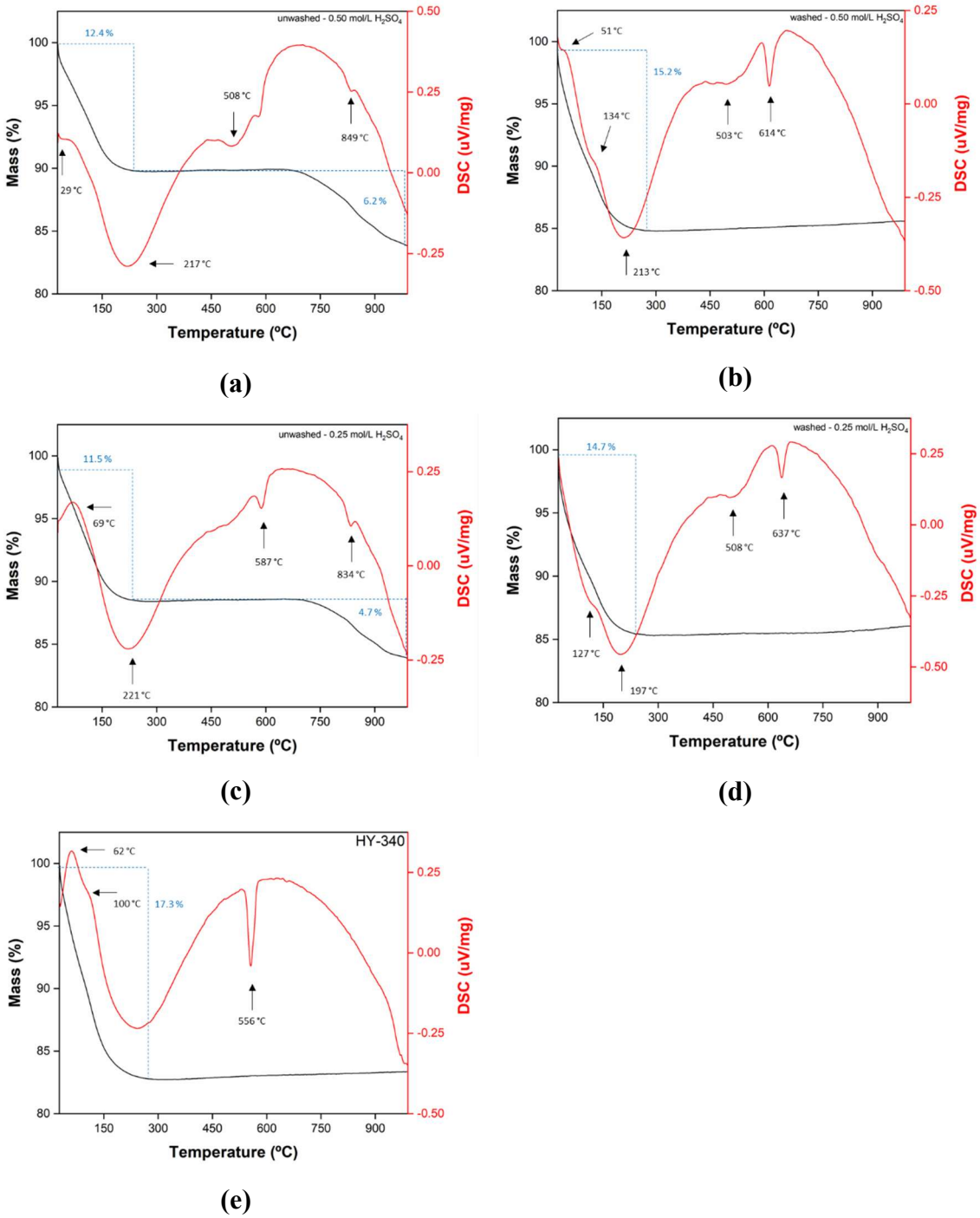

Figure 6.8. TG-DSC of niobic acid precipitated at 90±0.50 ºC and 200 rpm with 0.50 mol/L H_2SO_4 (a) unwashed and (b) washed; with 0.25 mol/L H_2SO_4 (c) unwashed and (d) washed and (e) commercial niobic acid HY-340.

Figure 6.9 shows the SEM images of the precipitated niobic acid. It can be observed that particles are amorphous and agglomerated. Amorphous material contains more adhering solution after filtration and this can influence in the purity of the product after drying and increase its tendency to caking. Through the chemical elemental mapping and backscattering images, it was possible to identify regions with the presence of a secondary phase, attributed to potassium sulphate formation, in the unwashed solids and a residual of K and S in the washed precipitated solids.

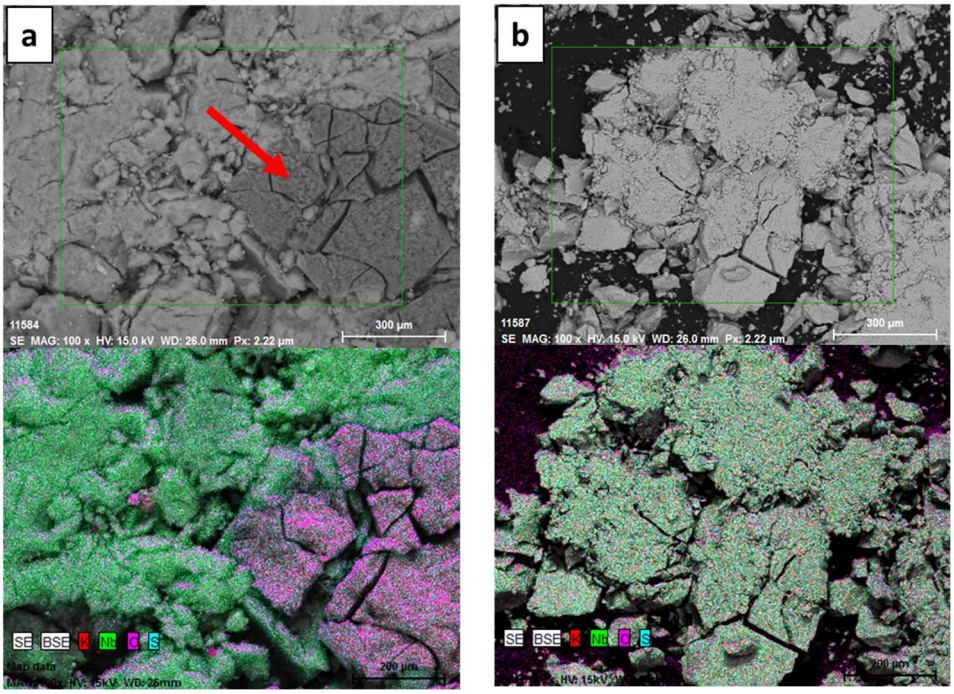

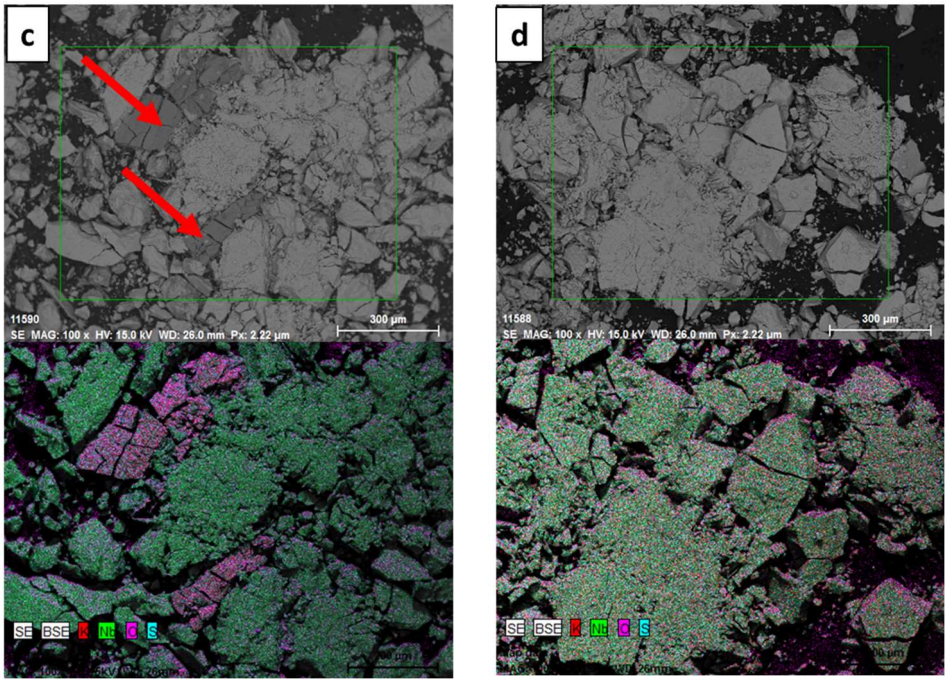

Figure 6.9. SEM backscattering images and chemical mapping of niobic acid precipitated at 90±0.50 ºC and 200 rpm with 0.50 mol/L H_2SO_4 (a) unwashed and (b) washed and with 0.25 mol/L H_2SO_4 (c) unwashed and (d) washed. Red arrow: regions with potassium niobate phase.

Table 6.4 shows the particle size distribution (D50 and D90) of niobic acid precipitated under different conditions, by addition of 0.25 and 0.50 mol/L H_2SO_4, both before and after the washing protocol. In addition, to compare the results, commercial niobic acid HY-340 was also analysed.

Table 6.4. Size of the particles of precipitated niobic acid with 0.25 and 0.50 mol/L H_2SO_4 addition at 90±0.50 ºC and 200 rpm before and after the washing protocol and commercial HY-340.

Samples	D50 (µm)	D90 (µm)
0.50 mol/L H_2SO_4		
Unwashed	12.53 ± 0.73	70.01 ± 0.73
Washed	34.41 ± 0.55	82.45 ± 0.55
0.25 mol/L H_2SO_4		
Unwashed	18.63 ± 0.75	86.76 ± 0.75
Washed	35.81 ± 0.66	94.54 ± 0.66
Commercial		
HY-340	22.28 ± 0.60	67.62 ± 0.60

From the D50 of the precipitated solids at 0.25 mol/L H_2SO_4, larger particles were observed before washing when compared to solids precipitated at 0.50 mol/L H_2SO_4. The washing protocol may promote an increase in the median size of particles. This may be attributed to the removal of smaller particles or particles agglomeration during the washing. The commercial niobic acid HY-340 presents slightly smaller crystals in both D50 and D90, meaning that the particle size distribution is narrower when compared to the obtained experimentally, especially the washed samples. Besides clear impact of the washing protocol in particle size and size distribution, the presence of impurities in the precipitated solids may also influence on particle size.

The control of the particle size is very difficult during the process of crystallization, specially via precipitation. One factor is that new particles are being generated during the process, which results in a product with different particle size (Nývlt et al., 2001). Furthermore, the solids in this study were produced using a batch process, different from industry that is usually a continuous process. As a result, continuous processes are expected to produce solids with a narrower particle size distribution. Additionally, controlling the supersaturation during the precipitation process and in the mixing of solution can enable a better control of particles size distribution.

6.3.2 Niobic acid calcination

Washed niobic acid precipitated with addition of 0.50 and 0.25 mol/L H_2SO_4 was calcined at 900 ºC for 5 hours. The solids contain a proportion of 89.20 and 90.18% of Nb_2O_5 and 2.11 and 1.44 % of K_2O, respectively. Due to the presence of residual potassium in the solids, less than 2%, the XRD analysis shows the presence of a potassium niobate phase as $K_2Nb_8O_{21}$ in addition to Nb_2O_5, as shown in Figure 6.10. The undefined peaks could be related to other minor intermediate potassium niobate phases such as $K_6Nb_{10.81}O_{30}$, $K_2Nb_6O_{16}$ and $K_2Nb_6O_{41}$.

According to the Figure 6.1, niobium oxide exists in many polymorphic forms and its crystallinity changes with heat treatment. In temperatures above 300 ºC the solid presents an amorphous structure and as the temperature increases its structure changes (Filella and May, 2020; Ko and Weissman, 1990; Pinto et al., 2017; Siddiki et al., 2019).

$K_2Nb_8O_{21}$ is usually synthesized by fusion of Nb_2O_5 and a source of potassium (KCl, $KHCO_3$) at higher temperatures (600 to 1100 ºC) and time of reaction (Teshima et al., 2008; Xu et al., 2008; Cheng et al., 2018; Guo et al., 2020; Liu et al., 2014). With an orthorhombic structure, this material exhibits unique properties to technological applications, high photocatalytic activity and good dielectric properties (Teshima et al., 2008;Liu et al., 2014). This phase also presents potential to be used in electronic batteries (Cheng et al., 2018).

The FTIR spectra of calcined niobic acid is presented in Figure 6.10. As the solids were calcined at high temperature, bands related to the presence of OH bonds were not identified. The bands observed between 1000 to 400cm^{-1} can be attributed to Nb_2O_5 (Huang et al., 1999). However, other studies also identify bands around the same wavenumber related to potassium niobate phases (De Andrade et al., 2000; Kudo and Sakata, 1996; Liu et al., 2002; Wang et al., 2007). No clear distinction between the peaks and these two compounds could be made based on existing literature.

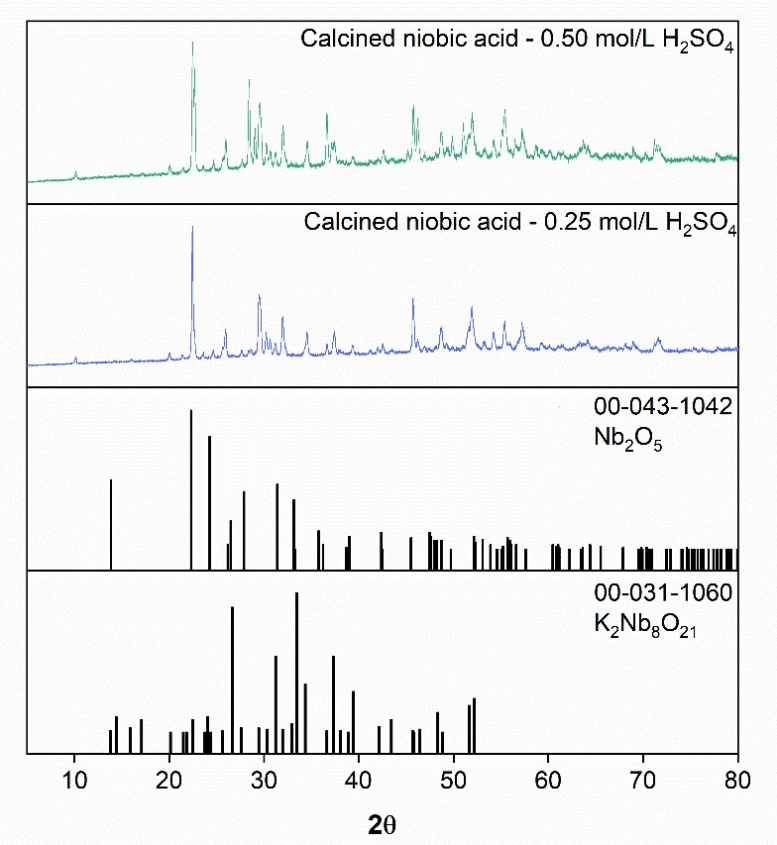

Figure 6.10. XRD of calcined niobic acid precipitated at with addition of 0.50 and 0.25 mol/L H_2SO_4 after washing protocol.

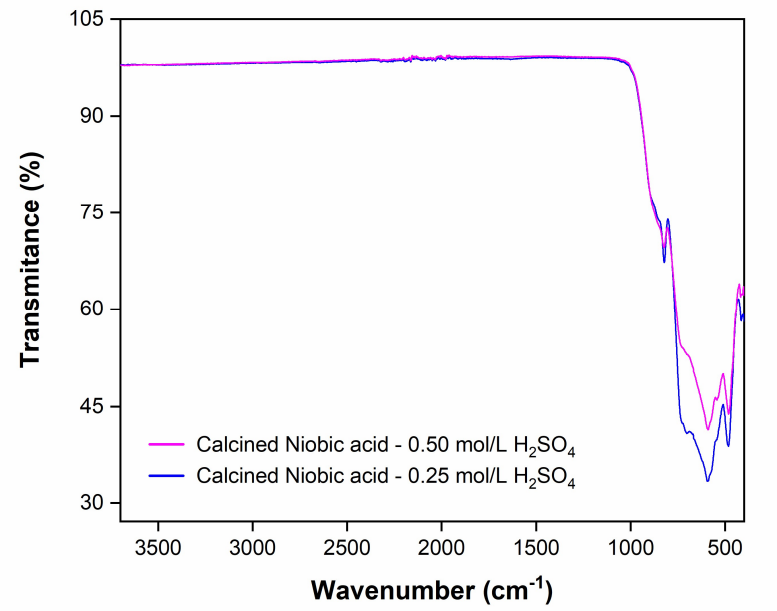

Figure 6.11. FTIR spectra of calcined niobic acid precipitated at with addition of 0.50 and 0.25 mol/L H_2SO_4 after washing protocol.

SEM images of calcined niobic acid is presented in Figure 6.12.

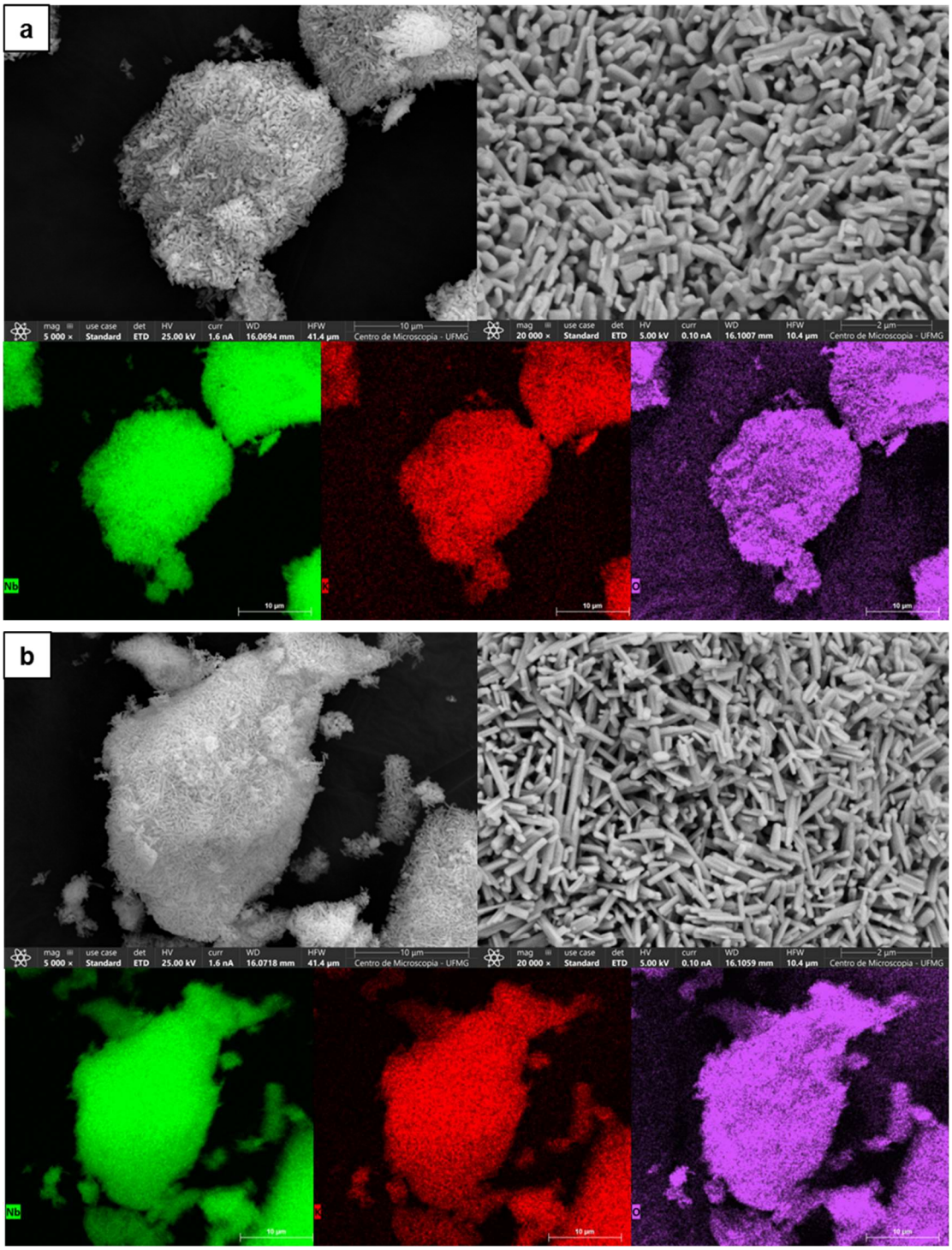

Figure 6.12. SEM of calcined niobic acid precipitated at with addition of (a) 0.50 and (b) 0.25 mol/L H_2SO_4 after washing protocol. Chemical mapping: green: Nb, red: K and purple: O.

From the SEM images (Figure 6.12) of calcined niobic acid of both conditions (0.50 and 0.25 mol/L H_2SO_4 after washing) it is noticeable that the sample was composed of many rod-like crystals smaller than 1 micron, typical morphology of $K_2Nb_8O_{21}$ particles (Teshima et al., 2008). The calcined niobic acid (precipitated by addition of 0.50 mol/L H_2SO_4) presented smaller agglomerates of particles compared to the other condition. The morphology of the solids could stick to each other and form agglomeration clusters (Guo et al., 2020). This can be related to the chemical composition of the solids. According to Teshima et al. (2008), the concentration of Nb directly influence crystal size and shape.

The elemental chemical mapping of calcined solids shows that the elements Nb, K and O are homogeneously distributed throughout the rod-like crystals. The chemical composition by XRF displays the presence of 63.04 % of Nb, 1.20 % of K and 0.04 % of S to calcined niobic acid precipitated from 0.50 mol/L H_2SO_4 and 62.34 % of Nb, 1.75 % of K and 0.06 % of S to those calcined niobic acid precipitated from 0.25 mol/L H_2SO_4.

The size of the particles can be seen in Table 6.5. The size of the particles was nearly similar in both samples of calcined solids, presenting a median size of 31.76 ± 0.73 and 36.34 ± 0.72 µm for washed agglomerated solids with 0.50 and 0.25 mol/L H_2SO_4, respectively.

Table 6.5. Size of the particles of calcined niobic acid precipitated at with addition of 0.50 and 0.25 mol/L H_2SO_4 after washing protocol and commercial niobium oxide - high purity.

Samples	**D50 (µm)**	**D90 (µm)**
0.50 mol/L H_2SO_4		
Washed	31.76 ± 0.73	93.50 ± 0.73
0.25 mol/L H_2SO_4		
Washed	36.34 ± 0.72	109.38 ± 0.72
Commercial		
High Purity	28.78 ± 0.52	63.46 ± 0.52

Despite its similar morphology, the particles obtained from this study by calcination of precipitated solids were larger compared to those reported in the literature (Cheng et al., 2018; Guo et al., 2020; Xiao et al., 2008; Xu et al., 2008), since the size is directly related to the method of synthesis of the precursor solid. The precipitated particles before calcination exhibited a narrower size distribution compared to the calcined particles. This suggests that particle agglomeration may have occurred during the calcination process. The particles size distribution width of washed precipitated solids increased with the calcination, resulting in a more heterogeneous material.

6.4 Conclusions

This study investigated the precipitation process of niobic acid from potassium niobate and sulfuric acid solutions, as well as its thermal conversion into niobium oxides. The modeling of the system by PHREEQC and OLI Studio predicted the pH of 3 as the optimal condition to niobic acid formation, due to the highest initial supersaturation indices at this value.

An amorphous niobic acid was obtained by precipitation with different concentrations of H_2SO_4, similar to the commercial niobic acid. Analysis of the samples revealed that the washing protocol effectively removed impurities potassium and sulphur, resulting in products closer to the reference composition of commercial niobic acid HY-340. From the XRF analysis the maximum 64.38 % of Nb was achieved by the solid precipitated with 0.50 mol/L H_2SO_4. However, a residual of ~2 % of potassium still presents in the solid, even after 8 cycles of washing.

The physico-chemical characterization of precipitated solids show that a potassium sulphate phase (K_2SO_4) was formed during the precipitation. The results also indicated that the concentration of the precipitating agent (0.25 or 0.50 mol/L H_2SO_4) influenced the chemical composition, particle size, and morphology of the obtained materials.

Due to the presence of residual potassium, calcination of the washed samples of precipitated solid revealed also a minor amount of crystalline phase $K_2Nb_8O_{21}$. The morphology of the calcined solids showed rod-like agglomerated particles, homogeneously distributed, with agglomerate size of approximately 30 μm and small individual particles of less than 1 micron.

The results highlight the importance of controlling parameters such as supersaturation index, operation, calcination temperature, and purification protocols to ensure high-quality final products.

6.5 References

Brandão, R.F., Quirino, R.L., Mello, V.M., Tavares, A.P., Peres, A.C., Guinhos, F., Rubim, J.C., Suarez, P.A.Z., 2009. Synthesis, characterization and use of Nb2O5 based catalysts in producing biofuels by transesterification, esterification and pyrolysis. J. Braz. Chem. Soc. 20, 954–966. https://doi.org/10.1590/S0103-50532009000500022

Brayner, R., Bozon-Verduraz, F., 2003. Niobium pentoxide prepared by soft chemical routes: Morphology, structure, defects and quantum size effect. Phys. Chem. Chem. Phys. 5, 1457–1466. https://doi.org/10.1039/b210055j

Carniti, P., Gervasini, A., Biella, S., Auroux, A., 2006. Niobic acid and niobium phosphate as highly acidic viable catalysts in aqueous medium: Fructose dehydration reaction. Catal. Today 118, 373–378. https://doi.org/10.1016/j.cattod.2006.07.024

Chan, X., Pu, T., Chen, X., James, A., Lee, J., Parise, J.B., Kim, D.H., Kim, T., 2017a. Effect of niobium oxide phase on the furfuryl alcohol dehydration. Catal. Commun. 97, 65–69. https://doi.org/10.1016/j.catcom.2017.04.019

Chan, X., Pu, T., Chen, X., James, A., Lee, J., Parise, J.B., Kim, D.H., Kim, T., 2017b. Effect of niobium oxide phase on the furfuryl alcohol dehydration. Catal. Commun. 97, 65–69. https://doi.org/10.1016/j.catcom.2017.04.019

Chen, Y., Wang, Z., Liu, S., Zhang, G., 2022. Modified niobic acid via acidification by various liquid acids for dehydration of succinic acid to succinic anhydride. Colloids Surfaces A Physicochem. Eng. Asp. 650, 129644. https://doi.org/10.1016/j.colsurfa.2022.129644

Cheng, X., Zhu, H., Yu, H., Ye, W., Zheng, R., Liu, T., Peng, N., Shui, M., Shu, J., 2018. K2Nb8O21 nanotubes with superior electrochemical performance for ultrastable lithium storage. J. Mater. Chem. A 6, 8620–8632.

https://doi.org/10.1039/c8ta01411f

De Andrade, J.S., Pinheiro, A.G., Vasconcelos, I.F., De Araújo, M.A.B., Valente, M.A., Sombra, A.S.B., 2000. Structural studies of KNbO3 in niobate glass-ceramics. J. Phys. Chem. Solids 61, 899–906. https://doi.org/10.1016/S0022-3697(99)00387-X

Deblonde, G.J.P., Bengio, D., Beltrami, D., Bélair, S., Cote, G., Chagnes, A., 2019. Niobium and tantalum processing in oxalic-nitric media: Nb2O5·nH2O and Ta2O5·nH2O precipitation with oxalates and nitrates recycling. Sep. Purif. Technol. 226, 209–217. https://doi.org/10.1016/j.seppur.2019.05.087

Fan, W., Zhang, Q., Deng, W., Wang, Y., 2013. Niobic acid nanosheets synthesized by a simple hydrothermal method as efficient Brønsted acid catalysts. Chem. Mater. 25, 3277–3287. https://doi.org/10.1021/cm400192q

Filella, M., May, P.M., 2020. The aqueous solution thermodynamics of niobium under conditions of environmental and biological interest. Appl. Geochemistry 122, 104729. https://doi.org/10.1016/j.apgeochem.2020.104729

Foo, G.S., Wei, D., Sholl, D.S., Sievers, C., 2014. Role of Lewis and brønsted acid sites in the dehydration of glycerol over niobia. ACS Catal. 4, 3180–3192. https://doi.org/10.1021/cs5006376

Guo, C., Qian, Z., 1993. Acidic and catalytic properties of niobic acid crystallized at low temperature. Catal. Today 16, 379–385. https://doi.org/10.1016/0920-5861(93)80077-E

Guo, Z., Liu, L., Hou, Z., Wang, Y., Yu, J., Jiang, H., 2020. Fabrication of K2Nb8O21 microcrystalline with good dispersion by molten salt synthesis. Ferroelectrics 554, 197–203. https://doi.org/10.1080/00150193.2020.1705111

Hara, M., 2014. Heterogeneous Lew i s Ac i d Cata l ysts Workab l e i n Water. Chem. Soc. Japan 87, 931–941.

Huang, B.X., Wang, K., Church, J.S., Li, Y.S., 1999. Characterization of oxides on niobium by raman and infrared spectroscopy. Electrochim. Acta 44, 2571–2577. https://doi.org/10.1016/S0013-4686(98)00385-5

Jun Park, Y., Kang, K.M., Ho Kang, J., Ho Han, S., Seong Jang, H., Yeon Lee, J., Yoon,

T.S., Nah, Y.C., Kim, D.H., 2022. Enhancement of electrochromic response and cyclic durability of WO3 thin films by stacking Nb2O5 layers. Appl. Surf. Sci. 582, 152431. https://doi.org/10.1016/j.apsusc.2022.152431

Ko, E.I., Weissman, J.G., 1990. Structures of niobium pentoxide and their implications on chemical behavior. Catal. Today 8, 27–36. https://doi.org/10.1016/0920-5861(90)87005-N

Kudo, A., Sakata, T., 1996. Effect of ion exchange on photoluminescence of layered niobates K4Nb6O17 and KNb3O8. J. Phys. Chem. 100, 17323–17326. https://doi.org/10.1021/jp9619806

Lebarbier, V., Houalla, M., Onfroy, T., 2012. New insights into the development of Bronsted acidity of niobic acid. Catal. Today 192, 123–129. https://doi.org/10.1016/j.cattod.2012.02.061

Liu, H., Zhang, Z., Hu, L., Gao, N., Sang, L., Liao, M., Ma, R., Xu, F., Fang, X., 2014. New UV-A Photodetector Based on Individual Potassium Niobate Nanowires with High Performance. Adv. Opt. Mater. 2, 771–778. https://doi.org/10.1002/adom.201400176

Liu, J.F., Li, X.L., Li, Y.D., 2002. Novel Synthesis of Polymorphous Nanocrystalline KNbO3 by a Low Temperature Solution Method. J. Nanosci. Nanotechnol. 2, 617–619. https://doi.org/10.1166/jnn.2002.152

Luisa Marin, M., Hallett-Tapley, G.L., Impellizzeri, S., Fasciani, C., Simoncelli, S., Netto-Ferreira, J.C., Scaiano, J.C., 2014. Synthesis, acid properties and catalysis by niobium oxide nanostructured materials. Catal. Sci. Technol. 4, 3044–3052. https://doi.org/10.1039/c4cy00238e

Nakajima, K., Baba, Y., Noma, R., Kitano, M., N. Kondo, J., Hayashi, S., Hara, M., 2011. Nb2O5•nH2O as a heterogeneous catalyst with water-tolerant lewis acid sites. J. Am. Chem. Soc. 133, 4224–4227. https://doi.org/10.1021/ja110482r

Nakajima, K., Fukui, T., Kato, H., Kitano, M., Kondo, J.N., Hayashi, S., Hara, M., 2010. Structure and acid catalysis of mesoporous Nb2O 5·n H2O. Chem. Mater. 22, 3332–3339. https://doi.org/10.1021/cm100391q

Nikishina, E.E., Lebedeva, E.N., Drobot, D. V., 2012. Niobium- and tantalum-containing

oxide materials: Synthesis, properties, and application. Inorg. Mater. 48, 1243–1260. https://doi.org/10.1134/s002016851213002x

ODY, K.D.S., 2018. Estudo das propriedades do óxido de nióbio a partir de uma perspectiva computacional. UNIVERSIDADE TECNOLÓGICA FEDERAL DO PARANÁ.

Pinto, M.B., Soares, A.L., Mella Orellana, A., Duarte, H.A., De Abreu, H.A., 2017. Structural, Electronic, and Thermodynamic Properties of the T and B Phases of Niobia: First-Principle Calculations. J. Phys. Chem. A 121, 2399–2409. https://doi.org/10.1021/acs.jpca.6b11383

Qiu, J., Li, X., Qi, X., 2019. Raman Spectroscopic Investigation of Sulfates Using Mosaic Grating Spatial Heterodyne Raman Spectrometer. IEEE Photonics J. 11, 1. https://doi.org/10.1109/JPHOT.2019.2939222

Rade, L.L., Lemos, C.O.T., Barrozo, M.A.S., Ribas, R.M., Monteiro, R.S., Hori, C.E., 2018. Optimization of continuous esterification of oleic acid with ethanol over niobic acid. Renew. Energy 115, 208–216. https://doi.org/10.1016/j.renene.2017.08.035

Rodrigues, L.A., da Silva, M.L.C.P., 2010. Synthesis of Nb2O5·nH2O nanoparticles by water-in-oil microemulsion. J. Non. Cryst. Solids 356, 125–128. https://doi.org/10.1016/j.jnoncrysol.2009.11.002

Siddiki, S.M.A.H., Rashed, M.N., Ali, M.A., Toyao, T., Hirunsit, P., Ehara, M., Shimizu, K. ichi, 2019. Lewis Acid Catalysis of Nb2O5 for Reactions of Carboxylic Acid Derivatives in the Presence of Basic Inhibitors. ChemCatChem 11, 383–396. https://doi.org/10.1002/cctc.201801239

Souza, C.R., Vaughan, J., Rocha, S.D.F., Birchal, V.S., 2021. Manufacturing reactive magnesia from nickel laterite waste solution via nesquehonite precipitation. Hydrometallurgy 204. https://doi.org/10.1016/j.hydromet.2021.105725

Su, T., Jiang, H., Gong, H., Zhai, Y., 2010. An alternative approach of solid-state reaction to prepare nanocrystalline KNbO3. J. Mater. Sci. 45, 3778–3783. https://doi.org/10.1007/s10853-010-4431-6

Takagaki, A., Nishimura, S., Ebitani, K., 2013. Mechanistic studies of solid acids and

base-catalyzed clean technologies. Heterog. Catal. Clean Technol. Spectrosc. Des. Monit. 125–171. https://doi.org/10.1002/9783527658985.ch6

Tanabe, K., 2003. Catalytic application of niobium compounds. Catal. Today 78, 65–77. https://doi.org/10.1016/S0920-5861(02)00343-7

Tanabe, K., 1987. Niobic acid as an unusual acidic solid material. Mater. Chem. Phys. 17, 217–225. https://doi.org/10.1016/0254-0584(87)90057-5

Tanabe, K., Okazaki, S., 1995. Various reactions catalyzed by niobium compounds and materials. Appl. Catal. A, Gen. 133, 191–218. https://doi.org/10.1016/0926-860X(95)00205-7

Teshima, K., Niina, Y., Yubuta, K., Nakazawa, T., Suzuki, T., Shishido, T., Ishizawa, N., Oishi, S., 2008. Environmentally friendly growth and characterization of photocatalytic K2Nb8O21 crystals. Jpn. J. Appl. Phys. 47, 629–632. https://doi.org/10.1143/JJAP.47.629

Tokio Iizuka, K.O. and K.T., 1983. Acidic and Catalytic Properties of Niobium Pentoxide. Appl. Catal. https://doi.org/10.1016/s0166-9834(00)81514-6

Ushikubo, T., Iizuka, T., Hattori, H., Tanabe, K., 1993. Preparation of highly acidic hydrated niobium oxide. Catal. Today 16, 291–295. https://doi.org/10.1016/0920-5861(93)80068-C

Wang, Y., Yi, Z., Li, Y., Yang, Q., Wang, D., 2007. Hydrothermal synthesis of potassium niobate powders. Ceram. Int. 33, 1611–1615. https://doi.org/10.1016/j.ceramint.2006.07.013

Xiao, X., Dong, G., Xu, C., He, H., Qi, H., Fan, Z., Shao, J., 2008. Structure and optical properties of Nb 2 O 5 sculptured thin films by glancing angle deposition. Appl. Surf. Sci. 255, 2192–2195. https://doi.org/10.1016/j.apsusc.2008.07.071

Xu, C.Y., Zhen, L., Yang, L., He, K., Shao, W.Z., Qin, L.C., 2008. A facile molten salt route to K2Nb8O21 nanoribbons. Ceram. Int. 34, 435–437. https://doi.org/10.1016/j.ceramint.2006.10.007

Zhao, Y., Zhou, X., Ye, L., Chi Edman Tsang, S., 2012. Nanostructured Nb 2 O 5 catalysts . Nano Rev. 3, 17631. https://doi.org/10.3402/nano.v3i0.17631

CHAPTER 7 – GENERAL CONCLUSIONS / CONCLUSÕES GERAIS

English

This study developed and validated a new route for recovering niobium compounds from Fe-Nb alloy fines through alkaline leaching with KOH and approximately 88% of niobium was recovered, resulting in a niobium-rich liquor. From this liquor was possible to crystallized potassium niobate (mixed of phases: $KNbO_3$ and $K_4Nb_6O_{17}$). The crystallized solid was used as source of niobium to precipitation of niobic acid using H_2SO_4 solution yielded an amorphous solid that was subsequently calcined to produce niobium oxide. Residual potassium in the precipitated material led to the formation of a potassium niobate phase ($K_2Nb_8O_{21}$) during calcination, indicating the need for further purification steps to enhance the product's quality.

The solubility of niobic acid and potassium niobate under alkaline conditions was investigated experimentally and supported by thermodynamic modeling using OLI Studio. Niobic acid pseudo-solubility increased with the temperature and decreased slightly at higher concentrations of KOH. The pseudo-solubility of potassium niobate decreased as KOH concentration increased but rose with higher temperatures.

The cooling crystallization of potassium niobate was further studied. The pre-concentration of the leached liquor and cooling rate was investigated. The 40 wt% pre-concentrated liquor achieved a crystallization yield of up to 95% when cooled from 100 to 30 ºC. The different cooling rate in the crystallization showed that lower cooling rates enhanced the crystallinity and improved the morphology of the crystals. Particle size analysis highlighted the slow kinetics of potassium niobate formation, with significant particle growth observed over time. Thermal treatment of potassium niobate revealed that higher calcination temperatures increased crystallinity and led to the formation of stable $KNbO_3$.

Precipitation studies of niobic acid were guided by thermodynamic predictions from PHREEQC and OLI Studio, which identified a pH of 3 as the optimal condition for the precipitation, where showed higher supersaturation index. Experimental results confirmed the production of amorphous niobic acid with residual content of potassium

and sulfur. A washing protocol was implemented to removal of impurities such as potassium and sulfur, though trace amounts of potassium remained, contributing to the formation of crystalline $K_2Nb_8O_{21}$ after calcination. The calcined solids exhibited rod-like morphologies, with well-distributed agglomerates and fine individual particles.

In conclusion, this work demonstrates an efficient route for recovering niobium compounds from secondary sources. It was highlighted the importance of controlling process parameters such as supersaturation, cooling rates during crystallization, concentration of the precipitant agent, calcination temperature and time, and purification steps. This study provides the basis for future recovery and valorisation of niobium-containing products from waste materials towards circularity and highlights the feasibility of recovering niobium compounds from secondary sources under mild temperature and pressure conditions.

Português

Este estudo desenvolveu e validou uma nova rota para a recuperação de compostos de nióbio a partir de finos da liga Fe-Nb por meio de lixiviação alcalina com KOH, recuperando aproximadamente 88% do nióbio, resultando em um licor rico em nióbio. A partir deste licor, foi possível cristalizar niobato de potássio (mistura de fases majoritárias: $KNbO_3$ e $K_4Nb_6O_{17}$). O sólido cristalizado foi utilizado como fonte de nióbio para a precipitação de ácido nióbico usando solução de H_2SO_4, gerando um sólido amorfo que foi posteriormente calcinado para produzir óxido de nióbio. O potássio residual no material precipitado levou à formação de uma fase de niobato de potássio ($K_2Nb_8O_{21}$) durante a calcinação, indicando a necessidade de etapas adicionais de purificação para melhorar a qualidade do produto.

A solubilidade do ácido nióbico e do niobato de potássio em condições alcalinas foi investigado experimentalmente e apoiado por modelagem termodinâmica usando o OLI Studio. A pseudo-solubilidade do ácido nióbico aumentou com a temperatura e diminuiu ligeiramente em concentrações mais altas de KOH. A pseudo-solubilidade do niobato de

potássio diminuiu conforme a concentração de KOH aumentou, mas aumentou com temperaturas mais altas.

A cristalização por resfriamento do niobato de potássio foi estudada mais detalhadamente. Investigou-se a pré-concentração do licor lixiviado e a taxa de resfriamento. O licor pré-concentrado a 40% em massa alcançou um rendimento de cristalização de até 95% quando resfriado de 100 ºC a 30 ºC. Diferentes taxas de resfriamento na cristalização mostraram que taxas de resfriamento mais baixas aumentaram a cristalinidade e melhoraram a morfologia dos cristais. A análise do tamanho de partículas destacou a cinética lenta de formação do niobato de potássio, com crescimento significativo das partículas ao longo do tempo. O tratamento térmico do niobato de potássio revelou que temperaturas de calcinação mais altas aumentaram a cristalinidade e levaram à formação de $KNbO_3$ estável.

Estudos de precipitação de ácido nióbico foram guiados por previsões termodinâmicas do PHREEQC e OLI Studio, que identificaram o pH 3 como a condição ideal para a precipitação, apresentando maior índice de supersaturação. Resultados experimentais confirmaram a produção de ácido nióbico amorfo com conteúdo residual de potássio e enxofre. Um protocolo de lavagem foi implementado para remoção de impurezas como potássio e enxofre, embora traços de potássio tenham permanecido, contribuindo para a formação de $K_2Nb_8O_{21}$ cristalino após a calcinação. Os sólidos calcinados exibiram morfologias em forma de bastão, com aglomerados bem distribuídos e partículas individuais finas.

Em conclusão, este trabalho demonstra uma rota eficiente para a recuperação de compostos de nióbio a partir de fontes secundárias. Destacou-se a importância de controlar parâmetros de processo, como supersaturação, taxas de resfriamento durante a cristalização, concentração do agente precipitante, temperatura e tempo de calcinação e etapas de purificação. Este estudo fornece a base para futuras iniciativas de recuperação e valorização de produtos contendo nióbio a partir de materiais residuais, promovendo a circularidade, e destaca a viabilidade da recuperação de compostos de nióbio de fontes secundárias sob condições moderadas de temperatura e pressão.

CHAPTER 8 – ORIGINAL CONTRIBUITIONS

PAPERS

- Journal of Separation and Purification Technology – Submitted and under revision

"Crystallization-based recovery of niobium compounds from alkaline liquor"

- Inorganic Chemistry Journal – Submitted

"Investigation of solubility of niobium compounds under alkaline conditions"

CONFERENCES

- ***BIWIC 2023 – 28th International Workshop on Industrial Crystallization – Estocolmo/SE***

"Precipitation of hydrated niobium oxide (niobic acid) from potassium niobate and sulfuric acid solutions"

- ***ISIC 2023 – Internationa Symposium on Industrial Cystallization – Glasgow/UK***

"Atmospheric crystallization of potassium niobate from Fe-Nb alloy fines liquor"

- ***Semana do Conhecimentos – UFMG: IC Vitória Sipoli***

"Estudos de compostos de nióbio obtidos a partir do licor alcalino dos finos de liga Fe-Nb"

- ***ICHS 2024 – 1st International Circular Hydrometallurgy Symposium – Mechelen/BE***

"Niobium circularity: Linking the chain aiming at sustainable innovation"

- ***BIWIC 2024 – 29th International Workshop on Industrial Crystallization – Delft/NL***

"Cooling crystallization of potassium niobate in aqueous medium"

- 3rd place prize for the best poster presentation.

- ***AiChe 2024 – Annual Meeting – San Diego/EUA***

"Solubility investigation of niobium compounds in alkaline medium"

APPENDIX

CHAPTER 4

Table A1. Equilibrium constants values for hydro-complexes of niobium at 25ºC*.

REACTION	log K	REFERENCE
$Nb(OH)_{5(aq)} + H_2O = Nb(OH)^{6-} + H^+$	-6.32 -6.76	Yajima et al., 1992 and 1994 - citated by Fillela and May, 2020
$Nb(OH)_{5(aq)} = Nb(OH)_4^+ + OH^-$	-14.60	Babko et al., 1963
$Nb(OH)_{5(aq)} = NbO_3^- + H^+ + 2H_2O$	-7.40	
$Nb(OH)_{5(aq)} + 2H_2O = Nb(OH)_7^{-2} + 2H^+$	-14.66	ΔG_f data from Peiffert et al., 2010
$7Nb_6O_{19}^{8-} + 2H^+ = 6Nb_7O_{22}^{9-} + H_2O$	3.95	Petrus et al., 2022
$5Nb_6O_{19}^{8-} + 22H^+ = 3Nb_{10}O_{28}^{6-} + 11H_2O$	79.40	
$4Nb_6O_{19}^{8-} + 17H^+ = H_9Nb_{24}O_{72}^{9-} + 4H_2O$	185.29	
$6Nb(OH)_4^+ = Nb_6O19_8^- + 14H^+ + 5H_2O(l)$	-70.54	Noseck et al., 2021
$6Nb(OH)_4^+ = HNb_6O_{19}^{7-} + 13H^+ + 5H_2O(l)$	-56.54	
$6Nb(OH)_4^+ = H_2Nb_6O_{19}^{6-} + 12H^+ + 5H_2O(l)$	-43.54	
$6Nb(OH)_4^+ = H_3Nb_6O_{19}^{5-} + 11H^+ + 5H_2O(l)$	-31.94	
$Nb_6O_{19}^{8-} + H^+ = HNb_6O_{19}^{7-}$	16.11 11.87	Etxebarria et al., 1994 and Petrus et al., 2022
$Nb_6O_{19}^{8-} + 2H^+ = H_2Nb_6O_{19}^{6-}$	27.97 23.21	
$Nb_6O_{19}^{8-} + 3H^+ = H_3Nb_6O_{19}^{5-}$	39.91 32.80	

* The chemical reaction of niobium complexes in aqueous media and their equilibrium constants are presented in Table A1. Furthermore, Fillela & May (2020) collected the thermodynamic data available in a variety of systems containing different anions (F^-, Cl^-, Na^+, NO_{3-} $C_2O_4^-$, $C_3H_2O_4^{2-}$, $C_4H_4O_4^{2-}$).

Table A2 shows the pH behavior of niobic acid in KOH solution with time was monitored during the equilibrium study after the filtration of each sample. It is possible to observe that the pH values decreased during the experiment in each concentration of KOH. This may indicate a partial neutralization of the solution with niobic acid. At 0.50 mol/L, the

highest concentration of KOH, the pH had a greater reduction in its value over time, which may suggest a greater interaction between KOH and niobic acid and more aqueous niobium available in solution.

Table A2. pH values of niobic acid in KOH solution during the equilibrium test.

Time (h)	0.10	0.25	0.50
	(mol/L) KOH		
	pH		
1	13.30	13.69	14.49
2	13.45	13.60	14.45
24	13.37	13.49	13.97
72	12.75	13.39	13.65
120	12.43	13.50	13.60
174	12.58	13.53	13.25
192	12.64	13.32	13.10
312	12.50	13.31	12.90

FTIR and XRD of niobic acid at 100 hours of experiment (Figure A1), when the most of compound had partially dissolved in the KOH solution (Figures 4.3- 4.5) shows a difference in bands 400 to 800 cm^{-1}, that indicates a change in the structure of the solids at 0.10 and 0.50 mol/L KOH when comparing with the niobic acid without previous contact with KOH solution. The niobic acid in 0.25 mol/L KOH shows a slight difference at 500 cm^{-1} with the same transmittance of niobic acid without contact in KOH solution. This behaviour may be related to a small interaction between the solid and the solution and can be corroborate by the small change in pH values during the experiment (see Table

A2). The XRD also shows a change in the structure of amorphous niobic acid, with a reduction of the peaks.

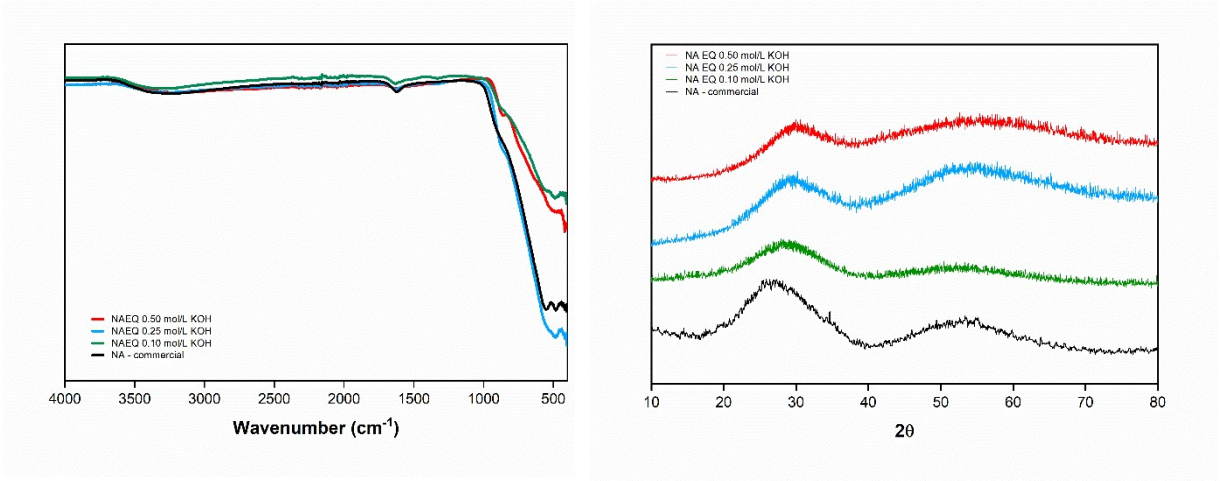

(a) **(b)**

Figure A113. (a) FTIR and (b) XRD of niobic acid commercial and after 100 hours in the different concentrations of KOH solution at 30 ± 0.5 ºC.

Table A3. Fitted equations of solubility by equilibrium study and Crystal 16.

Condition	Fitted Equation	R^2
	Equilibrium study	
0.10 - 0.50 mol/L KOH	C (g/L) =0.77±0.11*T (°C) –0.07±0.04	0.9590
	Potassium Niobate	
0 mol/L KOH	C (g/L) = 5.56±0.60*T (°C) – 90.92±3.30	0.9556
0.10 mol/L KOH	C (g/L) = 2.43±0.34*T (°C) – 33.55±11.06	0.9273
0.25 mol/L KOH	C (g/L) = 1.93±0.05*T (°C) – 49.73±2.02	0.9969
0.50 mol/L KOH	C (g/L) = 1.52±0.09*T (°C) – 31.05±3.66	0.9786
1.00 mol/L KOH	C (g/L) = 1.34±0.03*T (°C) – 42.02±1.74	0.9982

Niobic Acid		
0.75 mol/L KOH	C (g/L) = 2.76±0.08*T (°C) – 86.09±3.78	0.9968
1.00 mol/L KOH	C (g/L) = 2.27±0.40*T (°C) – 68.33±3.21	0.9821
1.50 mol/L KOH	C (g/L) = 5.90±0.92*T (°C) – 335.94±6.16	0.9085
2.00 mol/L KOH	C (g/L) = 5.65±1.20*T (°C) – 332.06±7.80	0.8104

Table A4 shows the chemical composition of potassium niobate crystallized from an alkaline liquor (Souza et al., 2024) as a mix of phases: $K_4Nb_6O_{17}$ and $KNbO_3$, and niobic acid from CBMM.

Table A4. Chemical composition by XRF of niobic acid and potassium niobate.

Content (%)	**Nb**	**O**	**K**	**Fe**	**S**	**Ta**	**Ca**	**Si**	**Al**
Potassium Niobate	44.26	24.4	26.22	0.24	0.04	<0.01	<0.01	<0.01	<0.01
Niobic Acid	69.36	30.05	-	-	-	0.08	0.09	-	-

Solubility of niobic acid in a range of 0 to 5 mol/L of KOH at different temperatures was measured. For this, the formation of other phases was allowed during the thermodynamic modeling of solubility of niobic acid, due to possible reactions with KOH. From 1.5 mol/L KOH Nb is consumed from the solution and react with potassium, forming potassium niobate as $KNbO_3$.

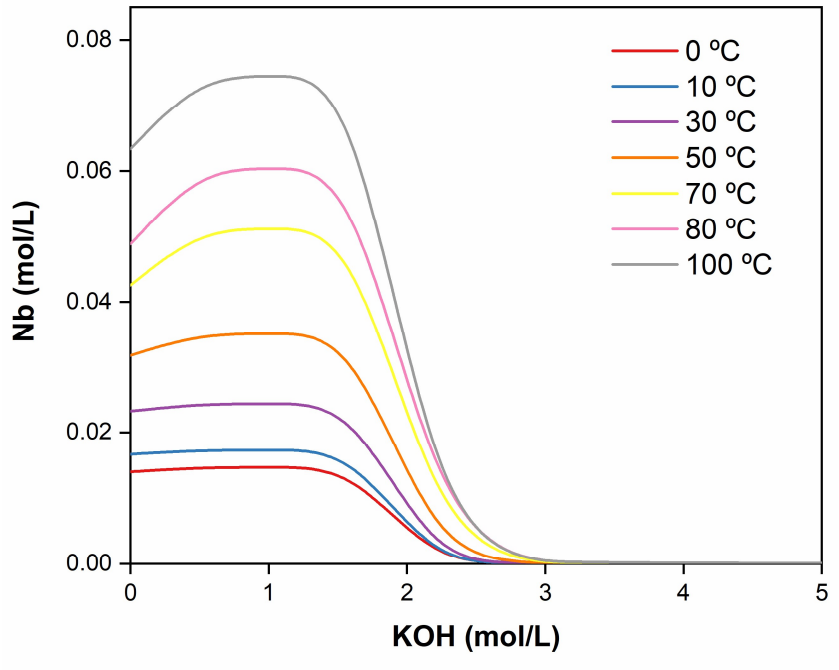

Figure A2. Solubility of $Nb_2O_5nH_2O$ in KOH dependence on temperature. Initial condition: [$Nb_2O_5nH_2O$] = 1 mol/L (OLI Studio databank – AQ thermodynamic framework).

According to the OLI Studio modeling, the solubility of the $KNbO_3$ phase in water is not linear with the temperature, as shown in Figure A3. The solubility exhibits a slight increase until 40ºC, followed by a rapid increase until reaching 90 ºC, the highest solubility point. Beyond this temperature, the solubility of potassium niobate decreases. The influence of the temperature and KOH concentration on the solubility of $KNbO_3$ given by OLI Studio can be seen in Figure A4.

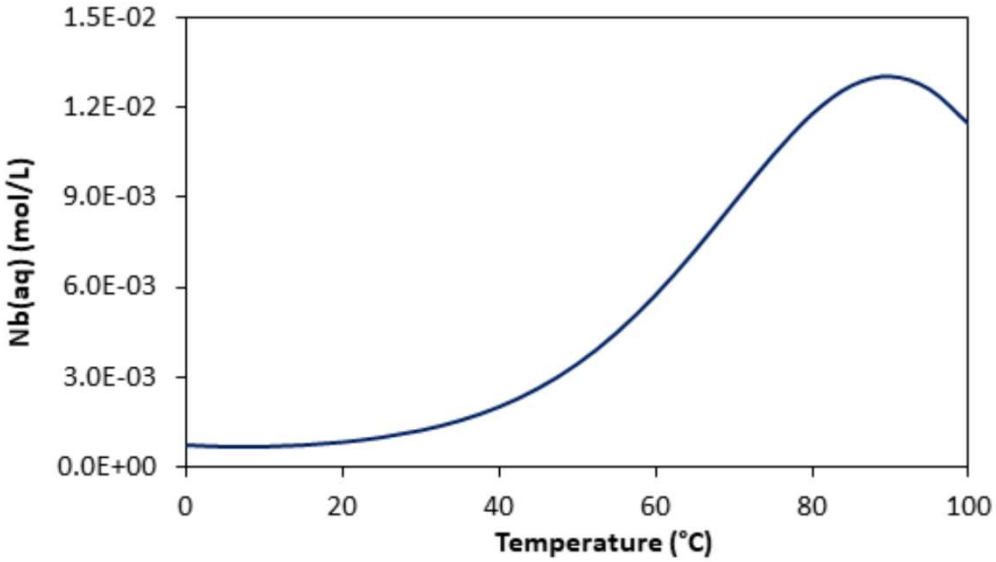

Figure A3. Solubility of $KNbO_3$ as a function of temperature. Initial condition: [$KNbO_3$] = 1 mol/L (OLI Studio databank – AQ thermodynamic framework).

The solubility of $KNbO_3$ is strongly affected by the temperature and solution concentration. The solubility of potassium niobate decreases with the increasing in KOH concentration. However, the solubility increases with the temperature when the KOH concentration is lower.

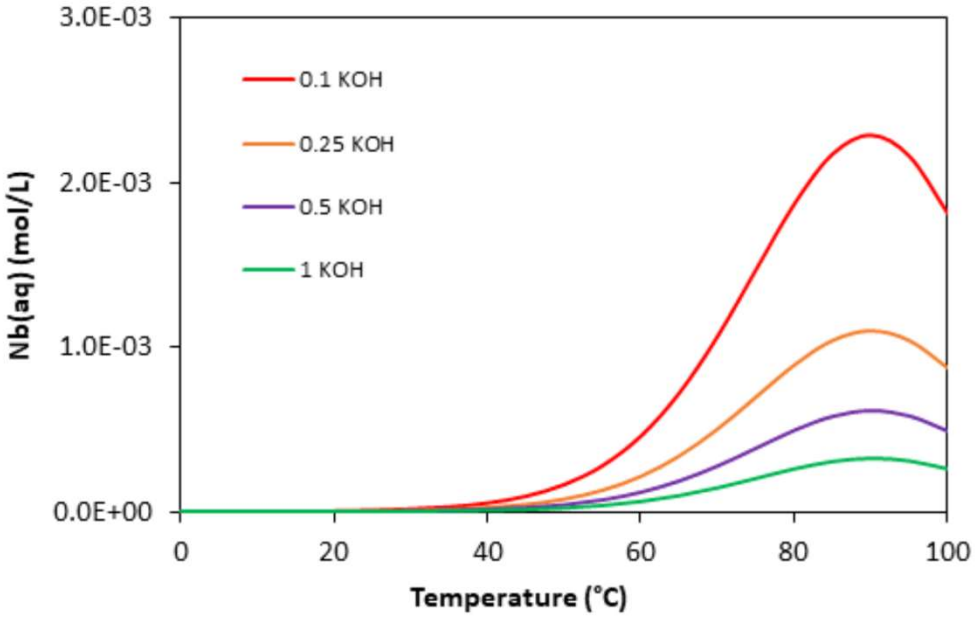

Figure A4. Solubility of $KNbO_3$ in KOH dependence on temperature. Initial condition: [KNbO3] = 1 mol/L (OLI Studio databank – AQ thermodynamic framework).